SPE TRANSACTIONS

devoted to plastics science and engineering

VOL. 1, NO. 3 JULY 1961

PUBLISHED BY THE SOCIETY OF PLASTICS ENGINEERS, INC.

SPE TRANSACTIONS

. . . publishes fundamental data in the field of plastics science and engineering. Each issue has a selection of polymer articles, both original and review type, including translations of significant articles from foreign publications. In addition to being readily available as a permanent reference source, SPE TRANSACTIONS is regularly indexed in the permanent literature. Also, the table of contents of quarterly issues of TRANSACTIONS is published in the preceding issue of the SPE Journal, also published by the Society.

Society of Plastics Engineers, Inc.

Executive and Business Offices
65 Prospect St.
Stamford, Conn.

1961 Officers of the Society —

President — FRANK W. REYNOLDS
Vice Pres., Eng. — JAMES R. LAMPMAN
Vice Pres., Adm. — JOHN DELMONTE
Secretary — MAURICE F. MALONE
Treasurer — JOHN N. BERUTICH
Exec. Secretary — THOMAS A. BISSELL

Neither the Society of Plastics Engineers, Inc., nor the SPE TRANSACTIONS is responsible for the views expressed by individual contributors either in articles published in SPE TRANSACTIONS or in technical papers presented at meetings of the Society.

Editor — MELVYN A. KOHUDIC
Layout, Production — LEE COOPER
Editorial Assistant — HELEN B. TIEDEMANN
Circulation Manager — LEWIS A. BERNHARD

SPE Publications Committee

MAURICE F. MALONE, *Adm.* — EUGENE C. QUEAR
DR. ALEX SACHER, *Chmn.* — DR. FRANK W. REINHART
DR. RAYMOND F. BOYER — IRVIN I. RUBIN
DR. JESSE H. DAY — DR. SIDNEY J. STEIN
DR. HERMAN F. MARK — PARKE WOODWORTH
FRANK A. MARTIN

Editorial Advisory Board

DR. FRANK W. REINHART, *Chmn.*

ROBERT W. BARBER — DR. HERMAN S. KAUFMAN
DR. EDWARD G. BOBALEK — JOHN P. LOMBARDI
DR. LUTHER BOLSTAD — DR. BRYCE MAXWELL
EDWARD F. BORRO, SR. — DR. FREDERICK J. McGARRY
BENJAMIN S. COLLINS — THOMAS F. McLAUGHLIN
WILLIAM CROLL — DR. ROBERT B. MESROBIAN
LAWRENCE M. DEBING — ROBERT E. MONICA
EDWARD J. FITZPATRICK — JULES PINSKY
RUSSELL M. HOUGHTON — ROBERT D. SACKETT
JOHN B. HOWARD — EDWARD W. VAILL

• SPE TRANSACTIONS is Published at 215 Canal St., Manchester, N. H. Address changes, undeliverable copies and orders for subscriptions should be sent to 65 Prospect St., Stamford, Conn.

• *Permit for second-class matter at the Post Office at Manchester, New Hampshire, at special postal rate provided in paragraph (d-2), Sec. 34.40 P.L. and R., of 1918, applied for.*

• *Copyright by the Society of Plastics Engineers, Inc., 1961. Reproduction in whole or part without written permission is strictly prohibited.*

— Subscription Rates —

SPE Members
1 Yr.—$10 2 Yrs.—$18 3 Yrs.—$25

Non-Members
(US and North America)
1 Yr.—$15 2 Yrs.—$28 3 Yrs.—$40

Non-Members *(Overseas)*
1 Yr.—$25 2 Yrs.—$47 3 Yrs.—$67

Table of Contents

VOLUME 1 • NO. 3

ABSTRACTS of Articles in this Issue 102

Best of ANTEC — SPE TRANSACTIONS explanation 104

Thermodynamic Diagrams for Polyethylene Resins 105

J. M. Lupton, E. I. du Pont de Nemours & Co. Inc., Polychemicals Department, Wilmington, Delaware.

Based on certain assumptions, thermodynamic diagrams are developed which can be used to estimate properties of resins not yet synthesized

The Strength of Glassy Polymers 109

J. P. Berry, General Electric Company, Research Laboratory, Schenectedy, New York

Actual polymer strength is less than that of theoretical expectations because of flaws which act as strength concentrators

Flow Patterns in a Non-Newtonian Fluid in a Single Screw Extruder 113

W. D. Mohr, J. B. Clapp and **F. C. Starr,** E. I. du Pont de Nemours & Co., Inc. Polychemicals Department, Wilmington, Delaware

Flow patterns of non-Newtonian fluids are shown to resemble those of Newtonian fluids, therefore simplified extrusion theory equations can be used for non-Newtonian conditions

The Effect of Extrusion Variables on the Fundamental Properties of Tubular Polyethylene Film 121

N. D. Huck and **P. L. Clegg,** Imperial Chemical Industries Ltd., Welwyn Garden City, Herts, England.

Properties of film are influenced by processing conditions and design features of the equipment in addition to the nature of the film

Effect of Gamma Radiation on Chemical Structure of Plastics 133

V. J. Krasnansky, M. S. Parker and **B. G. Achhammer,** National Bureau of Standards, Washington 25, D. C.

When plastic film samples were exposed to cobalt-60 gamma radiation in order to evaluate their respective stability, materials containing conjugated ring systems, ionic linkages and chlorine in their side groups proved to resist irradiation best

Inorganic-Organic High Polymers, Phenoxyaldehyde Resins of Titanium(IV), Zirconium(IV), and Hafnium(IV) 139

R. J. Landry and **E. H. Bartel,** U. S. Naval Ordnance Test Station, China Lake, California.

Calorobic resins which are metaloxene polymers of phenolaldehyde are now being synthesized, with emphasis placed on using refractory metals

Resins from Cyclohexane Oxide Derivatives and Fatty Acids 143

C. W. McGary, Jr. and **C. T. Patrick, Jr.,** Union Carbide Plastics Co., South Charleston, West Virginia

Resin preparation and the effect of curing agent and initiator concentration upon properties are discussed

EDITORIAL **Professor Giulio Natta,** Director of the Institute of Industrial Chemistry, Polytechnic Institute of Milan 147

abstracts of articles in this issue

THERMODYNAMIC DIAGRAMS FOR POLYETHYLENE RESINS

J. M. Lupton

E. I. du Pont de Nemours & Co., Inc., Wilmington, Del.

For resins of room temperature density 0.91 to 0.96 g/cc, enthaply and internal energy diagrams have been developed from 0 to 200°C and up to 1000 atmospheres. These diagrams can be used for estimating properties for which data are not available, and provide unified view of many properties of polyethylene under conditions of fabrication and use. Extent of crystallinity estimates can be made from enthalpy, internal energy, specific volume, compressibility and melting point data provided for hypothetical amorphous, crystalline and actual resins.

THE STRENGTH OF GLASSY POLYMERS

J. P. Berry

General Electric Co., Schenectady, N. Y.

The Griffith theory for brittle fracture predicts that the tensile strength should be inversely proportional to the square root of the size of a defect or flaw in the sample tested. The validity of this relation has been investigated for the glassy polymers, poly(methyl methacrylate) and polystrene. The results indicate that the strength of the polymers depends on two factors: (1) the surface energy, and (2) the inherent flaw size. The surface energy is primarily that dissipated in a viscous flow process and the inherent flaw size is related to the tendency of the polymer to craze under stress.

FLOW PATTERNS IN A NON-NEWTONIAN FLUID IN A SINGLE-SCREW EXTRUDER

W. D. Mohr, J. B. Clapp, and F. C. Starr

Polychemicals Department, E. I. du Pont de Nemours & Co., Inc., Wilmington, Del.

Flow patterns in the channel of a screw extruder have been investigated in a study utilizing a model extruder with stationary screw and a rotating, transparent barrel. Photographs of flow streamlines at conditions over the full range of output restriction are presented for a non-Newtonian fluid. A technique employing photographs of particle tracers was used with the same apparatus to permit quantitative measurement of velocity profiles with both a Newtonian and a non-Newtonian fluid.

THE EFFECT OF EXTRUSION VARIABLES ON THE FUNDAMENTAL PROPERTIES OF TUBULAR POLYTHENE FILM

N. D. Huck and P. L. Clegg

Imperial Chemical Industries, Ltd., Welwyn Garden City, Herts, England

The mechanism of formation of tubular polythene film is a complicated process, and extensive studies have

clip these briefs for easy reference on 3" x 5" or other suitable filing cards

shown that the properties of the film made are influenced profoundly and in a complex way both by the processing conditions used and by certain design features of the equipment. Studies of the effect of the extrusion variables on the more important film properties, both optical and mechanical, are reviewed in this paper. The results are discussed in terms of the fundamental nature of polythene film, its surface, its crystalline structure and its orientation.

EFFECT OF GAMMA RADIATION ON CHEMICAL STRUCTURE OF PLASTICS

V. J. Krasnansky, M. S. Parker, and B. G. Achhammer

National Bureau of Standards, Washington, D. C.

Twelve plastics representing various chemical structures were studied as part of a program to determine the utility of plastics as packaging materials in the high radiation presentation of food. The plastics were exposed to selected dosages of Cobalt-60 gamma radiation in vacuum and in air. Gas evolution and changes in infrared spectra as a result of irradiation were used to hypothesize the relative stability of these plastics to irradiation. Based on these facts it was found that plastics containing conjugated ring systems, ionic linkages, and chlorine in side groups were the most stable.

INORGANIC-ORGANIC HIGH POLYMERS, PHENOXYALDEHYDE RESINS OF TANTALUM (IV), ZIRCONIUM (IV), AND HAFNIUM (IV)

R. J. Landry and E. H. Bartel

U.S. Naval Ordnance Test Station, China Lake, Calif.

A new series of inorganic-organic high polymers have been synthesized namely; the metaloxene polymers of phenolaldehyde. Titanium (IV), Zirconium (IV) and Hafnium (IV) phenolaldehyde have been prepared and other metals especially the refractory type metals may merit further development as calorobic plastic materials. The hafnium resin has been compression molded into a rocket-nozzle insert shape with satisfactory rocket-firing results.

RESINS FROM CYCLOHEXENE OXIDE DERIVATIVES AND FATTY ACIDS

C. W. McCary, Jr. and C. T. Patrick, Jr.

Union Carbide Plastics Co., South Charleston, W. Va.

This article describes preparation of resins as described in the title above, and the effect of concentration of the diepoxide, dimer acid, and initiator (stannous octoate). Proportion of dimer acid and diepoxide has a marked influence on hardness and tensile properties of resins. Change in tensile properties upon aging correlates very well with change in hardness. Higher proportions of dimer acid produce softer, more flexible resins. The resins have unique electrical properties at temperatures up to 175°C, apparently because of the high proportion of hydrocarbon in the resin.

Best of ANTEC — SPE TRANSACTIONS

For those readers of TRANSACTIONS who may not know what "Best of ANTEC" means, there is a tradition in the Society whereby the best papers presented to the Society's Annual Technical Conference (ANTEC) are singled out for recognition and published as a group known as the Best of ANTEC.

In past years, all the papers were published in a single issue of the SPE Journal, official publication of The Society of Plastics Engineers. However, with the establishment of a second publication—SPE TRANSACTIONS— in January 1961, selection and publication, of necessity, had to be modified. Because the editorial scope of a paper is more suitable for publication in TRANSACTIONS rather than the SPE Journal is no valid reason for excluding that paper from Best of ANTEC consideration. Therefore, selections were based on value first, with the editorial scope of the paper determining whether it will be published in TRANSACTIONS or the Journal. As it developed, there were a total of 10 papers selected Best of ANTEC out of a field of 102, with six published in the April issue of the SPE Journal, the remaining four published on the pages that follow.

Actual selection is based on a system of numerical ratings assigned by members of the Society's Editorial Advisory Board after they have reviewed the papers. It is presumptuous to designate certain papers as being "best." However the philosophy behind the Best of ANTEC is to attempt to set some standard of technical quality, thereby providing incentive for the presentation of papers of a high value in the field and in the profession at future Conferences of the Society.

Thermodynamic Diagrams for Polyethylene Resins

Diagrams can be used to compute heat effects and changes in temperature, pressure, volume, and crystallinity in melting, cooling, molding, compression, and extrusion. Of great interest: The diagrams can be used to estimate crystallinity, specific heat, and other important properties of resins that have not yet been synthesized

J. M. Lupton

Polychemicals Department
E. I. du Pont de Nemours & Company, Inc.
Wilmington, Delaware

Diagrams showing the effects of pressure, volume, and temperature on thermodynamic properties such as enthalpy, internal energy, and entropy are well known for simple substances and serve many purposes in science and engineering. Such diagrams for thermoplastic resins have been less frequently used, reflecting many complications in acquiring and interpreting the necessary data. However, recent studies show that a series of assumptions can be used to develop useful new diagrams of wide scope for polyethylene resins.

Assumptions

Three primary assumptions are required:

Assumption 1: Semicrystalline polyethylene can be regarded as a mixture of a hypothetical purely amorphous phase and a hypothetical purely crystalline phase. The degree of crystallinity, X, is then defined as the weight fraction of crystalline phase.

Assuming that the value of an extensive property of the semicrystalline resin, such as volume, enthalpy, or internal energy, equals the sum of the values for the crystalline and amorphous phases, the degree of crystallinity is:

$$X = (V' - V)/(V' - V'') \quad (1)$$

$$= (H' - H)/(H' - H'') \quad (2)$$

$$= (U' - U)/(U' - U'') \quad (3)$$

where V, H, and U are the specific volume, specific enthalpy, and specific internal energy, respectively. Primes denote values for the amorphous phase; and double primes, for the crystalline phase. Symbols without primes or double primes denote values for the whole semicrystalline resin. These relations enable calculation of any one of the four quantities in each equation when the other three are known.

Assumption 2: The thermodynamic properties of polyethylene melts are independent of such molecular

structure features as chain branching, and through extrapolation can be used to provide estimates of the properties of the hypothetical purely amorphous phase. Experimental measurements on melts of high-density and low-density polyethylene resins show that melt specific heat is nearly independent of the degree to which the polymer is branched (1, 2). Thus, with sufficient accuracy for practical purposes, these values may be averaged and used to construct a single curve for the one-atmosphere enthalpy of any polyethylene melt as a function of temperature starting with T_m, the temperature above which (according to many different tests) all crystallinity disappears. Extrapolation to temperatures below T_m provides one-atmosphere enthalpies for the supercooled melt. These may be used as the one-atmosphere enthalpies of the hypothetical purely amorphous phase. In a similar fashion, one-atmosphere volumetric data on polyethylenes above T_m are nearly independent of branching and have frequently been extrapolated to temperatures below T_m to estimate amorphous specific volume. Recent measurements (3) show that the specific volumes of high-density and low-density polyethylene resins differ by less than 0.5% (the experimental uncertainty) at pressures up to at least 600 atmospheres. Since pressure affects enthalpy only through the pressure-volume-temperature relation, as shown by the equation

$$(\partial H/\partial P)_T = V - T\,(\partial V/\partial T)_P \qquad (4)$$

the effects of pressure on enthalpy must be similarly independent of chain branching. Thus, the single one-atmosphere T-H curve above, including the extrapolated portion, can be extended into a family of isobaric curves for the T-P-H relation of any melted, supercooled, or amorphous polyethylene.

Assumption 3: The physical and thermodynamic properties of the hypothetical purely crystalline phase are independent of chain branching and can be estimated from x-ray diffraction studies of polyethylene cell constants as a function of temperature (4), from x-ray diffraction determinations of the cell constants of hydrocarbon crystals at high pressures (5), and from the heats of fusion of crystalline polyethylene (2, 6, 7). Although uncertainties in the final estimates are substantial, they have minor effects on the diagrams. For example, compressibility is small enough that relatively large uncertainty has little absolute effect on either volume or pressure-enthalpy corrections.

As shown by many recent studies of polymer morphology, each of the assumptions above is subject to numerous and extensive qualifications. Nevertheless, the assumptions provide an effective basis for first approximations which are entirely adequate for many practical problems and which can serve as valuable points of departure when more accurate analyses are needed.

Construction of Diagrams

The enthalpy and internal energy diagrams in *Figures 1 to 3* were constructed by using standard physical and thermodynamic relations and the assumptions above with additional data (1, 2, 7) on the semicrystalline resins listed in *Table 1*; data for other resins may be incorporated as they become available. One atmosphere

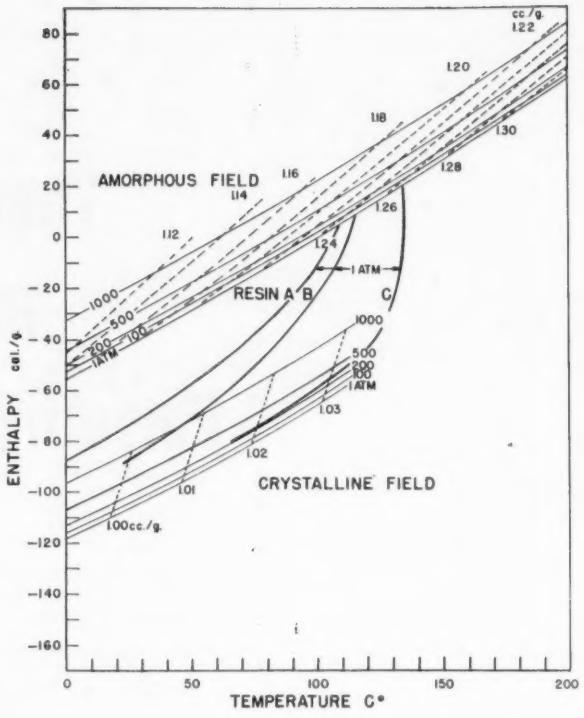

Figure 1. Enthalpy and internal energy diagrams. Slopes of curves represent specific heats at constant pressure

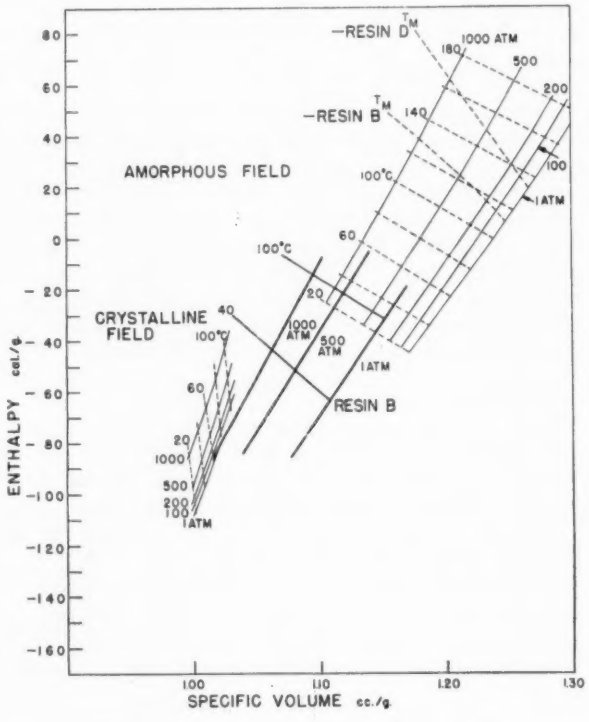

Figure 2. Enthalpy and internal energy diagrams. Included are curves for the effects of compression on the melting points of resins A and D

Table 1. Summary of Polyethylene Resins

Resin	Density at 23°C	Reference
A	0.915 g/cc	2
B	0.915*	7
	0.925*	
C	0.96	1
D	0.96	3

* Results based on data for two resins; see text.

and 100°C are used for all resins as convenient standard pressure and temperature. The term "amorphous field" is used to designate the families of curves for the amorphous phase; the reliability of the data and concepts involved appears sufficient to justify extending these curves through the ranges from 0 to 200°C and from 0 to 1000 atmospheres. Similarly, "crystalline field" designates curves for the crystalline phase extending through ranges from 0 to 110°C and 0 to 1000 atmospheres. Narrow lines are used to differentiate curves for these fields from curves for the semicrystalline resins. Curves for the effects of compression on the melting points of resins A and D are included in *Figure 2*; the location of such curves varies with the degree of chain branching.

Because only a few data are available on semi-crystalline resins, only limited tests of the accuracy of the diagrams have been feasible. When plotted on an enthalpy-volume diagram (not included), data for resin A—on which volumetric data were not published—imply a volume-temperature relation intermediate between the relations (8) for two resins with 23°C densities of 0.914 and 0.923 g/cc; the degree of consistency implies that uncertainties in the diagram are equivalent to volumetric uncertainties less than 0.005 cc/g.

In addition, careful inspection of *Figure 3* shows that the data for resin B are consistent with the isothermal tie lines implied between the amorphous and crystalline fields to within 0.01 cc/g, or 5 cal/g, or 5°C. However, study of the original report (7) indicates that the results plotted in *Figure 3* were obtained by combining volumetric data on a resin having 23°C density near 0.915 g/cc with enthalpy data on a resin having 23°C density near 0.925 g/cc. (The importance of small density differences was not then appreciated.) Because original data are lacking, correction for this difference in resins is not feasible. Since the directions of the discrepancies above are consistent with the difference in resins, portions of the discrepancies can be attributed to inadequacy in the semicrystalline data rather than to fundamental uncertainty in the diagram. Nevertheless, these uncertainties of 0.01 cc/g, or 5 cal/g, or 5°C appear to be conservative but reasonable guides to the use of the diagrams. If greater accuracy is needed, the diagrams should be used only for first approximations.

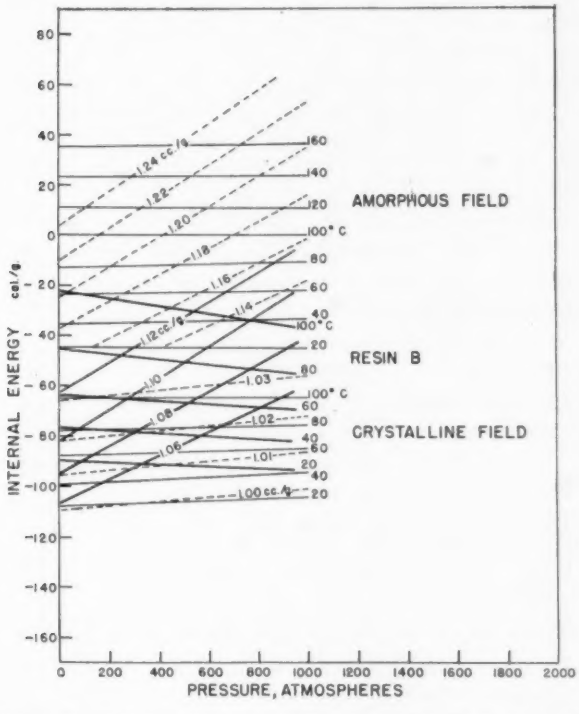

Figure 3. Enthalpy and internal energy diagrams. Data for resin B are consistent with the isothermal tie lines implied between the amorphous and crystalline fields to within 0.01 cc/g or 5 cal/g, or 5°C

Discussion

The diagrams summarize many physical properties succinctly. The slopes of the curves in *Figure 1* represent specific heats at constant pressure; a corresponding T-U diagram would show specific heats at constant volume. Compressibilities and thermal expansion coefficients can be computed from the volumetric data. Through equation 1, 2, or 3 such calculations can be made for resins that have not been synthesized, for example, for a resin with X = 0.6 at 50°C and 1 atmosphere. Conversely, as illustrated below, the diagrams can be used to follow changes in crystallinity from volumetric or thermal data.

The diagrams can obviously be used to compute heat effects and changes in temperature, pressure, volume, and crystallinity in a variety of processes. These include melting, cooling, molding, compression, and expansion under wide ranges of conditions.

Examples of particular interest are shown in *Figures 4 and 5*. *Figure 4* assumes that a mold is filled with melted resin B at 500 atmospheres and 160°C and then cooled at constant pressure. As heat is removed, the point representing the condition of the resin moves downward along the 500 atmosphere isobar. Since the process is isobaric, the decrease in enthalpy equals the heat removed. When the melting line for this resin is reached at B, a crystalline phase represented by A begins to appear and the moving resin point changes direction to move along the tie line.

If the resin behaved as a single-component system, the phase rule would require the resin point to continue along the tie line to A where the resin would be completely crystalline, but because of polymer complexity the point drops downward along the curved line, dashed in part to show where its location is not certain.

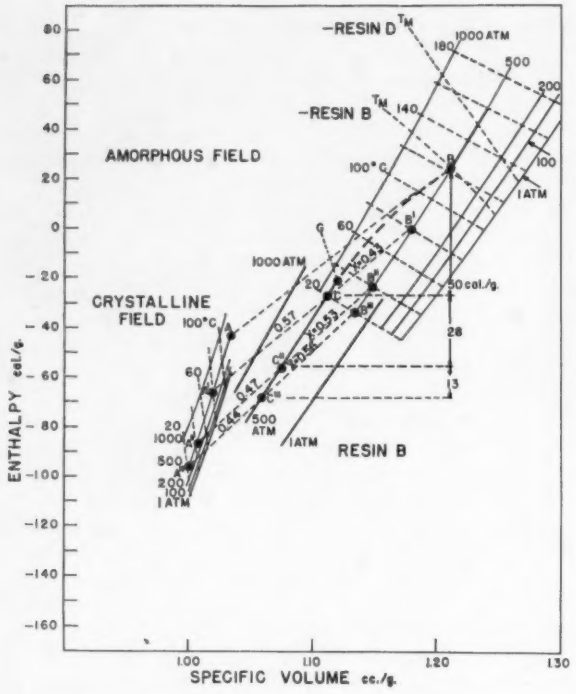

Figure 4. Diagram for following trends in crystallinity

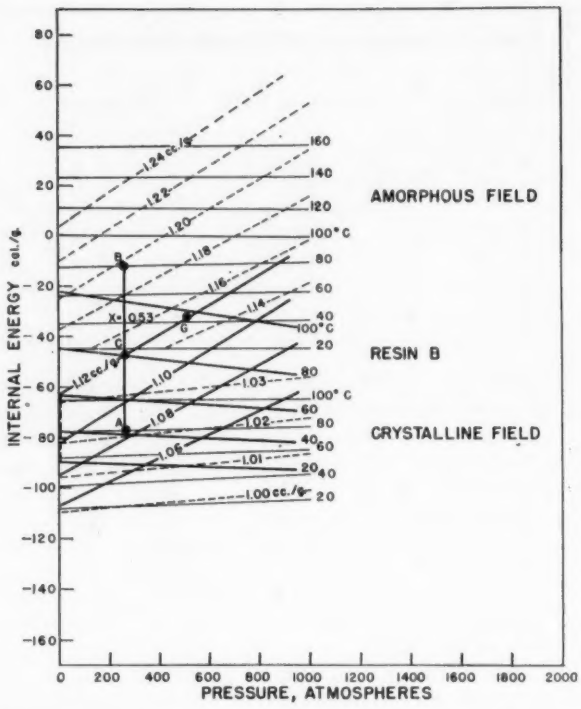

Figure 5. Internal energy as a function of pressure. Degree of crystallinity can be computed through the tie lines

As cooling continues, degree of crystallinity increases. This can be computed at any point through equations 1 or 2 or through the equivalent graphical rule that X equals the ratio of a tie-line segment, such as C'B', to the complete tie line, such as A'B'. Thus, the diagram provides means for following trends in crystallinity.

However, if the material in the mold entrance becomes rigid enough—for example, at G—the material within the mold can no longer be kept at constant pressure. Cooling then takes place at constant volume and the V-H diagram is no longer helpful. The process can be followed on the diagram in *Figure* 5 for internal energy as a function of pressure. At G in both diagrams, resin conditions are identical. As heat is removed, the point representing the resin moves downward along the isochore or line of constant volume. Since the process is isochoric, the decrease in internal energy equals the heat removed. As in the V-H diagram, degree of crystallinity can be computed through the tie lines. The example has been selected so that the resin reaches zero pressure at 60°C. Normal cooling cannot continue beyond this point; the resin must develop abnormal crystallinity, or negative pressure, or voids, probably the latter. Thus, the diagram indicates regions in which abnormal behavior can be expected.

These examples demonstate that the heat of fusion is usually large relative to other effects in melting or freezing polyethylene. Thus, supply or removal of this heat is of major importance in fabricating polyethylene.

Conclusions

A series of assumptions has been used to develop three diagrams showing relations among pressure, volume, temperature, and enthalpy or internal energy for polyethylene resins at temperatures from 0 to 200°C and at pressures from 0 to 1,000 atmospheres. The diagrams can be used to compute crystallinity, specific heat, and other important characteristics and to follow changes in these characteristics as the resins are heated or cooled. Accuracy appears sufficient for most engineering purposes. Effective estimates can be made for resins that have *not been synthesized*. The heat of fusion proves to be large relative to other heat effects in melting or freezing and, thus, is of major importance in many processes for fabricating polyethylene.

Literature References

1. Wunderlich, B., and Dole, M., *J. Polymer Sci.*, *24*, 201 (1957)
2. Dole, M., Hettinger, W. P., Jr., Larson, N. R., and Wethington, J. A., Jr., *J. Chem. Phys.*, *20*, 781 (1952)
3. Lupton, J. M., 134th Meeting, American Chemical Society, Chicago, Illinois, September 1958
4. Bunn, C. W., and Alcock, T. C., *Trans. Faraday Soc.*, *41*, 317 (1945)
5. Muller, A., *Proc. Roy. Soc.* London, Series A, *178*, 227 (1941)
6. Billmeyer, F. W., Jr., *J. Appl. Phys.*, 28, 1114 (1957)
7. Parks, W., and Richards, R. B., *Trans. Faraday Soc.*, *45*, 203 (1949)
8. Muus, L. T., unpublished

The Strength of Glassy Polymers

J. P. Berry

General Electric Research Laboratory, Schenectady, New York

In determining the strength of polymers, the secondary forces that determine viscous flow properties may be of greater importance than the intramolecular bonds. The actual strength which is proportional to the specific surface energy and inversely proportional to the effective flaw size, is much less than expected from theoretical considerations, because of the flaws which act as stress concentrators. The size of flaw appears to be related to polymer craze

The strength of all materials is much less than would be expected from a consideration of the molecular structure. This discrepancy generally arises because all samples tested contain flaws or defects which act as stress concentrators, and which thereby initiate the fracture process. The theoretical treatment of the problem, given by Griffith, (*1*) relates the tensile strength of the material (T), to the length of the defect (c), viz.

$$T = \left(\frac{2E\gamma}{\pi c}\right)^{1/2}$$

where E is the elastic modulus, and γ is the specific surface energy, defined as the amount of energy required to form unit area of fracture surface.

The tensile properties of the glassy polymers, poly (methyl methacrylate) and polystyrene have been investigated in relation to this theory, and the results indicate the importance of two factors in determining the strength of these polymers. The factors are: The specific surface energy and the effective flaw size. It is believed that a viscous flow process which occurs during fracture makes the largest contribution to the surface energy, but the factors which govern the size of the effective flaw in the polymer are, at present, not well defined.

Experimental Materials and Methods

The experimental materials were poly(methyl methacrylate) (Plexiglas II UVA) and a general purpose polystyrene. The viscosity average molecular weights were 3×10^6, and 3.5×10^5 respectively. To eliminate the effect of orientation or other inhomogeneities in the materials, the blanks from which the samples were made were selected at random over the sheets of polymer, taking an equal number in the transverse and longitudinal directions.

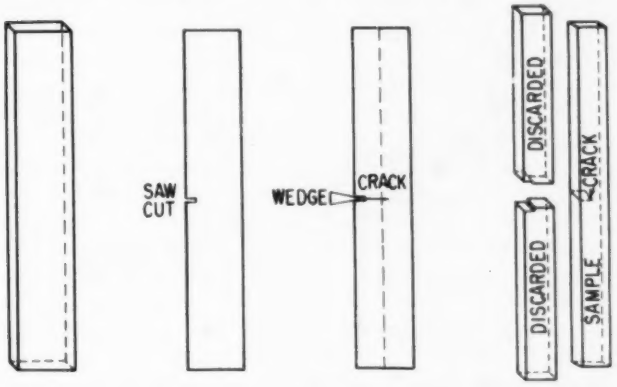

Figure 1. Method of preparation of tensile samples. The tip of the natural crack produced by driving the wedge into the sawcut is retained as the flaw in the sample used for testing.

As noted above, the Griffith treatment of tensile strength assumes that all samples tested contain defects. To assess the validity of the final equation, it was necessary to determine the tensile strength of polymer samples containing cracks of known size. To justify extrapolation of the results to conventional samples, it was clearly desirable that the defects which were introduced deliberately should, as far as possible, possess the same characteristics as those which would be expected to occur naturally. The technique which was devised to achieve this is illustrated in *Figure 1*. A fine sawcut was made in the edge of a strip of polymer. A wedge, driven

BEST OF ANTEC!

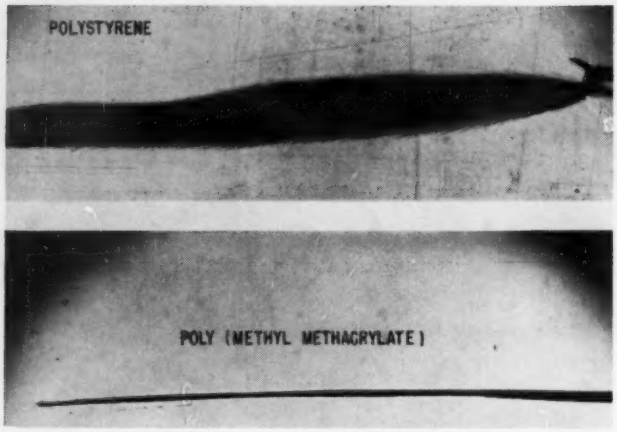

Figure 2. Comparison of crack morphology in poly(methyl methacrylate) and polystyrene samples. In the former polymer a crack consists of a simple single fissure, whereas, in polystyrene, many fine subsidiary cracks grow alongside the main crack.

into the sawcut, caused a natural crack to run across the sample, which was then cut down the midline and machined to confer a dumbbell shape. The length of the crack was determined by the final operations, and with care, samples were obtained containing cracks of sizes down to a lower limit of ~ 0.002".

The crack produced by this technique in poly(methyl methacrylate) samples was a simple single fissure. The behavior of polystyrene was more complex. When the wedge was driven into the sawcut in this polymer numerous fine secondary cracks were formed alongside the main crack. The difference in behavior of the two polymers is illustrated in *Figure 2*. Because of the complex nature of the crack in polystyrene it was somewhat more difficult to define its length, but this was taken as the distance of greatest penetration, whether by a primary or a secondary crack.

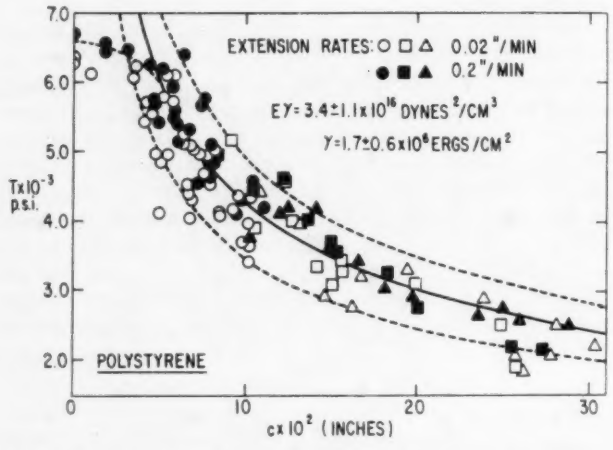

Figure 3. The dependence of tensile strength on crack size in poly(methyl methacrylate) samples under different experimental conditions: Extension rates; open symbols 0.5%/min, closed symbols 5.0%/min. Sample cross section; circles 0.42" x 0.19" squares 0.42" x 0.063", triangles 0.98 x 0.19", diamonds 0.98" x 0.063".

The length of the crack was determined by direct observation with a travelling microscope, suitably calibrated, measurements being made through both faces of the sample. The tensile strength of the samples was measured with a conventional tensile tester, the value of the ultimate stress being calculated from the area of cross-section at the fracture plane.

Surface Energy Calculations

The results of the tensile strength measurements on the two polymers studied are summarized in *Figures 3* and *4*. Included in these figures are the results of experiments at different strain rates, which gave experimental times varying by a factor of ten, and of experiments on samples of different dimensions. These variations were introduced to establish that the results were not strongly dependent on the experimental details. In both figures, the solid line is the theoretical inverse square root relation predicted by the Griffith theory. The value of the adjustable parameter $E\gamma$ was selected to give the best fit of the theoretical line to the data. Because of the considerable scatter in the results, it is not possible to define the value of $E\gamma$ with greater precision than is indicated by the broken lines. Even so, there is ample justification for assuming that the results can be represented by a relation of the form given by the Griffith theory. Taking the value of Young's modulus from the stress-strain curves, and assuming the value of $E\gamma$ based on the tensile strength data, the surface energy for the polymers can be obtained. It has the value of $3.0 \pm 0.8 \times 10^5$ ergs/cm² for poly(methyl methacrylate), and $1.7 \pm 0.6 \times 10^6$ ergs/cm² for polystyrene. These values agree quite well with those obtained by Benbow and Roesler (2) from experiments in cleavage, which involves a distinctly different mechanical system. Though the figures quoted are defined as the surface energies in terms of the Griffith theory, they are essentially adjustable constants obtained by a curve-fitting procedure. To assess the significance of the values quoted, it is of interest to compare them to values which are estimated from the

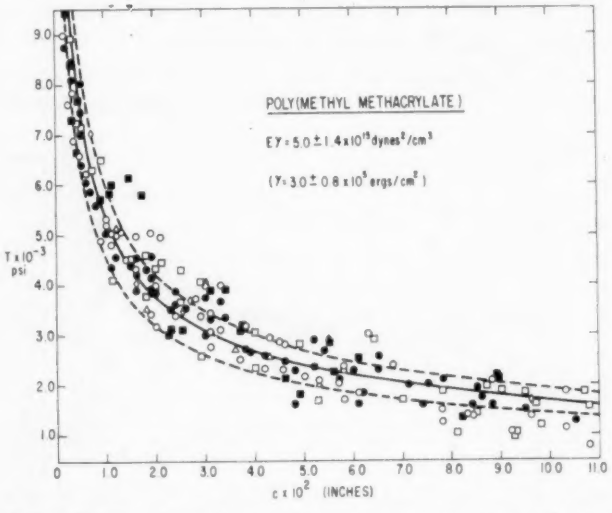

Figure 4. The dependence of tensile strength on crack size in polystyrene samples under different experimental conditions: Cross sections; circles 0.42" x 0.2", squares 0.98" x 0.2", triangles 1.42" x 0.2".

molecular structure of the materials. By definition, the surface energy is that required to form unit area of surface by separating two planes of atoms in the material. To simplify the calculation, the drastic assumption is made that the polymer molecules which pass through the reference plane are oriented normally to it, and are as closely packed as possible. Thus the maximum number of the strongest (chemical) bonds will be ruptured in separating the planes, and the value of the surface energy obtained should therefore represent the theoretical maximum. The value calculated in this way is ~ 500 ergs/cm^2, which is very much less than that determined experimentally. Some insight into this apparent anomaly is gained by a consideration of the experimental values of the surface energy of glass and steel. The observed surface energy of steel is ~ 10^6 ergs/cm^2, which is again several orders of magnitude greater than the theoretical value (3). The observed surface energy of glass is ~ 500 ergs/cm^2, (1) which, if anything is somewhat less than the theoretical value. It is well established that in the fracture of steel a considerable amount of energy is dissipated in a plastic work process which occurs in the vicinity of the fracture plane. X-ray diffraction studies of the fracture surface confirm this hypothesis, and provide an independent estimate of the amount of energy consumed in the plastic work process, which agrees quite well with the observed discrepancy in the surface energy values (3). There is no evidence for the occurrence of such a phenomenon when glass is fractured. These factors raise the possibility that the discrepancy between the experimental and calculated surface energies of the polymers studied is due to an analogous viscous flow process. Evidence for such a process is found in the color effects which are observed on the fracture surfaces of poly(methyl methacrylate) (4, 5, 6).

Optical Examination of Fractures

When examined by reflected light, the surface displays bands of color which are associated with specific areas of the surface, bounded by lines where the level sharply changes. There is a correspondingly abrupt change in the color at these boundaries, and within the areas so defined there is usually a more gradual transition in the direction of crack propagation (*Figure* 5). The colors also change, in regular order, as the angle of incidence of the light is changed, which indicates that the effect is due to optical interference at the fracture surface. A mechanism by which this could arise is illustrated in *Figure 6*. Because of the tensile stress applied to the sample, the material immediately ahead of the crack will be subjected to a relatively much higher tensile stress, normal to the plane of the crack. Under the influence of this stress the polymer molecules will tend to orient themselves in the direction of the stress. The region of orientation will be maintained ahead of the crack as it advances through the sample, and if it persists after the crack front has passed, the fracture surface will be covered by a region in which the polymer molecules are oriented normally to the surface. The refractive index of this layer will be different from that of the bulk material, and if the thickness is of the order of the wave-length of visible light, the colors observed can be accounted for. The orientation hypothesis is supported

Figure 5. Fracture surfaces of a poly(methyl methacrylate) tensile sample. The light and dark areas are of different colors in the original.

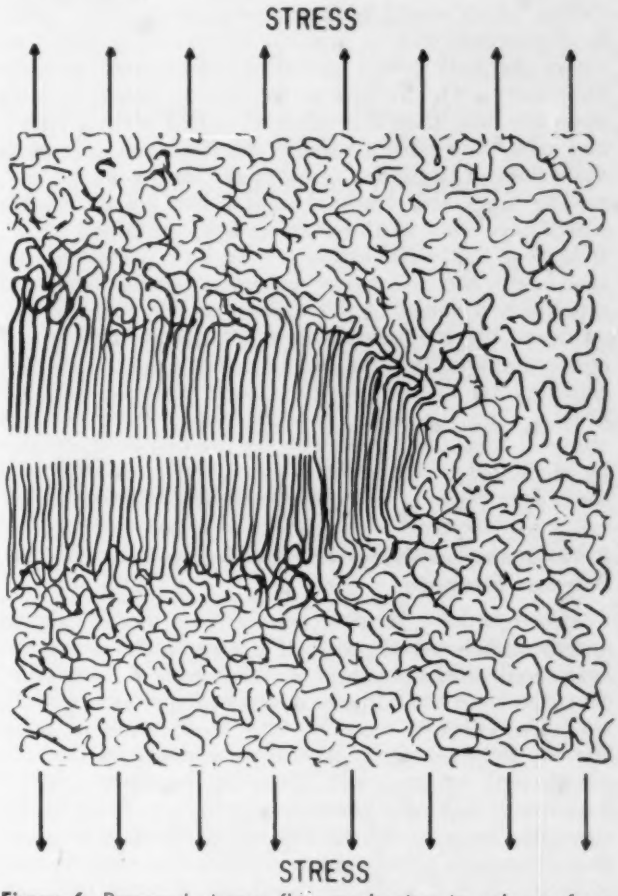

Figure 6. Proposed viscous flow mechanism in polymer fracture. The local tensile stress has a maximum value in the vicinity of the crack tip, and under its influence the molecules adopt an extended configuration.

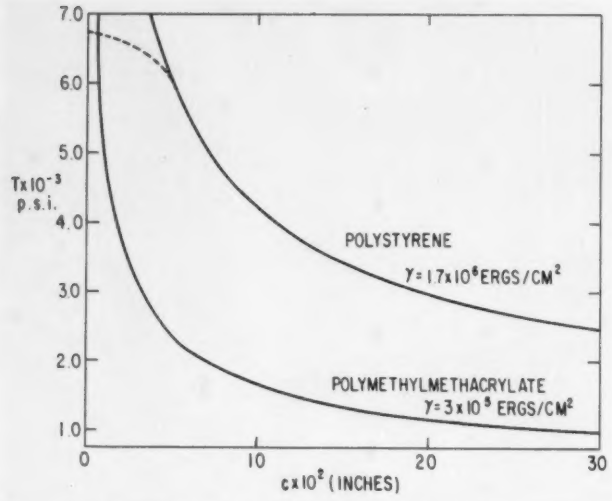

Figure 7. Comparison of the dependence of tensile strength on crack size in polystyrene and poly(methyl methacrylate) samples. Because of its greater surface energy polystyrene is intrinsically the stronger material, but the large inherent flaw size severely limits the tensile strength of conventional samples.

by the fact that the colors disappear under those conditions which would be expected to disrupt the postulated structure, such as exposure to solvents or heat. The colors also fade over a period of a few weeks at room temperature. The fracture surface of polystyrene is much more irregular than that of poly(methyl methacrylate), and such color effects, even if present, would be much more difficult to detect. Occasionally, however, flat mirror-like areas are produced, and colors are discernible which have some of the characteristics described above. It is clear that a mechanism of the type postulated can account for the discrepancy between the calculated and experimental values of the surface energy, since in carrying out the computation no account was taken of the energy required to bring the molecules from the random configuration to that in which, it is assumed, they are broken. The difference between the surface energies obtained from the experiments on the two polymers can be attributed to the greater interaction associated with the bulkier phenyl side-groups in the polystyrene.

Relationship of Effective Flaw Size to Polymer Strength

Although the agreement between the theoretical line and the experimental points of *Figures 1* and *2* may be considered satisfactory over a wide range of crack sizes, deviation from the agreement occurs for cracks of small size. The effect is more obvious in the case of polystyrene. Because of the inverse dependence of the tensile strength on crack size, given by the theory, such a deviation is inevitable for real samples with finite tensile strengths, since in the Griffith approach it is assumed that all samples tested contain defects. The effective size of such a defect, so far as the theory is concerned, can be calculated from the tensile strength of a conventional (uncracked) sample, using the established value of $E\gamma$ from the experimental results. For poly(methyl methacrylate) this is ~ 0.002", and for polystyrene it is ~ 0.043". It is evident, in carrying out the tensile experiments, that the difference in these values is due to the greater tendency of the polystyrene to craze, i.e., to develop cracks spontaneously under stress. In poly(methyl methacrylate) samples, fracture always occurred at the inserted crack, no matter how small, and very little crazing was detected. In samples of polystyrene, on the other hand, if the inserted crack was less than about 0.070" in size, a considerable amount of crazing was observed, and the samples frequently fractured at some point other than at the inserted crack.

It is interesting to compare the theoretical curves obtained with the two polymers studied (*Figure 7*). Because of the higher value of $E\gamma$, the curve for polystyrene lies above that for poly(methyl methacrylate), indicating that it is intrinsically the stronger material. However, because of its larger effective flaw size, deviation from the theoretical relation occurs at a larger value of crack size, and hence for a normal sample, i.e., one which does not contain an artificial crack, the tensile strength of polystyrene is much lower than that of poly(methyl methacrylate).

According to the Griffith equation, the tensile strength is related directly to the surface energy, and inversely to the (effective) flaw size. Thus high strength demands a large surface energy and/or a small effective flaw size. In the polymers studied the largest contribution to the surface energy is the energy dissipated in a viscous flow process, and that consumed in breaking the chemical bonds is negligible. In this respect they resemble metals rather than inorganic glasses. From this interpretation, it may be concluded that in consideration of the strength of polymers, the intermolecular (secondary) forces which determine the viscous flow properties are probably of greater importance than the intramolecular (chemical) bonds. Furthermore, the surface energy, and through it the strength, should be related to the visco-elastic properties as measured by the conventional creep and stress relaxation techniques. The size of the effective flaw appears to be related to the tendency of the polymer to craze, but the factors which govern this phenomenon are little understood.

Literature References

1. Griffith, A. A., Phil. Trans. Roy. Soc. A *221*, 163 (1921).
2. Benbow, J. J., and Roesler, F. C. Proc. Phys. Soc. *70B*, 201 (1947).
3. Felbeck, D. K. and Orowan, E., Welding J. Res. Suppl. *34*, 510-s (1955).
4. Higuchi, M., Rep. Res. Inst. Appl. Mech. (Japan) *6*, 173 (1958).
5. Wolock, I., Kies, J. A., and Newman, S. B., *Fracture*, John Wiley and Sons, New York (1959), p. 250.
6. Berry, J. P., Nature *185*, 91 (1960).

Acknowledgment

The author is indebted to Mr. Paul J. Krusic for his assistance in carrying out much of the experimental work and to Dr. A. M. Bueche for numerous stimulating discussions during the course of the investigation.

Flow Patterns In A Non-Newtonian Fluid In A Single-Screw Extruder

W. D. Mohr, J. B. Clapp, and F. C. Starr

Polychemicals Department,
E. I. du Pont de Nemours & Co., Inc.
Du Pont Experimental Station,
Wilmington, Delaware

Experimental observations on flow patterns of non-Newtonian fluids indicate that the flow patterns resemble those of Newtonian fluids The use of equations based on simplified extrusion theory is therefore supported.

The screw extrusion process is employed to develop pressure in thermoplastic polymer melts, some of which exhibit marked non-Newtonian behavior under usual operating conditions. Polyethylene is one example of a polymer melt which is non-Newtonian, that is to say, the shear rate and shear stress are not related by a single constant of proportionality over a range of conditions.

A previous study of flow patterns in a model extruder (3) was confined to observations of Newtonian flow behavior. A simplified theoretical analysis of the velocity distribution in a screw channel with a Newtonian fluid was presented, and the experimental observations were found to be in agreement with predictions from the theoretical analysis. No analysis or results for a non-Newtonian fluid were presented.

It is the purpose of this paper to expand upon the earlier work by presenting experimental observations on the flow behavior of a non-Newtonian fluid in an extruder channel. Photographs of flow patterns in a non-Newtonian fluid in a transparent barrel extruder are presented. Measurements of velocities of flow streamlines with Newtonian and with non-Newtonian fluids in the screw channel are presented and compared. This work was undertaken to determine the magnitude of the deviations from the velocity profiles predicted from Newtonian theory which result from non-Newtonianism of the fluid.

Theoretical Considerations

The expressions describing the distribution of velocities in an extruder screw channel have been presented previously (1, 2).

If

v = Velocity in the down-channel direction
U = Velocity of the inside barrel surface (π DN)
ϕ = Screw helix angle.

H = Distance from screw surface to position in channel as a fraction of the channel depth (reduced channel depth)

s = Velocity in the transverse-channel direction

$\underline{a}$ = Dimensionless pressure gradient parameter

$$\frac{h^2 \frac{dP}{dz}}{6 U \mu \cos \phi}$$

m = Speed of fluid

α = Angle of fluid motion relative to a plane perpendicular to the screw axis.

The velocity profile in the direction of the channel is then given by the equation

$$v = U \cos \phi \, [H - 3\underline{a} \, (H - H^2)] \qquad (1)$$

The equation for the velocity profile in the transverse channel direction, assuming no leakage over the flight, is

$$s = U \sin \phi \, [3 H^2 - 2H] \qquad (2)$$

The speed of the fluid is given by the vector sum of the two velocity components

$$m = \sqrt{v^2 + s^2} \qquad (3)$$

$$= \sqrt{\{U \cos \phi[H - 3\underline{a}(H - H^2)]\}^2 + \{U \sin \phi(3H^2 - 2H)\}^2}$$

The angle of fluid motion is given by the relation

$$\tan \alpha = \frac{v \sin \phi - s \cos \phi}{\sqrt{v \cos \phi + s \sin \phi}} \qquad (4)$$

$$= \frac{\cos \phi[H - 3\underline{a}(H - H^2)] \sin \phi - \sin \phi(3H^2 - 2H) \cos \phi}{\sqrt{\cos^2 \phi[H - 3\underline{a}(H - H^2)] + \sin^2 \phi \, (3H^2 - 2H)}}$$

The above expressions were derived using the following simplifying assumptions: 1. The bounding surfaces, screw and barrel, are plane surfaces; 2. The fluid has constant viscosity at all points in the channel (isothermal, Newtonian flow); 3. The channel is very wide and long relative to its depth; 4. There is no leakage flow over the screw flight; 5. The barrel moves relative to the stationary screw.

In the previous study with a Newtonian fluid (3), the observed flow distribution closely resembled the flow distribution predicted from the theoretical analysis, even though assumptions 1, 3, and 4, above, were not strictly fulfilled.

No adequate theory exists, even in simplified form, to describe the extrusion of a non-Newtonian fluid. The coupled action of down- and transverse-channel shear stresses in determining the viscosity at each point in the fluid makes a closed mathematical description of the flow seemingly impossible, even for an isothermal fluid.

As the degree of non-Newtonianism of the fluid decreases, the flow of fluid in the screw channel would be more closely described by equations developed for a Newtonian fluid. In any event, the effect of geometric variables (ϕ, N, h, D) should be approximately the same for any fluid with zero average axial pressure gradient.

For a Newtonian fluid, the output flow equation, neglecting flight edge effects and leakage flow, has been given by Squires (4) as

$$q = q_d - q_p = \frac{n\pi DNh(t/n - e) \cos^2 \phi}{2} - \frac{nh^3(t/n - e) \sin \phi \cos \phi}{12\mu} \frac{dP}{dl} \qquad (5)$$

where q = Volumetric flow rate from the extruder

q_d = Drag flow rate (flow with zero average axial pressure gradient)

q_p = Pressure flow

n = Number of flights

D = Diameter of screw

N = Rotational speed of screw

h = Channel depth of screw

t = Lead of screw

e = Axial flight width

μ = Fluid viscosity

P = Pressure

l = Distance along screw axis

From the previous definition of $\underline{a}$, the above equation can be rearranged.

$$q = q_d \, (1 - \underline{a}) = q_d - q_d \underline{a} = q_d - q_p \qquad (6)$$

Therefore, $$\underline{a} = \frac{q_p}{q_d} = \frac{\text{Pressure flow rate}}{\text{Drag flow rate}} \qquad (7)$$

From measurements, the parameter $\underline{a}$ may be defined as

$$\underline{a} = 1 - q/q_d \qquad (8)$$

where q is the measured volumetric flow rate and

$$q_d = \frac{n\pi DNL \, (t/n - e) \cos^2 \phi}{2} \qquad (9)$$

In the subsequent discussion of the results of observations of both Newtonian and non-Newtonian fluids in screw channels, the parameter $\underline{a}$ is computed from the expression

$$\underline{a} = 1 - q/q_d \qquad (8)$$

and is somewhat loosely spoken of as the ratio of pressure:drag flow. Irrespective of the verbal accuracy involved, the parameter a, as calculated above, uniquely describes the flow profile in the screw channel.

Equipment

A model extruder with a transparent barrel rotating about a stationary screw was used in this investigation. The screw had a diameter of 3.5 in., a lead of 3.5 in., and a length of 23.4 in. The width of the flight in the axial direction was 0.4 in., and the channel depth was 0.625 in. The barrel was 17.0 in. long, enabling the screw to protrude from the ends of the barrel into chambers of relatively large cross-sectional area in order to minimize entrance and exit effects. The fluid entered the inlet chamber through a 1½ in. nipple from a feed vessel, and left the discharge chamber through 6 inches of 1½ in. pipe. The rotational speed of the barrel could

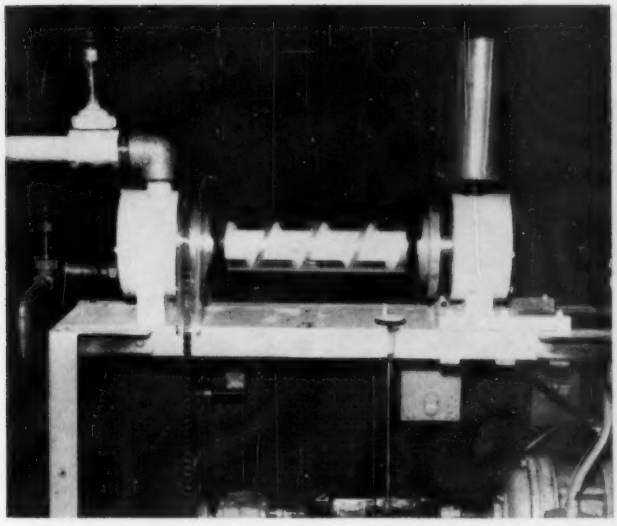

Figure 1. Model extruder with transparent barrel

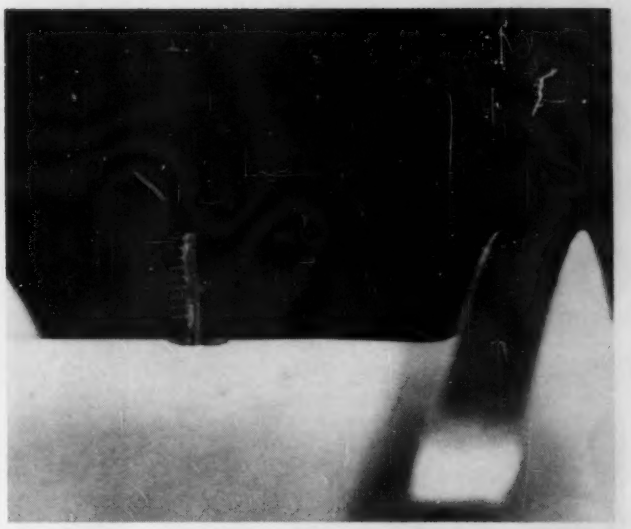

Figure 2. Side view of probe mounted in screw channel

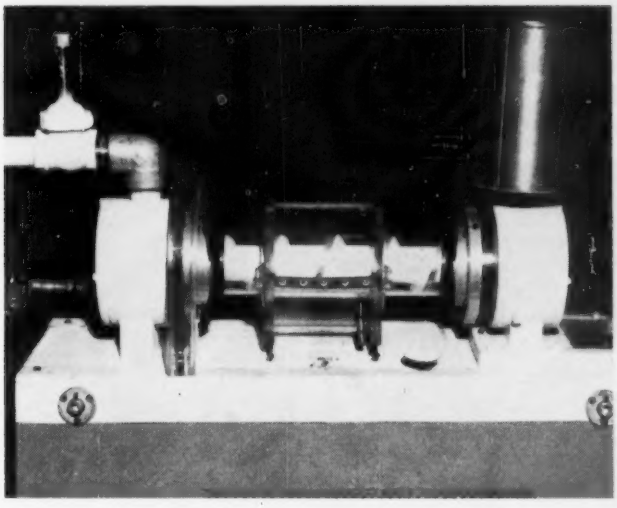

Figure 3. Extruder with transparent chamber in place

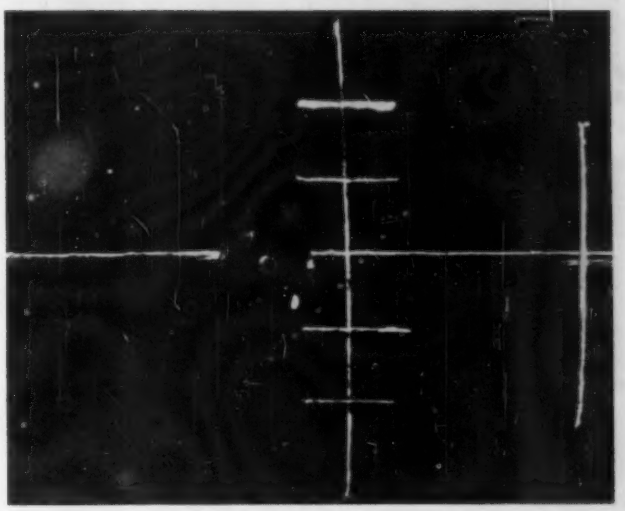

Figure 4. View of channel showing down channel motion of particles. Taken with camera 1

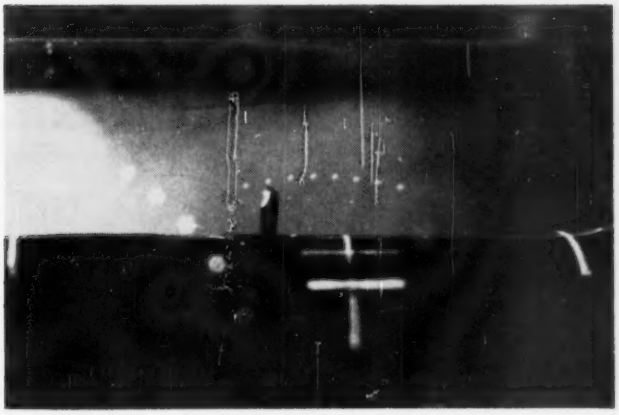

Figure 5. Cross-sectional view of channel showing particle depth. Taken with camera 2

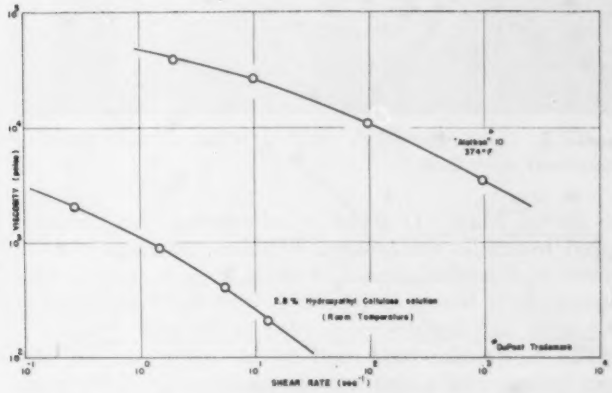

Figure 6. Viscosity as a function of shear rate for two non-Newtonian fluids. Data obtained with a cone and plate viscosimeter

Photographs of flow streams in an extruder channel (non-Newtonian fluid)

Angular spread of pattern increases as the ratio of pressure flow to drag flow is increased

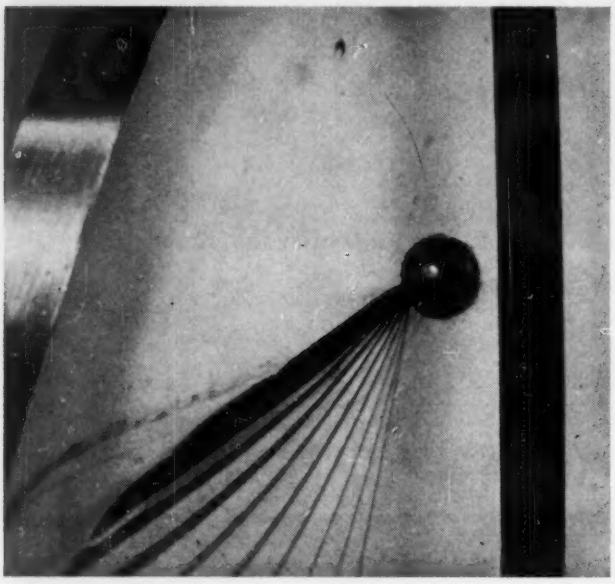

Figure 7. Ratio of Pressure to Drag Flow pressure gradient parameter $a = 0.20$

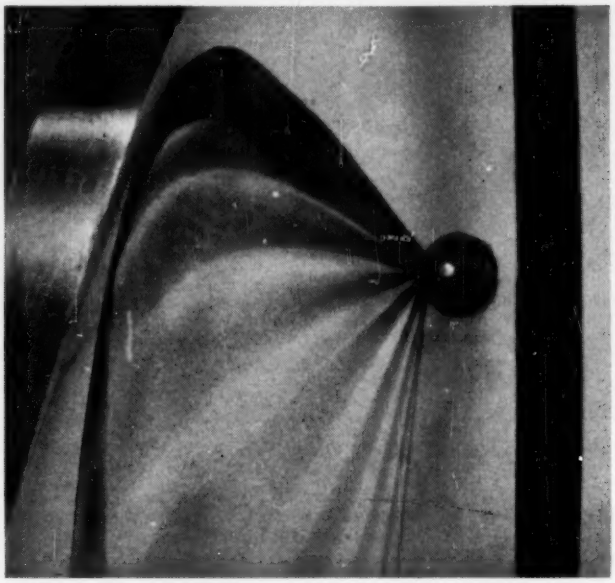

Figure 8. Ratio of Pressure to Drag Flow pressure gradient parameter $a = 0.42$

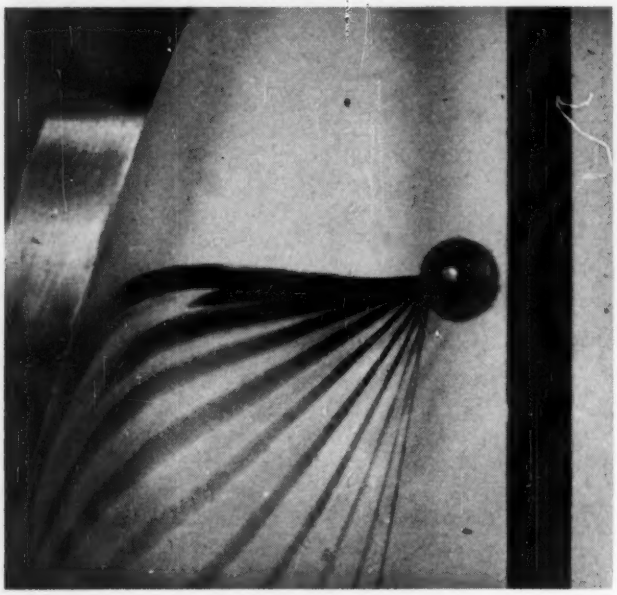

Figure 9. Ratio of Pressure to Drag Flow pressure gradient parameter $a = 0.64$

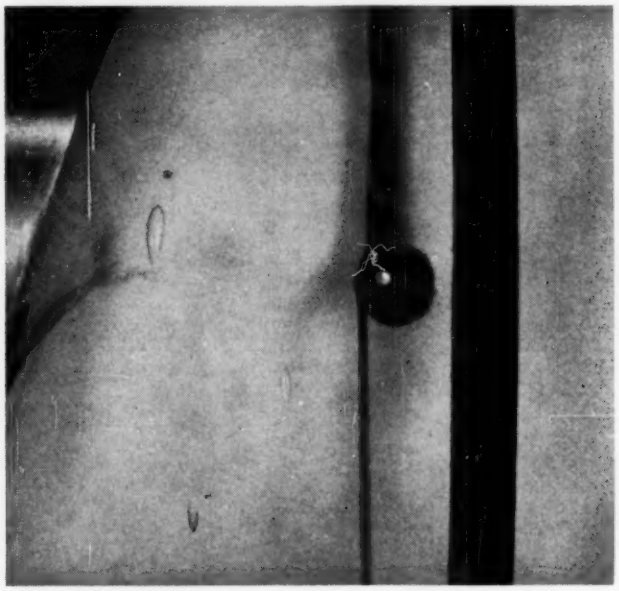

Figure 10. Ratio of Pressure to Drag Flow pressure gradient parameter $a = 1.00$

be altered from 0-10 RPM by adjustment of a variable-speed hydraulic transmission between the electric drive motor and a chain-sprocket drive to the barrel. This equipment is shown in *Figure 1*, with the feed vessel at the right, and the discharge pipe at the left.

The Newtonian fluid used in this study was 43° Be. corn syrup, with a viscosity of approximately 1500 poise at room temperature. The non-Newtonian fluid used was a 2.8% solution of hydroxyethyl cellulose in water. *Figure 6* shows the viscosity-shear rate relationship for this fluid. The data were obtained with a cone-and-plate viscometer.

The volumetric flow rate of the extruder was measured by means of a graduated cylinder and a stopwatch. A number of pipe caps, through which holes of various sizes had been drilled, were available to be placed on the discharge pipe to provide the different fixed output restrictions. The rotational speed of the barrel was measured by timing the rotation through a given number of revolutions.

Non-Newtonian Flow Patterns

For the purpose of displaying flow patterns in the channel, a special probe was fabricated of hypodermic tubing and installed in the center of the screw channel, *Figure 2*. The probe extended perpendicularly from the screw surface to within 1/32 in. of the barrel. Eleven small tubes, evenly spaced from screw surface to barrel, extended from the body of the probe, the top of which was closed. The inlet end of the probe was connected to a syringe by hypodermic tubing passing through the hollow core of the screw. In this way, streams of colored fluid could be injected at eleven different depths into the screw channel.

For the photographs of the flow patterns in the screw channel, *Figures 7 through 10*, the barrel was rotated at 2.3 RPM while black fluid was injected into the channel through the probe. This black fluid consisted of a dispersion of black India ink in some of the hydroxyethyl cellulose solution. The photographs were taken with the axis of the body of the probe pointing at the camera. Flow-pattern photographs were taken only with the non-Newtonian fluid during this phase of the study.

In *Figures 7 through 10*, the screw flight is seen in the upper left and lower right hand corners of the photographs. The black stripe just to the right of the probe was a circumferential line drawn on the rotating barrel to give an accurate picture of the line of barrel motion, which was from top to bottom in these pictures. The screw axis appears horizontal in this view, and the discharge end of the extruder is to the left of the pictures. The black fluid injected through the probe into the clear bulk fluid appears as a dark, fan-shaped pattern against the light background of the screw surface. The stream moving in the direction nearest that of the barrel is from the tube on the probe nearest the barrel, and the streams at progressively higher angles are from tubes progressively toward the root of the screw. The angular spread of the pattern increases as the ratio of pressure flow to drag flow is increased from 0.20 to 1.0 in *Figures 7 through 10*, respectively. A comparison between these photographs and those presented in the earlier paper on flow patterns in an extruder channel (3) shows the flow distribution for the Newtonian and the non-Newtonian fluids to be qualitatively the same. That is, in both cases, for all degrees of pressure flow ($a = 0$ to 1.0), the angle of motion of the fluid measured from a plane perpendicular to the screw axis is always in the range 0°-180°. A component of fluid velocity is thus in the direction of the output end of the extruder at all depths in the channel, irrespective of whether the fluid is Newtonian or non-Newtonian, when any output is permitted from the extruder. For the condition of zero output ($a = 1.0$), the only components of fluid velocity are in a plane perpendicular to the axis of the screw (angle of motion either 0° or 180°), and the axial velocity component is zero at all depths in the channel.

Measurement of Velocity Profiles

The photographs obtained of the flow patterns in a screw channel give an excellent qualitative picture of the flow in the channel. The distortion of flow by the probe made quantitative measurement of velocity profile impossible. In order to obtain the necessary quantitative information of velocity profile, a technique was developed which utilized photographs of tracer particles dispersed in the fluid.

Certain modifications and additions to the equipment described above were necessary to obtain photographs of tracer particles in the fluid. First, the special probe used to inject the black fluid was removed from the root of the screw. Second, the distortion introduced by the curvature of the transparent "Lucite" barrel was reduced by fitting a transparent, box-like chamber around the barrel. The box remained stationary around the rotating barrel, and the space between box and barrel was filled with water. Neoprene seals at the ends between the box and the rotating barrel rendered the chamber watertight. The system is shown in place in *Figure 3*.

Two cameras with optical axes mutually perpendicular were focused on the same spot in the channel. Camera #1 was positioned with optical axis perpendicular to the screw axis so that a view was obtained of fluid in the screw channel looking directly at the screw root. Camera #2 was positioned to give a view of a cross section of fluid in the channel at the point viewed by Camera #1. The optical axes of the cameras were perpendicular to two sides of the transparent water-filled box. Brackets were placed on the apparatus to which the cameras could be properly fixed in the correct position relative to each other and relative to the view desired of the screw channel.

Parallax corrections for each camera were obtained from photographs taken of scales placed in the fluid in the channel. No distortion was evident for the depth in the channel from photographs taken with Camera #2. The effect of parallax on measurements of particle travel taken with Camera #1 was found to be 5% from top

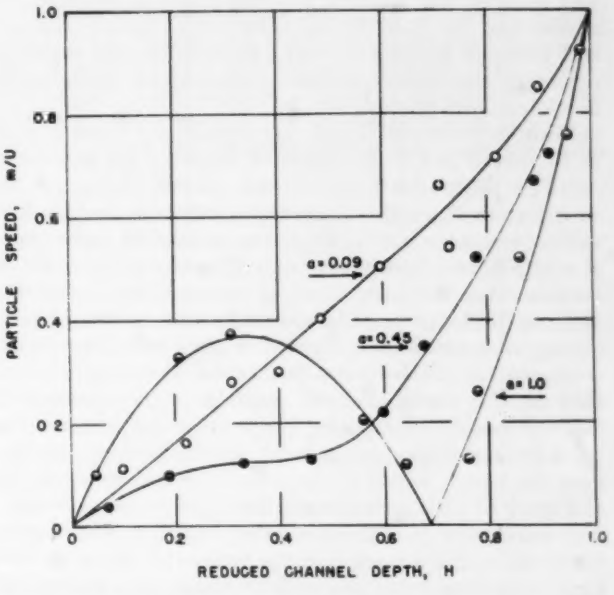

Figure 11. Particle speed as a function of channel depth for three degrees of pressure flow (Newtonian fluid)

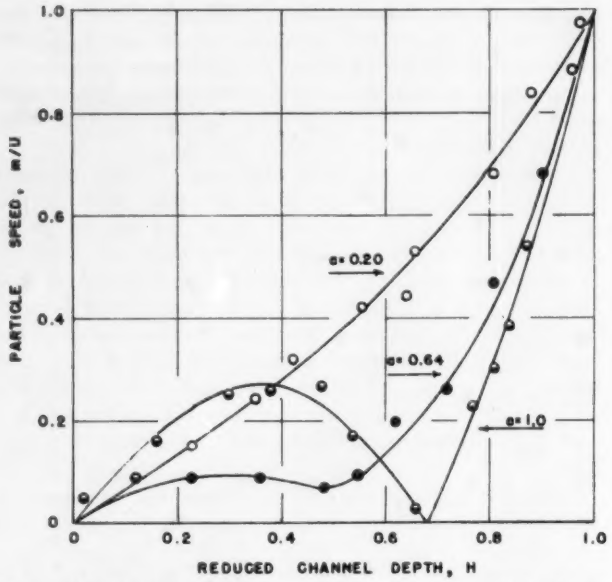

Figure 12. Particle speed as a function of channel depth for three degrees of pressure flow (Newtonian fluid). Note qualitative similiarity to Figure 11

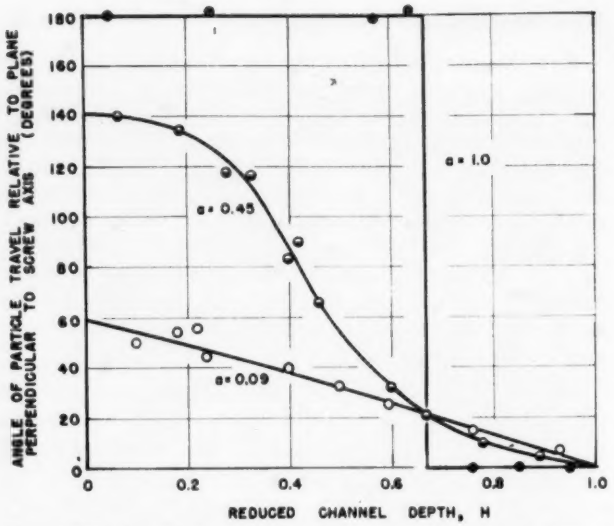

Figure 13. Angle of particle travel as a function of channel depth for three degrees of pressure flow (Newtonian fluid)

to bottom of the channel, and a linear correction was applied based on the depth at which a particle was viewed by Camera #2.

The tracer particles employed in this study were white resin beads of diameter 25-30 mils. The population density of particles in the fluid was adjusted so that several particles were in the useful range of view at all times. The screw surface was painted a flat black, and photographs were taken in a darkened room. Illumination was provided by a single "Strobolux" stroboscopic light which could be actuated at precise intervals of either 1.0 or 0.5 seconds. The duration of a single flash was of the order of 20 μ sec. The procedure employed was to open the shutters of both cameras, operate the strobe unit for 8-10 flashes, close the camera shutters, and advance the film in both cameras. On the resulting negatives the tracer particles appeared as black points in a clear background.

Positive prints of a pair of typical negatives appear in *Figures 4 and 5*. In *Figure 4*, showing the motion of particles down the channel, one particle trace can be seen just to the right of center, another at the far left. In this instance, the strobe unit was flashed eight times at a rate of one flash per second. Therefore, the distance between two adjacent dots in a trace represents the distance that the particle moved in one second. *Figure 5* was taken simultaneously with *Figure 4*, looking at the cross section of the same portion of the channel, and showing the depth of each particle in the channel. It can be seen by comparing these photographs that the particle at the left was moving relatively fast and was near the barrel, which is the faint light line near the top of *Figure 5*. The particle near the right center was moving more slowly, and was much closer to the screw, which is the black portion at the bottom of *Figure 5*. The large white trace that resembles a six-pointed star at the left center of *Figure 5* is an air bubble in the channel. The short piece of hypodermic tubing extending up from the screw in *Figure 5* was not present when data were being taken.

The processed films from both cameras were inserted together into a viewing apparatus, which projected the images on a ground-glass screen. In this way, the particle traces in one view of the channel could be matched to those in the other view, and measurements could be made. In the view of down-channel particle motion *Figure 4*, the distance between a given number of particle traces was measured, as well as the angle of the particle path with a plane perpendicular to the axis of the screw. These measurements were confined to a small area on either side of the horizontal center line of the photograph in order to minimize errors due to the curvature of particle motion around the screw axis. Measurements were made only on particles traveling within the

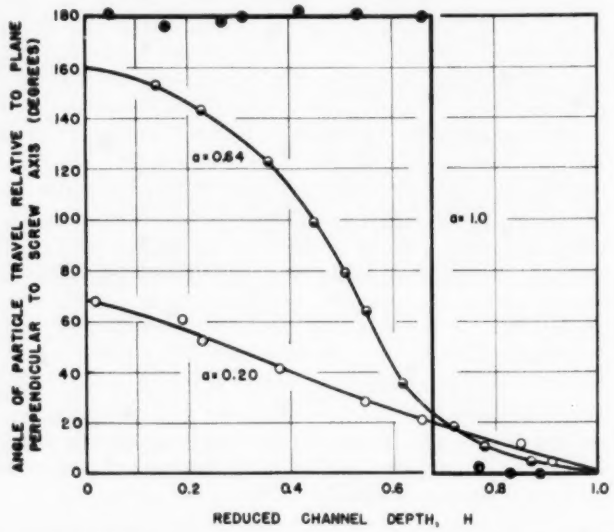

Figure 14. Angle of particle travel as a function of channel depth for three degrees of pressure flow (Non-Newtonian) fluid). Figures 13 and 14 are qualitatively similar, but Figure 14 has higher angle at lower channel depths

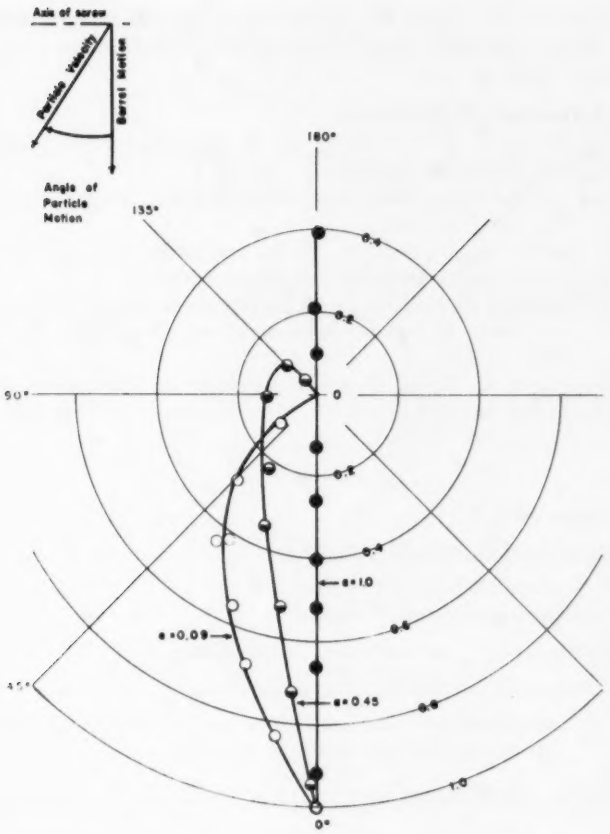

Figure 15. Angle of particle travel vs particle speed for three degrees of pressure flow (Newtonian fluid)

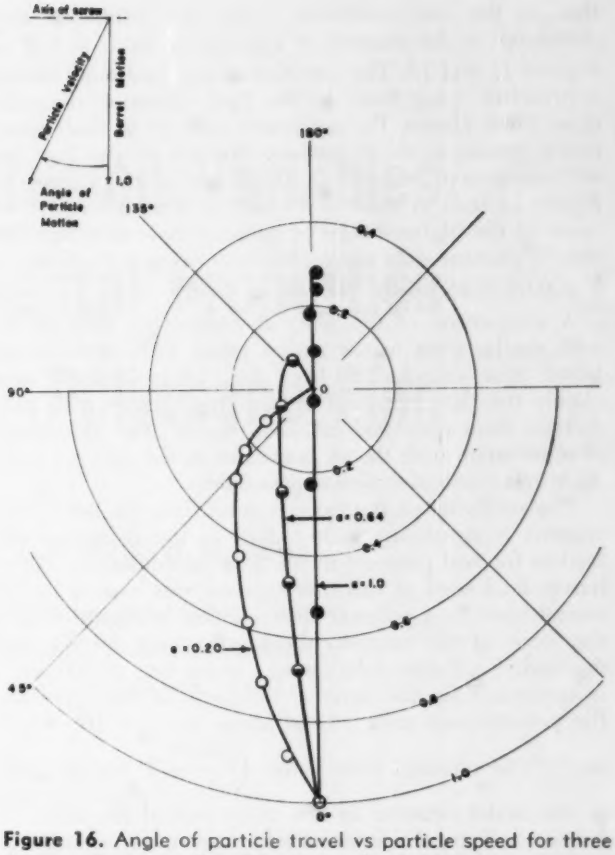

Figure 16. Angle of particle travel vs particle speed for three degrees of pressure flow (Newtonian fluid). Velocity component is smaller here than in Figure 15

center third of the channel between the flights, in order to minimize the influence of the flight edges upon the measurements. The distances as measured on the projected image were converted to actual distances by means of the scale on the screw and the parallax correction factor previously explained. In the channel cross section view *Figure 5*, measurements were made of the distances from screw to particle, and from screw to barrel surface. Sample calculations are in *Appendix I*.

The velocity data collected in this investigation are presented in the plots of *Figures 11 through 16*. The curves, as plotted, represent a smooth curve drawn by eye through all pertinent data points; about one-third of the data points are shown in the figures and are a representative selection from the whole. In *Figures 11 and 12*, tracer particle speed as a fraction of barrel velocity is plotted as a function of the particle reduced channel depth for Newtonian and non-Newtonian fluids respectively. The resulting curves for each fluid are very similar in appearance. In each case the data for the lowest value of the ratio of pressure flow to drag flow $\bar{a}$ were obtained with no restriction imposed upon the discharge pipe of the extruder. For the Newtonian fluid, this unrestricted discharge condition resulted in a value of $\bar{a} = 0.09$, or an output of 91% of the calculated drag flow. However, this same discharge condition produced an output of only 80% of the calculated drag flow or, a value of $\bar{a} = 0.20$, for the non-Newtonian fluid. The difference arises from the low shear rates and consequent relatively higher viscosities present in the discharge chamber and pipe in the case of the non-Newtonian fluid.

Figures 13 and 14 show the angle of particle motion plotted as a function of the reduced channel depth for the Newtonian and non-Newtonian fluids respectively. Once again, the resemblance between the curves for the two fluids is readily evident. A comparison of the curve for $\bar{a} = 0.64$ for the non-Newtonian fluid, and the curve for $\bar{a} = 0.45$ for the Newtonian fluid reveals that the former has a somewhat flatter appearance than the latter. This same difference in the flow behavior of the two fluids is also apparent in a comparison of *Figures 7 through 9* with similar photographs in (3). It can be seen that the flow patterns produced with the non-Newtonian fluid do not have as great an angular spread as those produced with the Newtonian fluid at comparable values of pressure flow. This effect is apparently due to a slight alteration in the transverse and down-channel velocity profiles arising from the non-Newtonianism of the fluid.

In the two polar plots *Figures 15 and 16* of particle velocity vs. angle of particle motion, the data for both fluid systems are once again seen to be qualitatively similar. A difference worth noting here is that, for the closed discharge condition, $\bar{a} = 1.0$, the maximum velocity in the 180° direction is greater in the Newtonian

than in the non-Newtonian fluid. The difference also shows up in the maxima of the curves for $\bar{a} = 1.0$ in *Figures 11 and 12*. The non-Newtonian fluid more nearly approaches "plug flow" in the 180° direction than the other fluid. Hence, the maximum velocity in that direction is greater in the Newtonian fluid. Note also that the 90° component of velocity is greater in the curves of *Figure 15* than in those of *Figure 16*. This is largely because of the higher values of pressure flow at which the non-Newtonian data were obtained ($\bar{a} = 0.20, 0.64$ vs $\bar{a} = 0.09, 0.45$ for the Newtonian fluid).

A comparison of the plots of *Figures 11 through 16* with similar plots in the earlier paper (3), which were based upon calculations from Eq. 1-4, will show how closely the data obtained in this study agree with predictions from simplified extrusion theory. The agreement of observation with theory is evident in the data for both Newtonian and non-Newtonian fluids.

The similarity of the experimental data for both fluid systems is significant with regard to the design of extruders for real polymer melts. The particular non-Newtonian fluid used in this investigation was chosen for its resemblance to a polymer melt. Notice in *Figure 6* that the slope of the viscosity-shear rate curve for the hydroxyethyl cellulose solution at a shear rate of 0.6 sec^{-1}, is approximately the same as the slope of the curve for the polyethylene melt (5) at shear rates of $10^1 - 10^2$ $sec.^{-1}$. The nominal shear rate $\left(\frac{\pi DN}{h}\right)$ encountered in the model extruder in this study was of the order of 0.6 $sec.^{-1}$. Typical nominal shear rates in a conventional extruder are in the range $10^1 - 10^2$ $sec.^{-1}$. For this reason, the flow behavior shown in this study for the hydroxyethyl cellulose solution in the model extruder should approximate that of a polymer melt at extrusion temperatures in a conventional extruder.

Conclusions

The flow distribution in an extruder channel has been described by equations derived from a simplified analysis of extrusion. One of the simplifying assumptions made in the analysis is that the fluid is Newtonian in its flow behavior. In the past it has been thought that the effect of this assumption did not lead to large error, and this impression has been borne out by the experimental observations of this study.

Photographs of flow patterns of a non-Newtonian fluid in an extruder channel have been presented. These photographs demonstrate that, with a non-Newtonian fluid, no material flows toward the rear of the extruder, and that the flow patterns resemble those of a Newtonian fluid. Data have been presented on the velocity distribution in a screw channel for both Newtonian and non-Newtonian fluids. The flow distribution for both fluids is shown to be qualitatively the same, and the behavior of both fluids is seen to agree reasonably well with predictions from simplified extrusion theory.

The conclusion to be drawn from these results is that non-Newtonianism of the fluid, to the extent usually encountered, does not greatly alter the picture of flow distribution in the channel as based on the equations developed for Newtonian fluids. This conclusion lends support to the use of the equations of simplified extrusion theory for calculations involving a non-Newtonian polymer melt.

Literature References

1. Carley, J. F., and Strub, R. A., *Ind. Eng. Chem.*, *45*, No. 5, 970-3 (1953).
2. Mohr, W. D., and Mallouk, R. S., *Ind. Eng. Chem.*, *51*, 765-70 (1959).
3. Mohr, W. D., Squires, P. H., and Starr, F. C., *Technical Papers, Vol. VI, SPE*, Jan., 1960.
4. Squires, P. H. Extrusion Theory, *Processing of Thermoplastic Materials*, Bernhardt, ed., Reinhold, New York (1959).
5. Westover, R. F., Processing Properties, *Processing of Thermoplastic Materials*, Bernhardt, ed., Reinhold, New York (1959).

Appendix I

Sample Calculations

Reduced Channel Depth:

Reduced channel depth,

$$H = \frac{\text{screw to particle distance}}{\text{measured channel depth}}$$

Measured distance from screw to particle = 14.5 mm

Measured channel depth = 26.5 mm.

$$H = \frac{14.5}{26.5} = 0.55$$

(Note: The measurements here are dimensions on a screen on which the photographs were projected.)

Particle Speed:

Parallax correction over entire depth of channel = 5%

Parallax correction = (H) (0.05) (Measured particle travel)

Measured particle travel = 11.4 mm.

Parallax correction = (0.55) (0.05) (11.4) = 0.31 mm.

Corrected particle = (measured travel) − (parallax correction) travel = 11.4 mm − 0.3 mm = 11.1 mm.

Actual particle travel = (corrected travel) (scale ratio)

Measurement scale: 69.0 mm (measured) = 2 in. (actual)

$$\text{Actual particle travel} = (11.1 \text{ mm}) \left(\frac{2 \text{ in.}}{69.0 \text{ mm}}\right) = 0.322 \text{ in.}$$

$$\text{Particle speed, } m = \frac{\text{(Actual particle travel)}}{\text{(Time for measured travel)}}$$

$$\text{Particle speed, } m = \frac{0.322 \text{ in.}}{2 \text{ sec.}} = 0.161 \text{ in./sec.}$$

$$\text{Fractional particle speed, } m/u = \frac{\text{Particle speed}}{\text{Barrel velocity}}$$

Barrel velocity, U = 0.387 in./sec.

$$\text{Fractional particle speed, } m/U = \frac{0.161}{0.387} = 0.42$$

The Effect of Extrusion Variables on the Fundamental Properties of Tubular Polythene Film

N. D. Huck, B. Sc. PhD and P. L. Clegg, B. Sc. PhD

Technical Service and Development Department
Imperial Chemical Industries Limited,
Plastics Division, Welwyn Garden City, England

For Blown Polythene Film

- *Higher extrusion temperature produces higher gloss film*
- *Increasing output rate increases haze in films*
- *Annealing chambers help to produce film of excellent quality*
- *Altering state of shear through die design affects film clarity*
- *Not only does magnitude of the transverse and machine direction drawing between die and freeze line affect mechanical properties, but also the order in which they occur*

More than 10 years have passed since the inception of the tubular process for the manufacture of polythene film, and it may seem surprising therefore, that although articles on individual aspects of tubular film extrusion have been published, a comprehensive treatment of the effects of process variables on the fundamental film properties, mechanical and optical, has not appeared. However, only in recent years has the wide range of properties obtainable from tubular polythene film been fully appreciated and the complexity of the mechanism of film formation been recognised.

The effects of extrusion variables on the fundamental phenomena determining the important optical and mechanical film properties, i.e. the nature of the surface of the film, its crystalline structure and the type of molecular orientation have been studied experimentally, and are discussed and illustrated by the results obtained.

Other important film properties, for instance blocking, slip, and proneness to develop a static charge, are certainly influenced by extrusion conditions, but they are not included as they are normally modified by the incorporation of suitable additives and may also be controlled at less critical stages of film production than those determining optical and mechanical properties.

To simplify presentation, the nature and the variation with extrusion conditions of the optical and mechanical properties of film are discussed separately in the two main sections of the article. In a discussion of these optical and mechanical properties it is essential to be familiar both with the methods used to measure them and with the main physical features of the film itself. This information is given in short introductions to each section.

OPTICAL PROPERTIES—THEIR NATURE, ORIGIN AND VARIATION

Definitions and Measurements

Percent Haze—Haze is defined as the percentage of transmitted light scattered by the film more than 2.5° from the normal incident beam, and has been measured according to ASTM method D1003-52.

No indication is given by this measurement of the complete polar light scattering diagram and important differences in texture may thus exist in films having the same percent haze value. In films used for display packaging, for example, not only should the measured haze be low but there should also be a relatively small amount of the wide angle scattering that occurs at small optical irregularities. The latter determines the apparent change of colour of a packaged article when viewed through the film.

The 45° specular surface gloss—Specular surface gloss has been measured as the proportion of light reflected from the film at an angle of 45°. For polythene film a large contribution to the specular reflection will be made by light undergoing multiple reflection within the film. Taking the first three of these reflections into account calculation shows that the maximum gloss value obtainable with low density polythene film is about 99 units (9.9% reflection).

High gloss is an important requirement of film to be used in display packaging. It is, however, inversely related to haze, though an exact relationship does not exist because of differences in the collimation of the incident light and in the range of angles over which the scattered light is measured in the two tests. To save much unnecessary duplication we have chosen to discuss haze rather than gloss throughout the text.

"See-through" clarity—"See-through" clarity is assessed by a visual test in terms of ability to resolve fine detail in a fairly *distant* object when viewed through film. The need for good "see-through" clarity in most polythene film is questionable and this applies particularly to the use of film as a packaging medium as the contents of the package are invariably in *close* proximity to the film. Whilst good "see-through" clarity is undoubtedly of psychological importance in selling film to the "middle man", it is doubtful if it attracts the final purchaser appreciably.

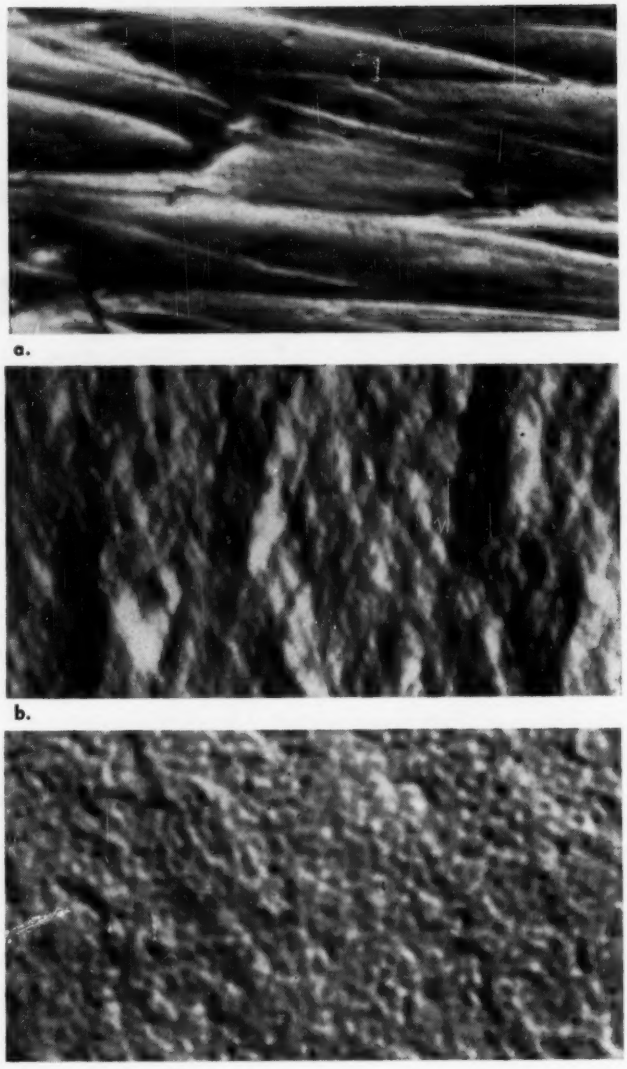

Figure 1. Basic types of surface irregularities on polythene film

a. 50 microns orange peel (x 90)
b. 50 microns extrusion haze (x 450)
c. 50 microns surface crystallisation irregularities (x 1800)

Origin of Factors Causing Light Scattering

There are only two major types of optical irregularity in polythene film, although light will also be scattered at inhomogeneities such as grain, microgels and particulate additives. These arise from: Surface irregularities caused by melt flow phenomena, and crystallization behaviour.

By far the greater proportion of light scattered by commercially available polythene film occurs at irregularities on the surface of the film where there is a large change of refractive index.

The most important surface irregularities are extrusion defects originating from the complex elastic melt flow

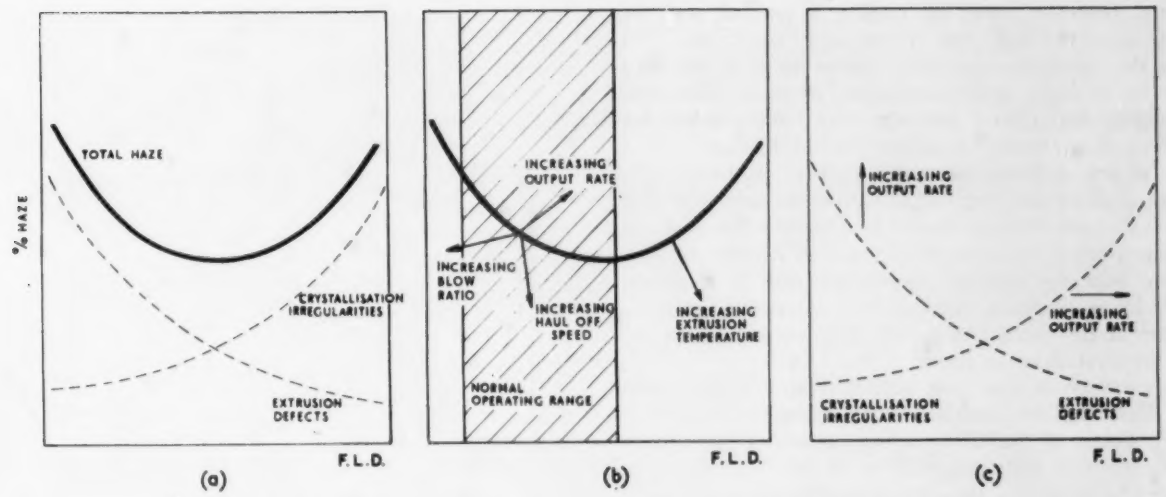

Figure 2 (a, b, and c). Characteristic variation of film hazewith freeze line distance

behaviour in the extrusion die itself, and are readily observed on the melt as it emerges from the die, (*see Figures 1a and 1b*). These are the only types of surface irregularities normally observed on film made from low density polythenes. Because they arise from melt flow phenomena their nature and magnitude will depend upon the particular flow properties of the polythene itself, and will also be influenced by the shear rate (output rate), the melt temperature and the die profile.

A second and also major cause of light scattering is surface irregularities arising from the growth and aggregation of crystallites at or near the surface of the film (*see Figure 1c*). This growth buckles the surface of the film and the magnitude and intensity of such irregularities, factors which determine how much light is scattered, depend upon the density of the polythene and upon the rates of nucleation and growth of crystallites through the cooling and drawing region. The important extrusion variables which most influence this growth are the temperature gradient at the freeze line, the distance from the die to the freeze line (the "freeze-line-distance" or "F.L.D."), and the cooling time, although orientation and, therefore, blow ratio (bubble diameter: die diameter), die gap etc., might also be expected to have some effect.

Crystallisation effects cause light scattering not only at the surface but also within the film at the boundaries of spherulites (narrower angle scatter) and between crystallites (wide angle scatter). It is the former type of scattering which is responsible for the translucent appearance of thick sections, e.g. mouldings. There are, however, only very small changes of refractive index at these internal optical irregularities, and in thin film the contribution made by this internal scattering to the total haze is normally small, though exceptions may be found in film made from the higher density polythenes.

Effect of Extrusion Variables on Principal Factors Causing Light Scattering

During the film forming operation there will be a change in the texture of the surface of the melt because of a decrease in the height of the extrusion defects and an increase in their length and breadth as the melt is drawn lengthways and blown sideways. However, as long as the polythene emerging from the die remains molten, the overall magnitude of the extrusion defects will decrease under the influence of surface tension. Thus, as the cooling time is increased by, for instance, increasing the freeze-line-distance, the magnitude of the extrusion defects finally frozen into the solid film will decrease and so therefore will the percent haze. On the other hand, as the freeze line distance increases the contribution to the total haze made by "crystallisation haze" increases because of the slower cooling times and larger crystalline aggregates that are formed. These two opposing effects are illustrated separately in *Figure 2a* and the sum of these curves may be considered to represent a characteristic curve for all types of polythene, both its precise shape and the position of its minimum along the abscissa depending upon the melt flow properties, the density and the crystallisation behavior of the particular polythene.

The general effects are shown in *Figure 2b* of changes in other important extrusion variables on the position of the characteristic haze curve; increases in blow ratio, output, haul-off speed and extrusion temperature move the curve in the direction shown by the arrows.

The effect of extrusion temperature—It is well known that the effect of increasing extrusion temperature is to produce a film having lower haze, higher gloss and higher clarity. Two effects combine to give these better optical properties, the first being that the melt is smoother at the higher temperatures, and the second that the size of the crystalline aggregates is reduced because of the higher cooling rates used to maintain a given freeze-line-distance at a higher melt temperature.

The effect of output rate—An increase in the magnitude of frozen-in melt surface irregularities and so in percent haze might be expected with increasing output rate everywhere up the left hand side of the characteristic curve (*Figure 2a*); this is shown in *Figure 2c*. To maintain a constant freeze-line-distance at an increased out-

put rate, however, more air cooling is needed and the cooling rate through the freeze line increases. This causes the crystallisation haze curve to shift towards higher freeze lines, again shown in *Figure 2c*. The relative magnitudes of these two opposing factors determine the effect of increasing ouput rate on total haze.

The effect of blow ratio—An increase in blow ratio and consequent drawing of the melt reduces the size of the extrusion defects finally frozen into the film; at the same time if this change is made at a constant output rate and the haul-off speed adjusted to maintain film thickness constant, there is an increase in the cooling time at the same freeze-line-distance and so an increase in crystallisation haze.

The variation of film haze with output and blow ratio rate is illustrated for a particular polyethene in *Figure 3*.

The effects of bubble cooling arrangements—From the foregoing it follows that film of low haze can be produced by adjusting the cooling conditions to minimise the effects of extrusion and crystallisation irregularities. This may be achieved by providing slow cooling near the die so as to allow the most rapid decay of the extrusion irregularities, and then following this by rapid quench at or near the freeze line to reduce the size of the crystallisation irregularities. Techniques involving the use of an annealing chamber between the die and the point where the air strikes the bubble give the required slow cooling process near the die and a fairly rapid quench at or near the freeze line, and though other factors such as bubble stability have to be taken into account when designing the optimum cooling arrangements, there is no doubt that major effects can be achieved in this way.

A passing reference should be made here to the excellent optical quality of flat film made by the chill roll casting technique. In this process heat is removed from the molten film far more efficiently than in the air cooled tubular process with the attendant problem of bubble control. A very high extrusion temperature can therefore be used so ensuring that the molten film has a surface substantially free from any form of extrusion irregularity. The final rapid quenching of the melt to form a solid film ensures minimum crystallisation defects.

Effects of Density and Crystallisation Characteristics

In general the minimum of the characteristic curve moves to shorter freeze-line-distances as the density of the polythene is increased, so that percent haze may be found to increase with increasing freeze-line-distance in the normal operating region. With polythenes of the same density but having different crystallisation rates, the minimum of haze occurs at lower freeze-line-distances for the sample crystallising more rapidly.

Effect of Melt Flow Behaviour on Film Haze

It has already been said that extrusion defects are predominantly responsible for the haze of film made from low and intermediate density polythenes giving the required medium or high level of toughness. It will be recalled that tubular polythene film suffers from two types of extrusion defect or surface irregularity. The first, which we call "extrusion haze", is a very fine surface irregularity (*see Figure 1b*); the second is large scale gross irregularity which is commonly called "orange-peel" or "apple-sauce" (*Figure 1a*). It is tempting to associate these defects respectively with mattness and distortion on monofilament. These are well-known defects (1, 2, 3) which occur with increasing output rate and may be described as: A surface roughness or mattness which is a high frequency surface irregularity occurring on an otherwise uniform extrudate and a distorted extrudate which has been described as turbulent, wavy, knobbly, or bamboo-like.

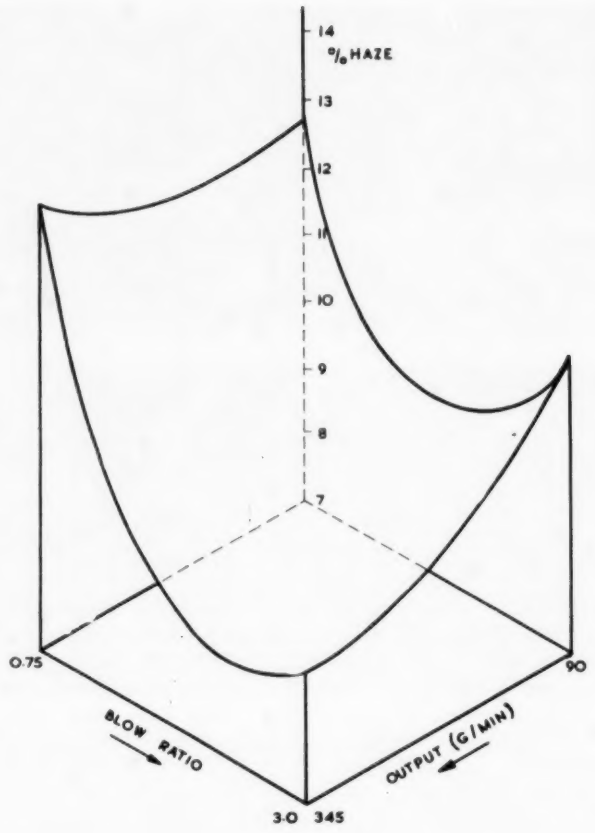

Figure 3. Variation of haze of film made from polythene A (0.925/4.0) with blow ratio and output rate

The problem of mattness has not been investigated as fully as has that of distortion (turbulence) but it is practically independent of the included die entry angle over the range 20°-140°; the effect of die length is not so certain, however, although most polythenes appear to show a decrease in mattness with a decrease in die length and an increase in die entry angle up to about 20°. Recent work indicates that with at least some polymers mattness occurs at a critical linear extrusion velocity through the die irrespective of the shear rate or shear stress.

It is on the other hand well-proven that distortion or turbulence is a die entry phenomenon, and, for a fixed die geometry, occurs at a critical shear stress or rate of shear.

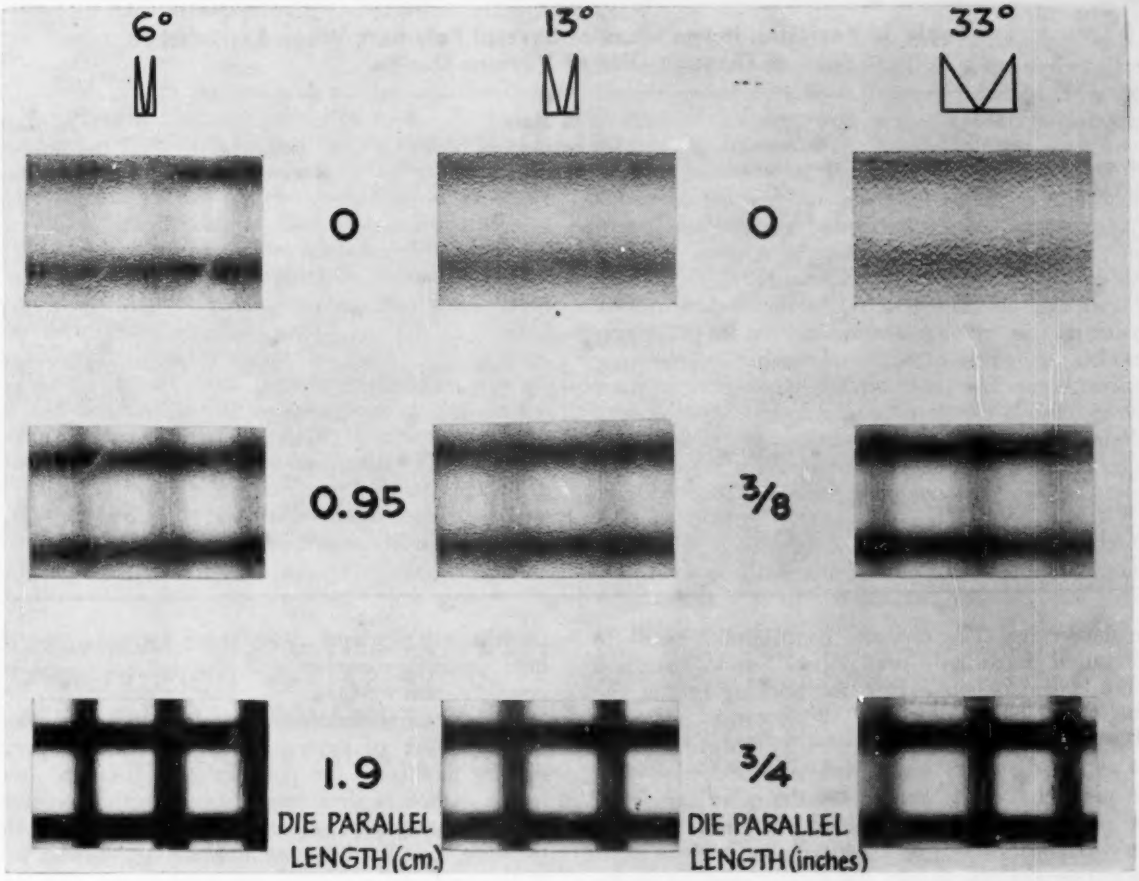

Figure 4. Variation of orange peel of films extruded from polythene (.930/4.0) through various die profiles

Variation of die geometry, i.e. die land length and die entry angle, is therefore a convenient way to study the occurrence of "extrusion haze," and "orange peel". However, there is a practical difficulty as it is well-known that polymers may be modified through being "worked" (i.e. subjected to high shear stresses in the melt). For a given extruder, the degree of working achieved on the screw is affected by the die design, as this largely controls the back pressure, i.e. the pressure the screw has to develop to force polymer through the die at the required output rate. Alterations to die design may thus affect the quality of the extrudate in two ways, first by providing a different flow path for the polymer and second, and indirectly, by modifying the polymer itself through alterations in the degree of shear experienced on the screw. When assessing the effect of changes in die profile it is therefore necessary to maintain a constant pressure along the screw by means of a throttling device; the effects of such throttling devices, i.e. of extrusion pressure, have then to be studied separately using constant die profiles. A further effect of change of die design may be to modify the state of shear of the polymer as it is presented to the die and this together with the other effects is discussed below.

Variation of Die Profile—"Extrusion haze" may possibly be caused by the relaxation of those molecules most highly sheared at the die/melt interface as the elastic melt emerges from the die. Short parallels and wide entry angles may, therefore, give minimum "extrusion haze". "Orange-peel" on the other hand is supposed to originate from turbulence in the die entry region; a long parallel would have the effect of smoothing out distortion originating in this region, and as with the effect of die entry angle on the critical point during monofilament extrusion, a narrow entry angle would be required to give film having the least "orange-peel".

The effect of die profile on "orange-peel" was illustrated most vividly using an experimental intermediate density polythene which gave film with very little "extrusion haze" and "crystallisation haze", but with a marked tendency to "orange-peel". From the photographs in *Figure 4* it can be seen that the intensity of "orange-peel" varies as would be expected if it is related to turbulence, that is, it increases with decreasing die parallel length and also, to a lesser extent, with increasing die entry angle.

Further experiments varying die parallel length and die entry angle using other types of polythene have given more complex results as, for example, in *Table 1*.

These results may be tentatively explained by supposing that "orange-peel" and "extrusion haze" may occur together and in a manner not readily distinguished

Table 1. Variation in the Haze of Several Polymers When Extruded Through Dies of Various Design

Polymer (density/M.F.I.)	Die parallel length inches	Extrusion temperature °C.	% Haze Die entry angle degrees 6	13	33	Extrusion temperature °C.	% Haze Die entry angle degrees 6	13	33
C	0		11.3	10.6	10.8		7.7	9.4	8.4
(0.925/4.0)	3/8	135	9.5	9.0	8.4	170	7.3	7.7	6.7
	3/4		10.9	8.9	7.8		7.8	7.0	6.6
D	0		16.0				13.3		
(0.920/1.0)	3/8	180	10.8	14.4		205	10.7	13.8	
	3/4		12.5	15.6	10.4		11.6	11.1	11.9
E	0		9.5						
(0.917/2.0)	3/8	155	7.1						
	3/4		7.5	7.4					
F	0		12.5		15.2		8.8		7.6
(0.917/7.0)	3/8	135		11.6		160		6.9	
	3/4		11.2		9.6		7.7		6.9

by the naked eye. The separate contributions made to the measured haze by "orange-peel" and "extrusion haze" are considered in *Figure 5a*. Looking first at the contribution which "orange-peel" or distortion makes to the measured haze, it can be seen that distortion increases as the die entry angle widens and decreases as the die parallel is made longer. On the other hand, we suggest that the contribution of mattness to the measured haze decreases as the die entry angle widens and increases slightly as the die parallel length is increased. Summing these opposing effects the graph of *Figure 5b* is obtained which is in fact derived from the data in *Table 1* for one particular polymer.

The precise effects of these variations in die profile will, of course, depend upon the flow properties of the particular polythene being used, and upon the relative response of "extrusion haze" and "orange-peel" to both die parallel length and die entry angle; there will in fact be an optimum design, i.e., one which will produce film with the best optical properties, for each type of polythene. Over and above these extrusion defects, the final optical properties will also be influenced by any crystallisation effects.

The effects of the shear history of the melt—The well-known effect of improving the optical properties of film by modifying the polymer itself through alterations in the degree of shear experienced on the screw is illustrated by the data summarised in *Table 2* for the low pressure die. In this case a throttling device, situated at the end of the screw, was used to vary the pressure developed along the screw.

The existence of another effect of equal importance may be best illustrated by the occurrence of the well known memory lines, which originate where the melt has rejoined after being divided by, for instance, the webs which are so often used to support the central mandrel or torpedo. The melt which has flowed around a web is sheared to a greater extent than that on either side of it, and as molten polythene takes a finite time to relax completely to a normal unoriented state after

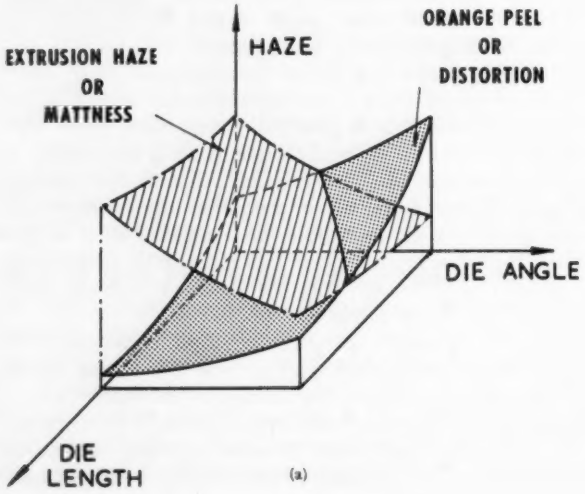

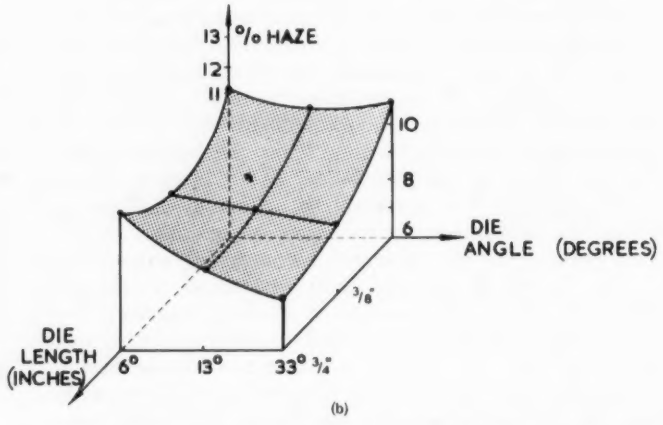

Figure 5 (a and b). Effect of die parallel length and die entry angle on film haze

being sheared, the die is presented with a non-uniform melt; in the regions of non-uniformities the film is clearer.

Any special design feature of the die which alters the state of shear of the melt presented to the die entry, such as a restriction, will have a similar effect. This is illustrated by the data summarised in *Table 2* for the high pressure die. In this die, which had an entry angle and parallel length similar to that of the low pressure die, the extrusion pressure was developed within the die itself at spiralling and constrictive overlapping flow channels designed to eliminate memory lines from previous divisions of the flow path.

This substantial improvement in the optical properties of film produced from high pressure dies is well-known, and because of this improvement as well as the improved thickness tolerance obtained with them there is an increasing tendency to use such dies. These effects do illustrate however, further practical difficulties in isolating the effects of any individual section of the die; for instance, a long parallel might also be expected to produce similar oriented flow and so clearer film.

MECHANICAL PROPERTIES—EFFECT OF EXTRUSION VARIABLES ON MECHANICAL PROPERTIES OF POLYTHENE FILM

Measurements of the tear and tensile strengths have always been used as an indication of the mechanical strength of tubular polythene film. In recent years experience has shown that some form of impact test together with a tear test gives a working assessment of the toughness and durability necessary in the extensive produce prepacking, building and agricultural applications. The mechanism of the impact failure of polythene film and the various types of tests which have been used to measure impact strength have been discussed and classified in a previous article (4), the salient features of which are summarised briefly below.

Under impact loading conditions, as for instance in a dropping sand-bag test, a slit-like failure may occur along the machine direction, either in the body of the film or more probably down one of its edge folds. Such failures, usually termed "brittle", are in fact "localised high-temperature shock failures" caused by the production of a sharp neck in the transverse direction and subsequent failure of the necked portion at a low overall elongation. This localised failure is caused by the adiabatic temperature rise that occurs in the neck. The magnitude of this temperature rise, which may be as high as some tens of degrees Centigrade, depends on the shape of the neck developed. This in turn depends on the orientation and the density of the film; an increase in either of these will lead to an increase in the sharpness of the neck, hence to a higher neck temperature during rapid deformation and consequently to a greater likelihood of failure. A simple if indirect measure of neck sharpness is the natural draw ratio* of the film determined in the transverse direction, and a good correlation exists between this and the impact strength of film (4).

A neck is rarely if ever formed when drawing in the machine direction and impact failure normally follows necking in the transverse direction to give a slit in the machine direction; with film made under conditions giving a very high impact strength, on the other hand, failure occurs randomly and sometimes circularly.

Table 2. The Effect on Film Haze of Extrusion Pressure Varied Using a Throttle or Unthrottled High Pressure Die

Polythene (density/MFI)	Film Haze %			
	Pressure (increased using throttle on L.P. die) p.s.i.			Pressure in H.P. die p.s.i.
	700-1100	2000-2500	4000	3900-4400
F. (.918/7.0)	15.3	10.3	8.6	5.3
I. (.920/2.0)	12.9	11.5	10.5	7.2
E. (.922/2.0)	7.0	6.8	6.3	3.8
A. (.925/4.0)	12.5	8.4	7.6	5.0
G. (.929/8.0)	6.3	5.9	5.9	4.8

Definition and Measurement of the Mechanical Properties of Film

Impact strength—We have measured the impact strength using the well-known dropping dart test developed by the Monsanto Chemical Company (5). The quantity used to assess the impact strength is the weight of the dart at which 50% of the samples tested fail, i.e. F_{50}. In service, the region of practical importance is less than 1% failure (F_1) and a limitation of F_{50} is that films with the same F_{50} value can have quite different F_1 values. A further limitation is that the most likely point of failure is along one of the edge-folds rather than in the face of the film. The impact strength of an edge-fold can be determined using the same equipment but placing the edge-fold to one side of the point of impact so as to pass through the region of maximum stress around the head of the dart at the moment of impact.

Tear strength—The tear strength was determined by using a method similar to the well-known Elmendorf test, and like tensile strength is measured in both the machine and transverse directions. The tear in the specimen is initiated with a small slit and the specimen is stretched and cold drawn to the breaking point everywhere along the line of the tear. The numerical value quoted is a measure of the work done in propagating this tear and this depends upon the geometry of the sample and its elongation to break. These two quantities together control the amount of film drawn during the tearing process.

A limitation of the Elmendorf type test is that the tear is free to run towards or along the weakest line, which is generally in the transverse direction. The length of the tear is thus variable, particularly if initiated in the

* The natural draw ratio is the ratio of the cold drawn length of a specimen to its original length.

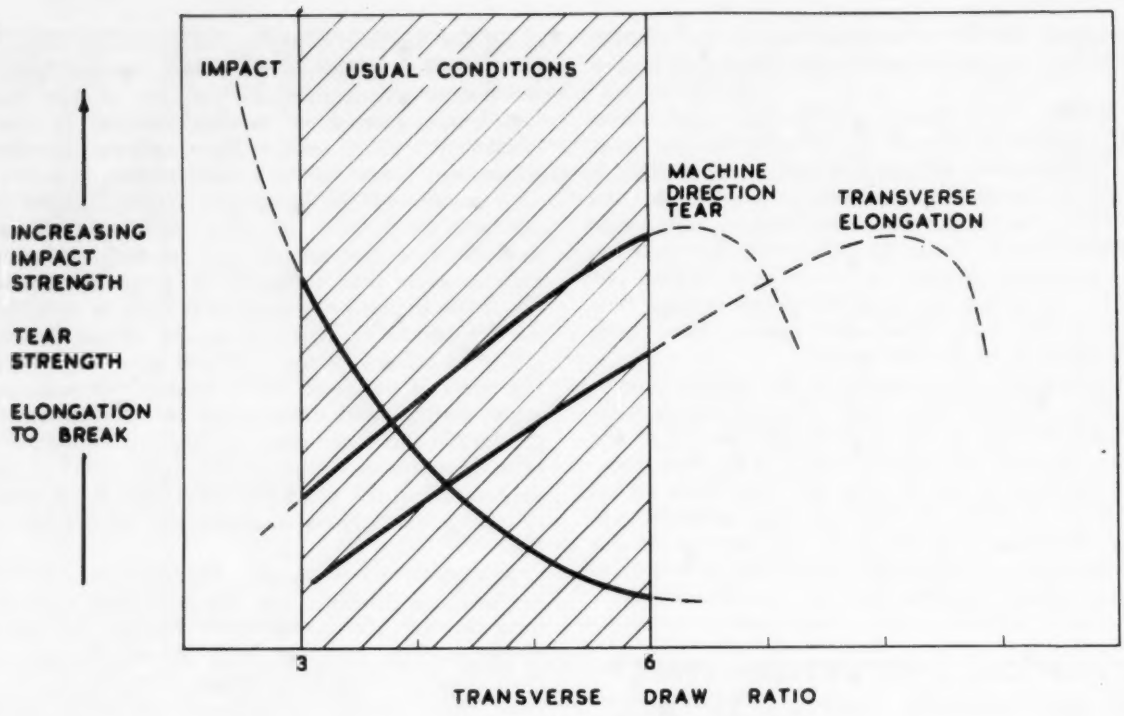

Figure 6. Characteristic relationships between tear and impact strengths and elongation at break

machine direction, and will affect the energy absorbed i.e. the measured tear strength. Thus the interpretation of this test is not straightforward; it has nevertheless proved of some value in assessing the likely durability of film in service.

Tensile properties—The tensile data were determined on conventional equipment at an extension rate of 12 inches per inch per minute. The tensile strength at break gives no information about serviceability; in spite of this it is a property often discussed. Elongation at break, like impact and tear strength, is affected by the way in which a neck develops after yield; it is therefore broadly related to these other mechanical properties.

Characteristic relationship between tear strength, impact strength and elongation at break—The exact relationship between these properties is undoubtedly complex, but all three depend significantly on the way in which polythene film draws when strained at different rates. The following discussion is over-simplified but may provide a useful working hypothesis.

The elongation of polythene film can take place either uniformly, as when the elongation to break is low, or through a neck. As the sharpness of the neck increases so does the draw ratio and, up to a limit, the elongation to break. If the neck becomes too sharp and the draw ratio (measured at a low testing speed) too great, the elongation to break of the sample drops to a low value. This is because failure occurs at the neck almost as soon as it initiates and before the bulk of the sample can cold draw. The type of failure is, in fact, identical with the "localised high-temperature shock failure" discussed previously.

A low draw ratio in the transverse direction favours a low tear strength in the machine direction, i.e. when the

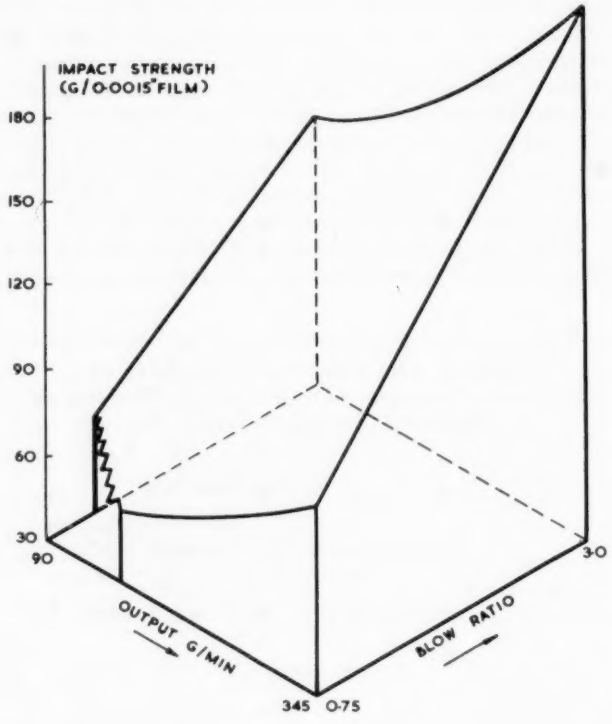

Figure 7. Variation of impact strength with blow ratio and output rate—polythene A (0.925/4.0) at A F.L.D. of 18"

tear runs along the machine direction and the specimen is therefore stretched to break at a low elongation in the transverse direction. This same low draw ratio would, however, give a high impact strength (4); in the extreme case of low draw ratio one has the high impact and low tear strength of planar oriented films. A generalised sketch of this inverse relationship between impact strength and machine direction tear strength is given in *Figure 6*, in which both are plotted against transverse draw ratio, though they could equally well be plotted against an extrusion variable, transverse draw ratio decreasing as the blow ratio increases.

The left hand limb of the tear strength curve corresponds to tough tears and the right hand limb to tears that are becoming localised adiabatic heating failures. This latter is the type of failure that occurs during impact testng and the difference in position of the two curves along the draw ratio axis arises from the marked difference in testing rate involved; the tear test is much slower. The curve for elongation to break in the transverse direction is similar in shape to the tear strength curve, increasing with draw ratio before finally falling fairly sharply to a low value. The maximum of this curve lies at the highest draw ratio as tensile testing is carried out at the slowest speed. The shaded portion of *Figure 6* covers the range of draw ratios normally found in the transverse direction. The draw ratio in the machine direction is, by contrast, either equal to unity (i.e. no neck forms at all) or low and thus the resulting tear strengths in the transverse direction are never very high; these are also less influenced by extrusion conditions. The relative levels of machine and transverse direction tear strengths are in fact shown in *Figure 8*.

Factors Affecting Orientation and Effect of Extrusion Variables on Orientation

There is little doubt that orientation is the major factor controlling the mechanical properties. There are three sources of stress imposing orientation during blown film formation:—

(a) the shear stress causing flow of the visco-elastic melt through the die.
(b) the circumferential stress arising from the blowing process.
(c) the longitudinal stress applied by the nip rolls.

Orientation arising in the die is small compared with that from melt drawing and does not directly influence the orientation finally frozen into the film; its importance lies in that it may affect the way in which the melt draws.

In the blown tubular process, using the normal blow ratios of between 1.5 and 3:1 a large draw down in the machine direction is required to produce film 0.0010-0.0015 in. thick from a die with an annular gap of between 0.015 and 0.040 inch; for example, film 0.0015 in. thick made at a blow ratio of 2:1 from a die with an annular gap of 0.030 in. will be drawn down in the machine direction in the ratio

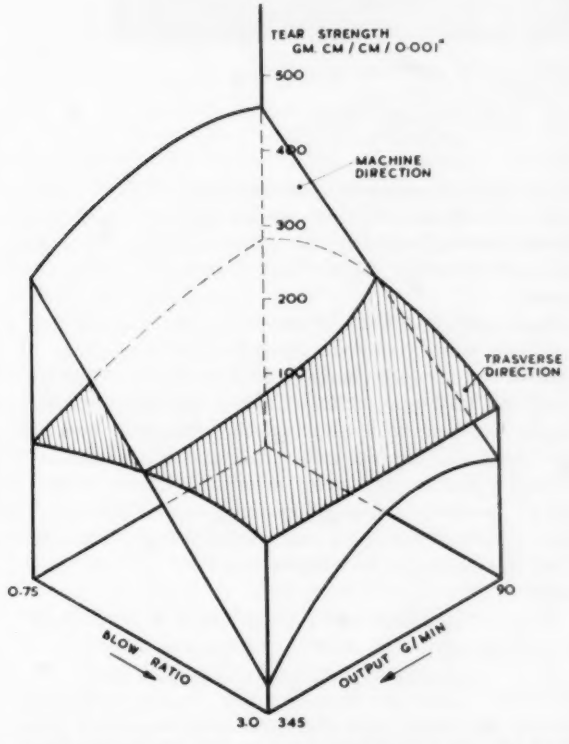

Figure 8. Variation of tear strength with blow ratio and output rate—polythene A (0.925/4.0) at A F.L.D. of 14"

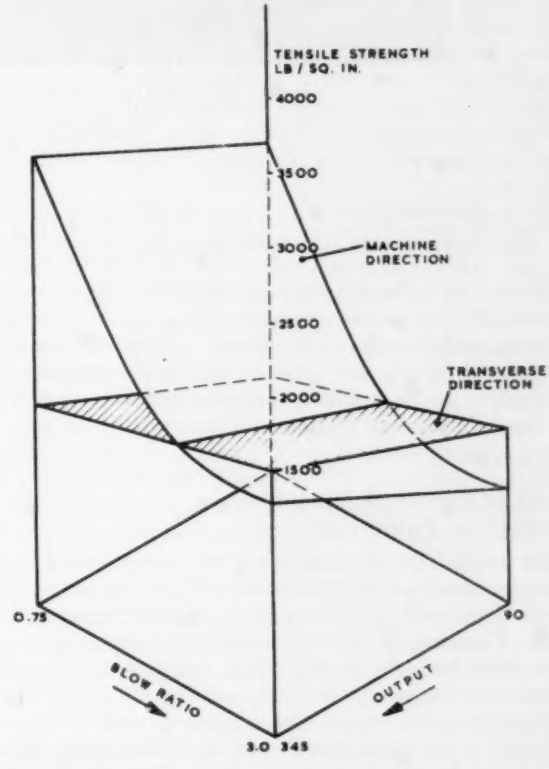

Figure 9. Variation of tensile strength with blow ratio and output rate—polythene A (.925/4.0) at A F.L.D. of 14"

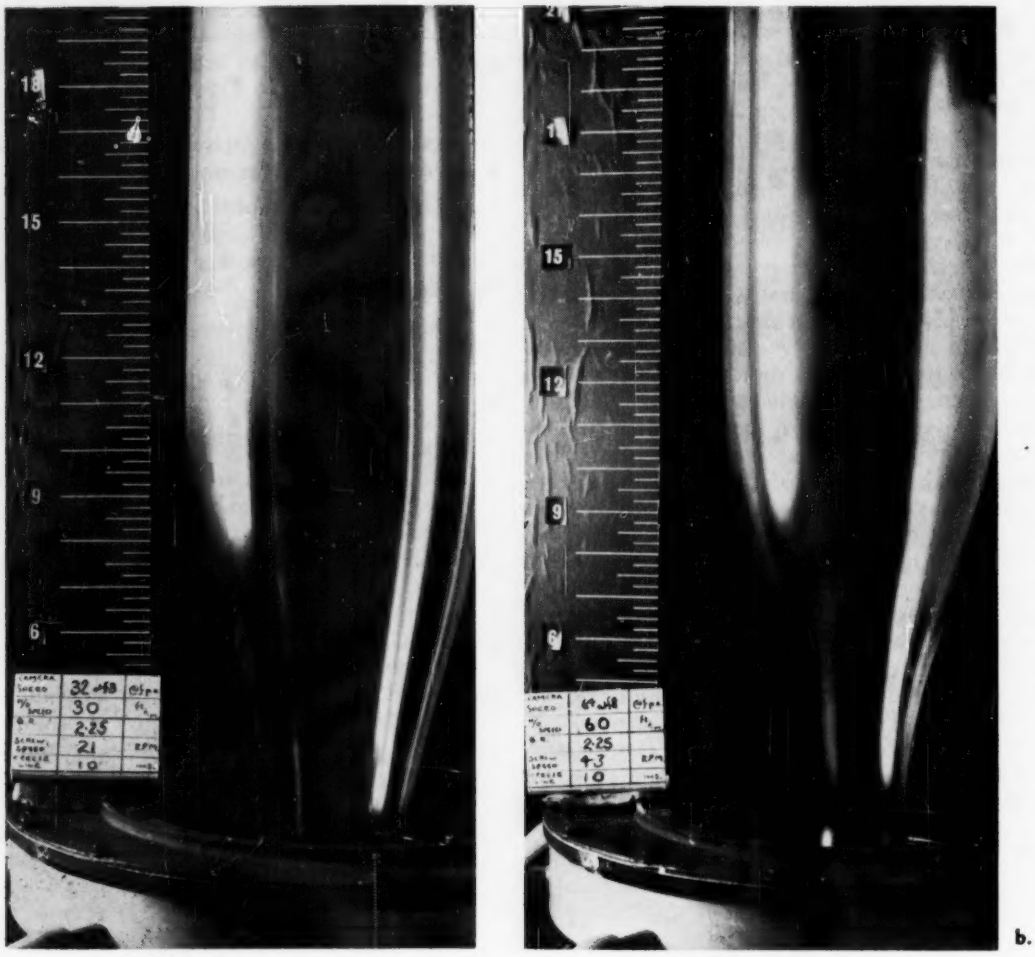

Figure 10 (a and b). Variation of bubble shape with extrusion conditions
a. Low output, low F.L.D. impact strength 99g.
b. High output, low F.L.D. impact strength 187g.

$$\frac{\text{die gap}}{\text{film thickness x blow ratio}} = \frac{0.030}{0.0015 \times 2} = 10{:}1$$

compared with the 2:1 ratio in the transverse direction. It therefore appears at first sight that machine direction drawing, and therefore orientation, will predominate in any normal blown film process; hence the familiar slit-like failure in the machine direction under impact loading conditions. That this is not necessarily so will be seen.

Effect of Extrusion Variables on Mechanical Properties

It is well known that the effect of decreasing the longitudinal or machine direction orientation by increasing the lateral blow ratio is to increase the impact strength and to alter the ratio of the tear and tensile properties in the machine and transverse directions; however, as far as the authors are aware no comprehensive study of the effect of other extrusion variables has been described. *Figures 7, 8 and 9* illustrate the impact, tear and some tensile properties of films produced over a wide range of blow ratios and output rates, the haul-off speed being varied to maintain a constant film thickness of 0.0015 in. The expected trends of these properties with blow ratio are immediately discernible. However, in addition, a general and unexpectedly large effect of output rate is also revealed.

An important effect of increasing the output rate at a constant freeze-line-distance is to alter the shape of the bubble; this change is illustrated in the photographs reproduced in *Figure 10*. It follows that the drawing behavior in the melt must have changed, and so the growth of the bubble below the freeze line was studied photographically; the order in which transverse and machine direction drawing occurred could then be calculated respectively from the profile of the bubble and from the changes in velocity between the die and the freeze line.

It was found that in the production of film having low impact strength, e.g. at low output rates, the shape of the bubble was basically similar to that of *Figure 10a*, and that both transverse and machine direction drawing occurred uniformly, with the latter predominating throughout, (*Figure 11a*). However, at the high output conditions giving film of higher impact strength, the order in

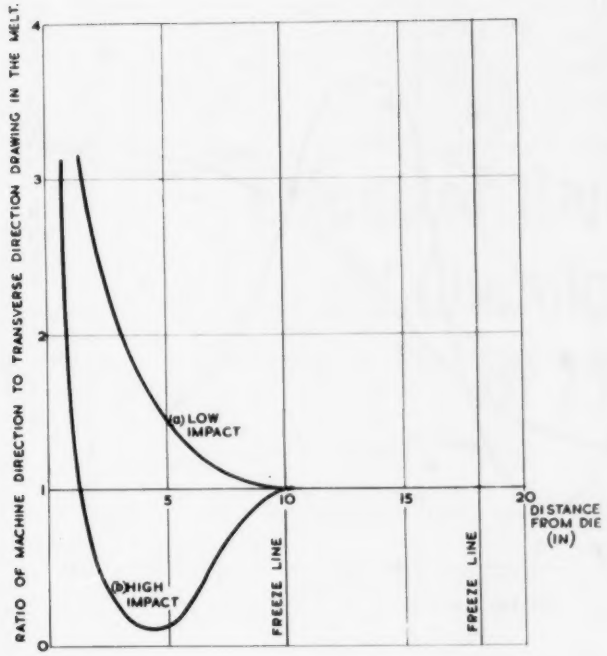

Figure 11. Variation of machine and transverse direction drawing with extrusion conditions

which transverse and machine direction drawing occurred changed, so that transverse drawing predominated in the region just before the freeze line, (*Figures 10b and 11b*).

The main criteria affecting the mechanical properties of tubular film are therefore not only the relative magnitude of the transverse and machine direction drawing between the die and the freeze line but also the order in which they occur. This is not altogether surprising because the relaxation times of molten polythene are comparatively short and most of the orientation imposed early in the drawing process will be forgotten. The most likely orientation to be frozen and retained in the film as well as the consequential crystallisation behaviour, are determined by the orientation existing in the melt at or just before the freeze line.

Any residual drawing occurring through the freeze line will also be of considerable importance, as the final crystalline structure will depend markedly on the conditions obtained during the period of its growth. That such drawing can occur in both directions after the first appearance of haze—indicating the growth of crystallites or crystalline aggregates to a size which scatters visible light—is well known. And indeed it is interesting to speculate whether the increased residual drawing that must occur in this region when operating at higher outputs, and thus at high bubble pressures, is a major factor in producing film of higher impact strength.

Some Factors Affecting Drawing Behaviour Between Die and Freeze Line

The bubble shape and so the mechanical properties of the film produced are affected significantly by the temperature gradient between the die and the freeze line and therefore by the particular cooling arrangements used. The effect cooling arrangements have in modifying the bubble shape and producing film of higher impact strength is illustrated by the results in *Table 3;* this was obtained by increasing the distance between the die and the point at which the cooling air stream strikes the molten bubble and at the same time increasing the flow of air to maintain a constant freeze-line-distance. As in the control of optical properties, however, factors such as bubble stability must also be considered in designing such equipment.

Table 3. The Effect of Raising the Air Cooling Ring on the Impact Strength of Film Made at a Constant Freeze Line Distance

Position of Cooling Ring	Impact Strength F_{50} (gm.)
Normal position near die	72
Raised ½"	78
Raised 3½"	96

Variation of Orientation, Birefringence and Impact Strength

A description of the type of orientation generally found in tubular polythene film has been discussed in detail by Holmes and Palmer (6). Briefly, there is a cylindrical symmetry about the machine direction, and the b axes of the crystallites are preferentially oriented in a plane perpendicular to this direction, (*Figure 12a*). Depending on the extrusion conditions the angle α made by the chain axes of the crystallites (c axes) may vary so that α increases with, for instance, an increase in blow ratio.

The measured birefringence is influenced both by the average value of the angle α and by the dispersion or distribution of orientation (δ) about this value; in the films previously examined and discussed by Holmes and Palmer this dispersion remained substantially constant.

Figure 12b shows the variation of birefringence and impact strength of films of constant thickness made at constant freeze-line-distances and haul off rate, the output rate and blow ratio increasing together. It can be seen that there is no correlation between birefringence and impact strength. However, X-ray diffraction data showed that the initial decrease of birefringence resulted primarily from an increase in α, the average angle of tilt of the c axes to the machine direction. And at the minimum and thereafter this angle of tilt remained substantially constant but the distribution of orientation about this angle increased; this increase of dispersion initially results in an increase of birefringence, but ultimately birefringence must decrease as the orientation becomes more random. It seems logical that the impact strength should increase under these conditions, particularly as the distribution of orientation is widening, until a random configuration is obtained.

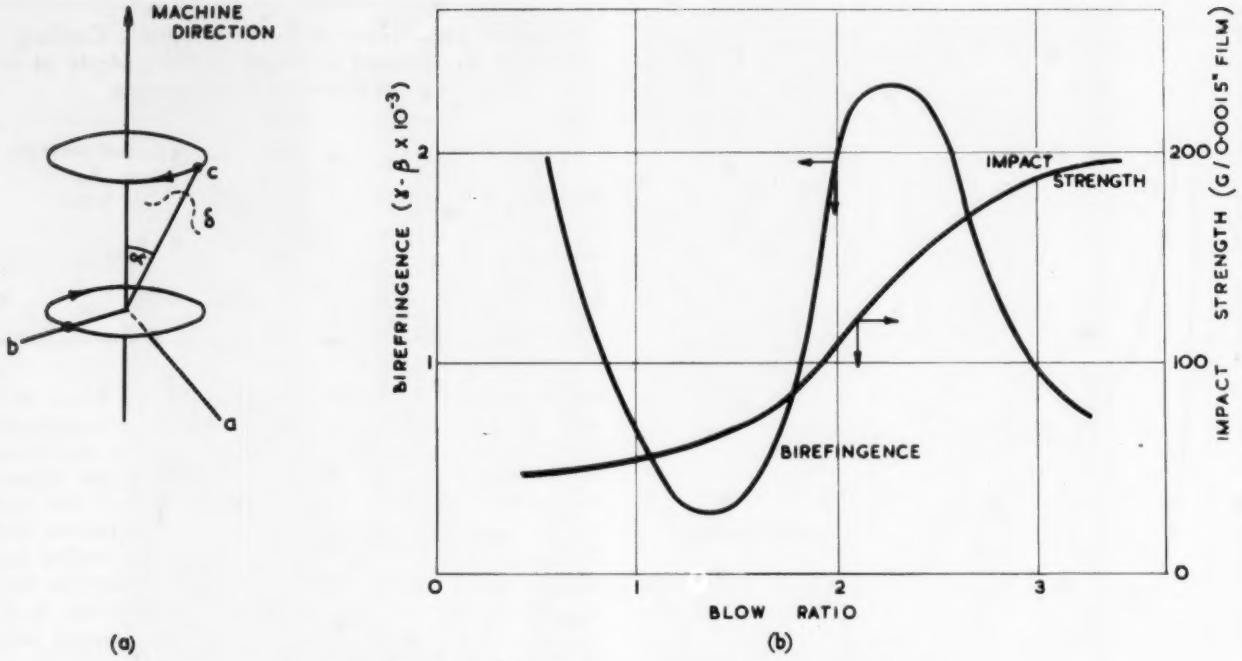

Figure 12 (a and b). Birefringence and impact strength of films made from polythene A (0.925/40)

In none of these samples was there any evidence of a significant change of orientation in the amorphous regions or of a significant amount of planar orientation. It is interesting to note, however, that more recently samples of film made under normal extrusion conditions from some experimental polythenes have shown some planar orientation.

Discussion

Various facets of tubular polythene film formation, and the criteria determining some important properties of the film produced, have been briefly reviewed above and these amply illustrate the complexity of this process; it has been seen that all the important mechanical and optical properties are closely related to all the processing conditions and the fundamental properties of the polythene. In the available space and time it has been possible to mention only briefly some of the salient features of film formation and much detail has of necessity been omitted.

Many aspects have to be taken into account by the polymer manufacturer in designing a film grade and by the very nature of polythene this frequently means that compromises have to be made; an example of this is the development of intermediate density polythenes, for which the flow properties have been adjusted to give high clarity film and the density increased at a sacrifice of toughness to give the required non-blocking characteristics. Thus there has been a growing use of additives, which have not been discussed and which can affect processing behaviour, to give further flexibility. It has been seen, however, that the interaction with the extrusion equipment is also very important and each type of polythene requires a certain different combination of processing conditions on each type of extrusion equipment in order to achieve the optimum film properties. That much can be achieved by adjustment of extrusion conditions and design of equipment has been shown, but there is undoubtedly still great scope for further research.

Literature References

1. Clegg, P. L., *Trans. Plast. Inst. 26,* 151 (1958); Rheology of Elastomers, p 174, Pergammon Press, London 1958.
2. Tordella, J. P., *J. App. Phys.* 27, 454 (1956); *Trans. Soc. Rheol. 1,* 203 (1957).
3. Bagely, E. B., Cabott, I. M., and West, D. C., *J. App. Phys.* 29, 109, (1958).
4. Clegg, P. L., Turner, S., and Vincent, P. I., *Plastics 24,* 31, (1959).
5. Supnik, R. M., and Adams, C. M., *Plast. Tech.* 2, 151, (1956).
6. Holmes, D. R., and Palmer, R. P., *J. Poly. Sci., 21,* 345, (1958).

Acknowledgments

The authors wish to acknowledge the considerable assistance of many colleagues in the Plastics Division of Imperial Chemical Industries Limited for their helpful discussions and criticisms and for the compilation of the data which have been included in this paper.

This article is a condensed version of the preprint appearing in Volume VII of the Technical Papers presented to the 17th Annual Technical Conference in Washington, D. C. January, 1961. The scope of the paper has not been changed but some minor points and most of the tabulated data upon which the arguments are based have been omitted.

Effect of Gamma Radiation on Chemical Structure of Plastics

V. J. Krasnansky, B. G. Achhammer, and M. S. Parker

Plastics Section,
National Bureau of Standards, Washington, D. C.

This article gives the order of stability of plastic films to radiation. Analysis of the products of polymer degradation suggest a close relationship between structure—branches and side chains—and stability to radiation

The stability of polymers on exposure to ionizing radiation has been studied extensively (1) and several attempts to correlate relative stability with chemical structure of polymers have been made (2, 3, 4). Such data are necessary to insure proper use of polymers in applications involving exposure to ionizing radiation.

This article reports on a study of the effects of Co-60 gamma radiation on the chemical structure of certain plastics. This study was part of a program to determine the utility of plastics as packaging materials in the high energy radiation preservation of food (5-10). Plastics films were considered because they provide flexible and transparent packaging materials. The effects of radiation on specific physical properties, such as tensile strength, elongation, and flexibility, have been studied previously by Sisman and Bopp (11). The materials chosen for this work were representative of various types of chemical structures. A previous study (12) is coordinated with this to present an evaluation of a wider spectrum of chemical structures.

The plastics films were exposed to Co-60 gamma radiation to a total dosage of 6 megarads, the suggested food sterilization dosage, and to other dosages for particular materials. The exposures were conducted in air and in vacuo. The gaseous products evolved as a result of the exposures were analyzed by mass spectrometry. Infrared spectrophotometry was used to detect any chemical structural changes.

Materials

The plastics materials used in this study and their structural formulas are given in *Table 1.*

All of the materials were obtained from commercial sources and were studied in film form except the polycarbonate which was studied only in powder form.

A 2500 curie Cobalt-60 gamma source at the National Bureau of Standards was used for all irradiations. This source, which is of the "swimming pool" type, was described in a previous paper (12). Dose rate was approximately 0.27 megarads per hour.

Procedure

The plastics films were cut into strips 3 inches wide, rolled up and inserted into glass tubes fitted with a break-off tip for mass spectrometric analyses. The specimens were evacuated to a pressure of 10^{-4} mm Hg for five days and then sealed off. The specimens which were to be irradiated in air were similarly evacuated to remove volatile impurities. The exposure tube was then filled with air at atmospheric pressure prior to sealing. To test the evacuation procedure the concentration of occluded gases in polyethylene films was measured. Samples of commercial polyethylene containing antioxidant were evacuated for three and five days and then fused in a xylene reflux bath at 137°C for four hours. The evolved gases were collected for analysis by mass spectrometry. Approximately 3×10^{-7} moles of air per gram of sample

Table 1. Plastic Films Studied

Type and Composition	Chemical Structure	Thickness inch
A. POLYESTERS		
1. Polyethylene Terephthalate (I) 2. Polyethylene terephthalate (II) (heat shrinkable)	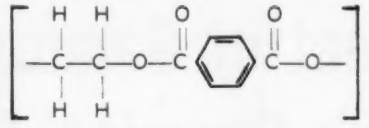	0.0005 0.0005
3. Polyethylene terephthalate and polyethylene isophthalate (III)	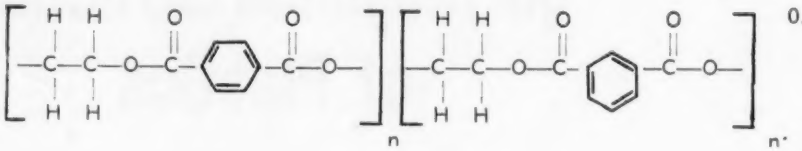	0.0005
B. POLYOLEFINS		
1. Polyethylene (density — 0.955)	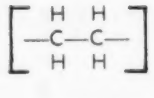	0.002
2. Polyethylene (density — 0.914)	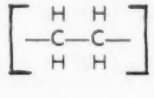	0.0015
3. Polypropylene	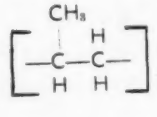	0.002
C. POLYAMIDES		
1. Hexamethylenediamine and adipic acid, 66	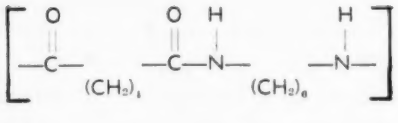	0.001
2. 11-amino undecanamide	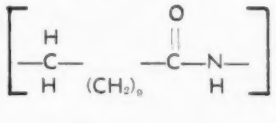	0.0017
3. Meta-xylylenediamine and adipic acid, MXD-6	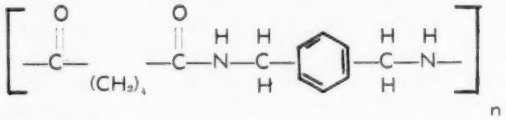	0.001 and 0.0015
D. MISCELLANEOUS		
1. Chlorinated Polyether	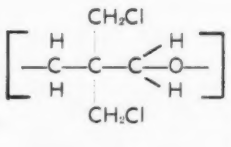	0.002
2. Polyacetal	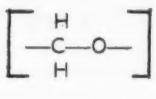	0.010
3. Polycarbonate	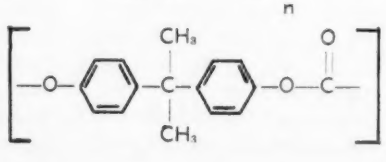	0.0015

was obtained from the specimen evacuated for three days while no gas was detected after five days evacuation.

After irradiation the gases evolved from the specimens were analyzed by mass spectrometry. The irradiated films were then examined by infrared spectrophotometry and the results were compared with those obtained with unirradiated films to determine the effects of the irradiation on the chemical structure of the films.

The magnitude of the errors inherent in these experiments was reduced by using specimens of approximately the same geometry, mass, and thickness. Errors introduced by diffusion of gases through the films were considered negligible.

Mass Spectrometer Analysis

The gas analyses were made on two Consolidated mass spectrometers at the National Bureau of Standards. The results are given in *Table 2* in mole percent. Traces of water in the products evolved from the specimens irradiated in vacuo are not included in the results.

Although efforts were made to maintain the mass and geometry of the specimens constant, different size specimens were used in several instances. The irradiation of eight rolls of polyamide 66 film, ranging in height from 0.5 to 3 inches and in weight from 0.1 to 3.6 grams, showed that the total amount of gas evolved per gram of sample as a result of a total dosage of 6 megarads was independent of the geometry and the size of the specimens used in this study.

The stability of the films was judged on the basis of total number of moles of gas evolved per gram of specimen exposed to the radiation in vacuo. It was assumed that the film giving the least amount of gas was the most stable. Undoubtedly this criterion of stability would not be satisfactory for many applications. For a better understanding of chemical changes occurring in an irradiated polymer and their relationship to stability, however, a knowledge of the amount and nature of gases evolved is necessary.

The materials given in *Table 3* are arranged according to the total amount of gases evolved. The first eleven materials evolved an amount of gaseous products less than five micromoles per gram sample as a result of irradiation: Polyamide MXD-6, polyester I, polyester III, polymonochlorotrifluoroethylene, polystyrene, rubber hydrochloride, chlorinated polyether, polyamide 11, polyamide 66, polycarbonate, and polyester II. The value of five micromoles was selected arbitrarily and should not be considered as having any special scientific significance. On the basis of this study these materials are suggested for primary consideration as packaging of foods for high energy radiation preservation. The remainder of the materials in *Table 3* are considered less stable because of greater evolution of gaseous products, although they may be quite acceptable for the application.

Selected polymers were irradiated to 36 and 3 megarads to study the effect of total dosage on the degradation mechanisms. The analyses of gases evolved are given in *Tables 4 and 5* in mole percent. Four polymers: polyamide MXD-6, polyamide 66, polyamide 11, and polyester III were irradiated to a 36 megarad dosage. The order of stability is polyamide MXD-6, polyester III, polyamide 66, and polyamide 11. The total number of micromoles of product per gram sample is 1.7, 17, 28, and 56, respectively. It was quite evident that polyamide MXD-6 was much more stable than the others at the higher dosage and that the general order of stability observed after 6 megarads dosage was retained.

Polyamide 66, and polyethylenes of low and high density were irradiated for a total dosage of 3 megarads. The mole percents of gases evolved are given in *Table 5*.

Table 2. Mass Spectra of Gaseous Products Evolved on Exposure to 6 Megarads of Gamma Radiation in Vacuum

PART A—POLYESTERS

Material Products	Polyester I	Polyester II	Polyester III
	Mole Percent		
Carbon Dioxide	56.3	82.0	24.0
Hydrogen	33.5	18.0	60.0
Carbon Monoxide	—	—	—
Butene	4.6	—	—
Pentene	1.6	—	—
Methyl Chloride	4.0	—	—
TOTAL	100.0	100.0	100.0

PART B—POLYOLEFINS

Material Products	Polyethylene High Density	Polyethylene Low Density	Polypropylene
	Mole Percent		
Carbon Dioxide	3.0	1.0	1.0
Hydrogen	92.0	91.0	95.0
Carbon Monoxide	5.0	1.0	1.0
Butane	—	3.5	—
Butene	—	1.5	—
Ethane	—	2.0	—
Methane	—	—	3.0
TOTAL	100.0	100.0	100.0

PART C—POLYAMIDES

Material Products	Polyamide MXD-6	Polyamide 11	Polyamide 66
	Mole Percent		
Carbon Dioxide	16.0	1.0	5.0
Carbon Monoxide	16.0	29.0	24.0
Hydrogen	68.0	66.0	71.0
Methane	—	4.0	—
TOTAL	100.0	100.0	100.0

PART D—MISCELLANEOUS

Material Products	Chlorinated Polyether	Polyacetal	Polycarbonate
	Mole Percent		
Carbon Dioxide	8.7	69.0	32.5
Hydrogen	85.8	7.5	1.5
Carbon Monoxide	—	—	66.0
Methyl Chloride	3.8	—	—
Methanol	—	2.0	—
Methane	—	15.0	—
Butene	1.4	—	—
Dimethyl Ether	—	6.5	—
Pentene	0.3	—	—
TOTAL	100.0	100.0	100.0

Table 3. Order of Stability of Plastics Films to Gamma Radiation[a]

Below 1 micromole	Polyamide MXD-6 Polyester I Polyester III Polymonochlorotrifluoroethylene[b] Polystyrene[b] Rubber hydrochloride[b]
1-5 micromoles	Chlorinated polyether Polyamide 11 Polyamide 66 Polycarbonate Polyester II
5-10 micromoles	Polyvinylidenechloride I[b, c]
10-15 micromoles	Polyethylene-coated Polyester[b] Polyvinylidene chloride II[b, c]
10-20 micromoles	Polyethylene (high density)[d] Polyethylene (low density)[d] Polypropylene
Above 50 micromoles	Polyacetal

[a] The order of stability is based on total pressure of gaseous products evolved on exposure in vacuum to 6 megarads of gamma radiation. The materials are arranged alphabetically in each range of pressures expressed in terms of number of micromoles per gram sample. No significance should be attached to the order of the materials in each pressure range.
[b] Data from reference 12 corrected for 6 megarad total dosage.
[c] Poly(vinylidene chloride) I and II each supplied by a different manufacturer.
[d] Data from this study and from Reference 12 corrected for 6 megarad total dosage.

The relative order of stability was the same as that observed at the 6 megarad dosage. The polyamide was more stable than the polyethylenes, producing 2.7 micromoles of gaseous product as compared to 8.2 and 8.3 micromoles of gaseous product from high density and low density polyethylenes, respectively.

The gases evolved from irradiated polyesters were principally hydrogen, carbon dioxide, and carbon monoxide. The methyl chloride and alkenes evolved from polyester I may be due to additives or impurities in the sample. The hydrogen chloride observed in the gases evolved from polyester III is believed to result from the breakdown of the coating on this material. The polyesters used in this study are aromatic esters and thereby have appreciable stability because of the energy sink of the phenyl group.

Table 4. Mass Spectra of Gaseous Products Evolved from Plastics Films on Exposure to 36 Megarads of Gamma Radiation in Vacuum

MATERIAL	POLY-AMIDE MXD-6	POLY-ESTER III	POLY-AMIDE 66	POLY-AMIDE 11
PRODUCTS		**MOLE PERCENT**		
Carbon Dioxide	25.0	20.0	1.5	0.5
Hydrogen	75.0	63.0	82.5	75.0
Carbon Monoxide	—	—	16.0	22.5
Methane	—	3.0	—	2.0
Hydrogen Chloride	—	14.0	—	—
Total	100.0	100.0	100.0	100.0

Table 5. Mass Spectra of Gaseous Products Evolved from Plastics Films on Exposure to 3 Megarads of Gamma Radiation in Vacuum

MATERIAL	POLYAMIDE 66	POLY-ETHYLENE (HIGH DENSITY)	POLY-ETHYLENE (LOW DENSITY)
PRODUCTS		**MOLE PERCENT**	
Carbon Dioxide	3.0	3.0	3.0
Hydrogen	71.0	90.0	91.0
Carbon Monoxide	26.0	6.5	—
Propane	—	0.5	2.5
Ethane	—	—	2.0
Ethene	—	—	1.5
Total	100.0	100.0	100.0

Hydrogen gas was the predominant volatile product in the irradiation of polyethylenes, followed by carbon dioxide, carbon monoxide, and in the case of the low density polymer, light hydrocarbons. The oxides may be a result of oxidation of the polyethylene prior to the irradiation.

The branches or side groups of polypropylene may be susceptible to cleavage by high energy radiation and this may account for the methane evolved and the absence of other light hydrocarbons in the gases evolved on irradiation of polypropylene.

The gases evolved from irradiated polyamides were predominantly hydrogen with relatively smaller varying quantities of carbon monoxide and carbon dioxide. The latter products may be a result of main chain fragmentation.

Lawton, Bueche, and Balwit (13) reported that nylon is crosslinked by ionizing radiation. Additional work in this laboratory extends this view to polyamide MXD-6. It was observed that polyamide MXD-6 upon exposure to cobalt-60 gamma radiation in vacuum to a total dosage

Table 6. Oxygen Absorbed as a Result of 6 Megarads Irradiation of Plastics Films in Air

MATERIAL	N_2/O_2
Air (Control)	3.78
Polyester II	3.90
Polyester I	4.22
Polyester III	4.47
Polyamide MXD-6	4.49
Polyethylene (Low Density)	4.62
Chlorinated Polyether	5.23
Polyamide 66	5.50
Polyethylene (High Density)	5.66
Polyacetal	8.82
Polyamide 11	11.84
Polypropylene	23.16

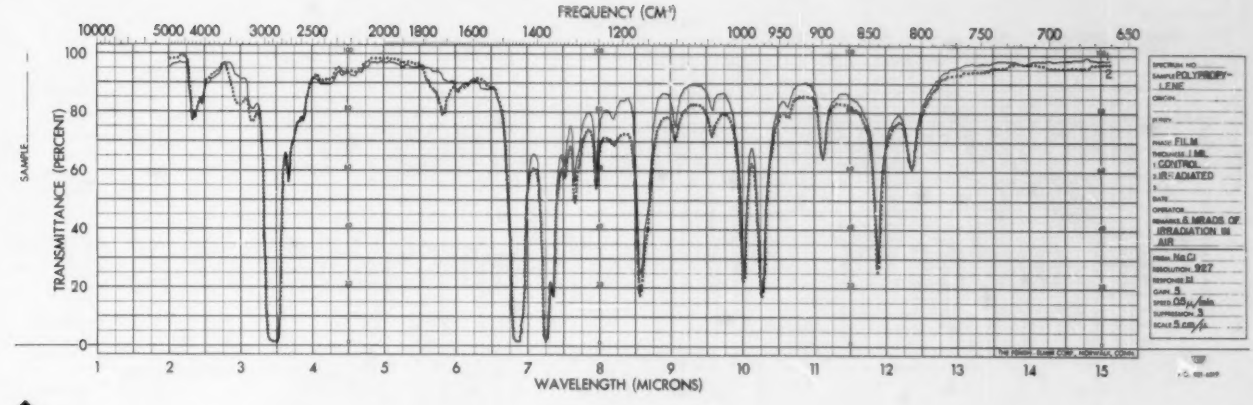
FREQUENCY (CM⁻¹)
10000 5000 4000 3000 2500 2000 1800 1600 1400 1200 1000 950 900 850 800 750 700 650
TRANSMITTANCE (PERCENT)
SAMPLE
WAVELENGTH (MICRONS)
1 2 3 4 5 6 7 8 9 10 11 12 13 14 15
POLYPROPYLENE
FILM
2 MIL
1 CONTROL
2 IR-IRRADIATED
6 MRADS OF IRRADIATION IN AIR
927
5 cm/μ

Figure 1. Polypropylene irradiated in air showed a slight increase in absorption at 5.8 microns—indicative of carbonyl formation, and at 2.9 microns—indicative of hydroxyl formation

of 1000 megarads was difficultly soluble in formic acid, in contrast to the ease of dissolving an unirradiated sample.

In the irradiation of chlorinated polyether the principal product is hydrogen. The methyl chloride and alkenes which are evolved suggest cleavage of the side groups and main chain, respectively. In polyacetal evolution of carbon dioxide, methane and light hydrocarbons suggest main chain cleavage. The polycarbonate yielded principally carbon dioxide, carbon monoxide, and relatively little hydrogen, suggesting some main chain cleavage.

Oxygen Absorption

The extent to which the films, irradiated in air, absorb oxygen was studied by the deviation of the ratio of nitrogen to oxygen in the products from the ratio in air. The ratios for the specimens irradiated in air are given in *Table 6*. The ratio obtained on a sample of air was 78.3/20.7 or 3.8. The materials exhibiting the greatest deviation were polypropylene, polyamide 11, and polyacetal with ratios of 23, 12, and 8.8, respectively. The others had ratios between 3.9 for polyester II and 5.7 for high density polyethylene.

The significant sorption of oxygen by polypropylene may be due to hydroperoxidation at the tertiary carbons. The tertiary hydrogens may be removed by irradiation and the free radical site then occupied by oxygen to form a peroxide which subsequently abstracts a hydrogen to form the hydroperoxide (14). No suitable explanation can be given at this time to explain the high oxygen absorption by polyamide 11. The polyacetal probably dissociates into [$-CH_2O-$] units which are then oxidized to formic acid and ultimately to carbon dioxide and water. Although water had been subtracted from the mass spectrometric results given in *Table 2*, it was observed condensed on the walls of the tube containing the irradiated polyacetal.

Infrared Spectrophotometric Analysis

Infrared spectra of the films were obtained on an Infracord or a Perkin-Elmer Model 21 spectrophotometer. The infrared spectra were determined before and after irradiation for a total dosage of 6 megarads in air and in vacuo to study changes in chemical structure. The polyesters, polyamides, polycarbonate, and polyethylenes showed no detectable changes.

A structural change in the polymers should be of the order of 2-3 percent before it can be detected by infrared spectrophotometry. Although polyethylene absorbed considerable oxygen as a result of a 6 megarad dosage, no oxidation was detected.

Polypropylene showed no change between the unirradiated specimens and those irradiated in vacuo. However, polypropylene irradiated in air showed a slight increase in absorption at 5.8 microns—indicative of car-

Figure 2. Chlorinated polyether showed increases in both hydroxyl and carbonyl concentration

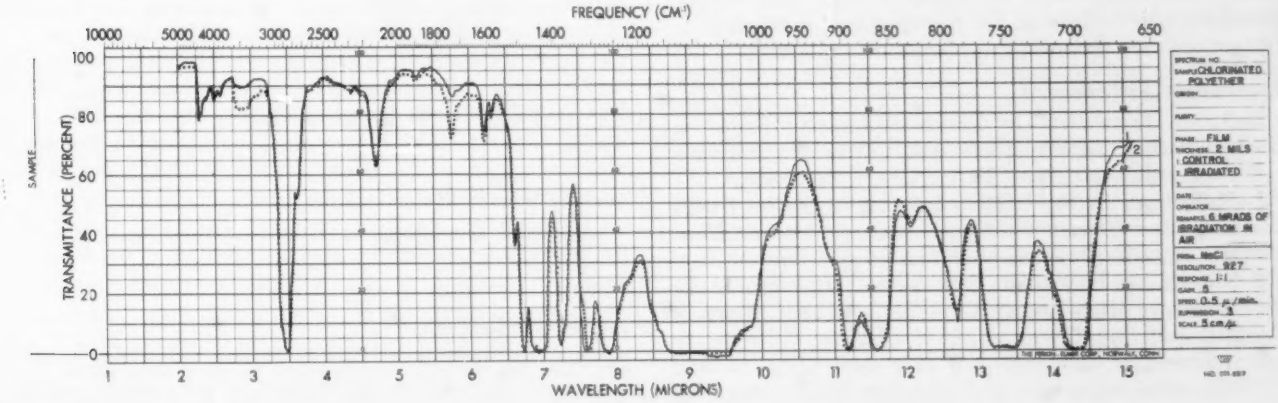
FREQUENCY (CM⁻¹)
10000 5000 4000 3000 2500 2000 1800 1600 1400 1200 1000 950 900 850 800 750 700 650
TRANSMITTANCE (PERCENT)
SAMPLE
WAVELENGTH (MICRONS)
1 2 3 4 5 6 7 8 9 10 11 12 13 14 15
CHLORINATED POLYETHER
FILM
2 MILS
1 CONTROL
2 IRRADIATED
6 MRADS OF IRRADIATION IN AIR
927
5 cm/μ

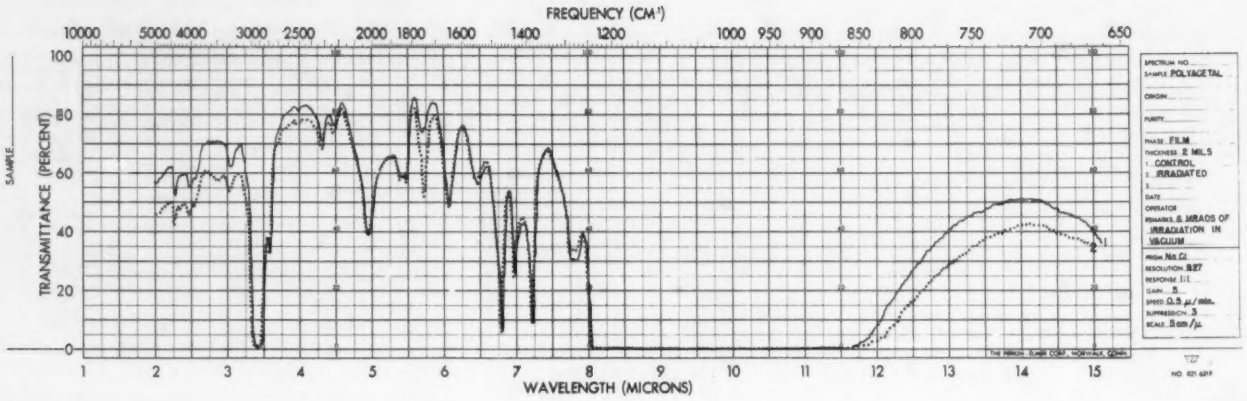
FREQUENCY (CM⁻¹)
10000 5000 4000 3000 2500 2000 1800 1600 1400 1200 1000 950 900 850 800 750 700 650
TRANSMITTANCE (PERCENT)
100 80 60 40 20 0
SAMPLE
1 2 3 4 5 6 7 8 9 10 11 12 13 14 15
WAVELENGTH (MICRONS)
SAMPLE POLYACETAL
PHASE FILM
THICKNESS 2 MILS
1 CONTROL
2 IRRADIATED
REMARKS 6 MRADS OF IRRADIATION IN VACUUM
RESOLUTION SLIT
SPEED 0.5 μ/min.
SUPPRESSION 3
SCALE 5 cm/μ

Figure 3. Polyacetal film showed strong carbonyl and weak hydroxyl adsorption after irradiation both in air and vacuo

bonyl formation, and at 2.9 microns—indicative of hydroxyl formation (See *Figure 1*). The chlorinated polyether irradiated in air showed increases in both hydroxyl and carbonyl concentration (See *Figure 2*). The polyacetal showed strong carbonyl and weak hydroxyl adsorption after irradiation both in air and vacuo (See *Figure 3*). No differences were observed between the specimens irradiated in air and in vacuo. Presumably the carbonyl and hydroxyl formation were due primarily to chain sciesion, and not oxidation.

Physical Observations

No visible changes in the characteristics of the films were observed except the embrittlement of the polyacetal and discoloration of the polyamides MXD-6 and 11. All films were colorless prior to irradiation except the polyacetal which was milky white. Upon irradiation the polyamide MXD-6 turned to a straw color and the polyamide 11 turned to a very faint yellow at higher dosages.

Conclusions

The results of this study indicate that the materials most stable to irradiation contain a phenyl group, an amide linkage, and possibly chlorine atoms. Five of the materials which produced less than five micromoles per gram of sample contain a phenyl group. None of the less stable polymers contains this group. The addition of an amide linkage seems to increase the stability of polymers containing the phenyl group. This stability is attributed to the ionic character of the amide linkage (15). No explanation can be offered for the apparent stabilizing effect of chlorine atoms in the polymer composition.

Literature References

1. Bovey, Frank A., The Effects of Ionizing Radiation on Natural and Synthetic High Polymers, Interscience Publishers, New York, New York (1958).
2. Ballantine, D. S., "Highly Intense Radiation Fields and Their Effects on High Polymers", *Modern Plastics 32*, 131 (November 1954).
3. Saeman, J. F., Millett, M. A., and Lawton, E. J., "Effect of High Energy Cathode Rays on Cellulose", *Ind. and Eng. Chem. 44*, 2848 (1952).
4. Achhammer, B. G., Tryon, Max, and Kline, G. M., "Chemical Structure and Stability Relationships in Polymers", Kunststoffe *49*, 600 (November 1959); *Modern Plastics, 37*, No. 4, 131 (December 1959).
5. Hannon, R. S., "Research on the Science and Technology of Food Preservation by Ionizing Radiations", Chemical Publishing Company, Inc., New York, New York (1956).
6. Proctor, B. E., and Goldblith, S. A., "Radiation Fundamentals and Their Applications in Food Technology", Advance in Food Research 3, 119-196 (1951).
7. Clifcorn, L. E., "The Food Industry's Attitude Toward Radiation Sterilization", *Nucleonics 13* (1), 39-41 (1955).
8. Proctor, B. E., Lockhart, E. E., Goldblith, S. A., Grundy, A. V., Tripp, G. E., Karel, M., and Brogle, R. C., "The Use of Ionizing Radiations in the Eradication of Insects in Packaged Military Rations", *Food Technology 8* (12), 536-540 (1954).
9. Le Clair, H. G., and Cobbs, W. H., Jr., "Effects of Radiation on Plastics Packaging Films", *Ind. Eng. Chem. 50*, 323 (1958).
10. Karel, M., and Proctor, B. E., "Cathode-Ray Irradiation of Cellophanes", *Modern Packaging 30* (5), 141-148, 202, 205 (January 1957).
11. Sisman, O., and Bopp, C. D., "A Summary of the Effects of Radiation on Some Plastics and Elastomers", *ASTM Special Publication No. 208*, 119 ('57).
12. Bersch, C. F., Stromberg, R. R., and Achhammer, B. G., "Effect of Radiation on Plastic Films", *Modern Packaging 32*, 117 (August 1959).
13. Lawton, E. J., Bueche, A. M., and Balwit, J. S., "Irradiation of Polymers by High Energy Electrons", *Nature 172*, 76 (1953).
14. Jellinek, H. H. G., Degradation of Vinyl Polymers, Academic Press Inc., Publishers, New York, New York (1955). See pages 223-229.
15. Little, K., "The Effect of High Doses of Ionizing Radiations on Organic High Polymers", *A.E.R.E., Harwell Report No. GP/R 1402* (1957).

This research was sponsored by Headquarters, Quartermaster Research and Engineering Command, Natick, Mass.

Acknowledgment

The authors thank the members of the Mass Spectrometry Section, 4.03, and the Molecular Structure and Properties of Gases Section, 5.07, of the National Bureau of Standards for the mass spectrometric analyses.

Inorganic-Organic High Polymers, Phenoxyaldehyde Resins of Titanium (IV) and Hafnium (IV)

R. J. Landry *and* **E. H. Bartel**

U.S. Naval Ordnance Test Station, China Lake, Calif.

This article describes preparation of hafnium and titanium phenoxide high-temperature resistant resins. It also suggests the possibility of combining such exotic elements as columbium and tantalum into copolymers of phenolic derivatives. . . .

The Materials Engineering Branch of the Engineering Department at U. S. Naval Ordance Test Station at China Lake, California, has been evaluating potential calorobic materials (1) for the past six years. Approximately 200-300 materials have been evaluated by various methods. A compression-molded physical mixture of titanium carbide, zirconium oxide or zirconium boride and CTL-91LD (Cincinnati Testing and Research Laboratories phenol-formaldehyde resin) gave excellent results as the nozzle insert part of a miniature combustion chamber, or subcalibre rocket motor (2, 3). A chemical combination of either of the above mentioned mixtures therefore should produce superior calorobic nozzle materials. Feasibility of chemically replacing part of the carbon with titanium, zirconium, hafnium or other metals in the phenolic resin structure was therefore investigated.

Titanium phenoxide and zirconium phenoxide (solvated) have been prepared by Funk and Roglet in 1944 (4), but hafnium phenoxide has never heretofore been prepared. The phenoxides are the intermediate products in the reaction process during the formation of phenoxyaldehyde resins. Phenoxyaldehyde resins of zirconium (IV), hafnium (IV), tantalum (V) and columbium (V) have never heretofore been reported in the literature.

Hafnium oxide, in the presence of graphite (charred areas of phenolic resin binder at the nozzle surface) at high temperatures may be converted to hafnium carbide. Titanium, zirconium and other metals can be assumed to behave in a like manner and the chemical kinetics of these polymers at high temperature will determine the calorobic value of the compounds. The hafnium and titanium resins of this series have been prepared by the U. S. Naval Ordance Test Station, inasmuch as they are considered to be the most promising of the series.

Preparation of Titanium (IV) Phenoxide by Double Decomposition

Titanium phenoxide is prepared by heating titanium tetrachloride in the presence of excess phenol. Hydrogen chloride gas is evolved as a by-product during the refluxing operation. The equation for the chemical reaction is:

$$TiCl_4 + 5C_6H_5OH \rightarrow Ti(OC_6H_5)_4 \cdot C_6H_5OH + 4HCl$$

60 grams of titanium chloride and 400 grams of phenol are introduced into a 3 neck resin flask having a condenser attached to one of the necks with a drying tube and liquid trap at the upper extremity. The resin flask is made in two approximately equal parts, the lower part being cylindrical and the upper part hemispherical. The upper part, with 3 neck outlets, is joined to the lower part by a peripheral flange which is sealed with a silicone grease. An aspirator-filter-pump hose attached to the liquid trap bottle evacuates the system. All mixing operations were conducted in a chamber under dry nitrogen atmosphere. Two thermometers were inserted in the other two flask necks, one with the bulb dipping in the liquid phase and the other bulb exposed to the gas phase. The resin flask containing a teflon coated

magnetic stirrer rests on a "Thermo-Stir" heater (The Scientific Glass Co.). The liquid is refluxed under a vacuum with the maximum liquid temperature being 264°F and the maximum gas temperature 195°F until the evolution of hydrogen chloride gas ceased. During the refluxing operation a reddish-orange precipitate of titanium (IV) phenoxide will appear. After the hydrogen chloride gas evolution ceased, the precipitate is allowed to settle to the bottom of the resin flask and the upper layer is decanted. The impure titanium (IV) phenoxide crystals are then washed on a Buchner funnel under vacuum with a minimum amount of carbon tetrachloride followed by a rinse with hexane. The purified crystals are finally dried in a vacuum to remove the last trace of hexane. The reddish-orange titanium (IV) phenoxide (solvated) crystals are soluble in benzene, carbon tetrachloride and carbon disulphide The crystals are slowly decomposed by water and converted to a yellow crystalline material. The purified titanium (IV) phenoxide (solvated) (1) crystals melt at 320°F (50% yield) as reported in reference 4.

Titanium (IV) Phenoxide Preparation by Ester Interchange

$$Ti(OPr)_4 + 4C_6H_5OH \rightarrow Ti(OC_6H_5)_4 + 4PrOH$$

Titanium-(IV) tetra-iso-propoxide	Phenol	Titanium-(IV) tetra-phenoxide	Isopropyl Alcohol

188.2 grams of phenol was placed in a one liter, three necked, round bottom flask. The phenol was dissolved in 100 ml. of toluene. The flask was fitted with a stirrer, addition funnel and a condenser. The solution was heated using an oil bath. After about 25 ml. of the toluene had been distilled out, the addition of $Ti(OPr)_4$ was started, while stirring. The oil bath temperature was maintained at 130°F. 143 ml. of $Ti(OPr)_4$ was added drop-wise over a 30 minute period. The PrOH distilled from the reaction vessel slowly. The oil bath temperature was increased to 155°F. Residual isopropyl alcohol was removed under reduced pressure over a two hour period. The product is a dark red solid.

Titanium (IV) Phenoxyaldehyde Resin Preparation

The purified titanium (IV) phenoxide (25.7 grams) was mixed with paraformaldehyde (16.2 grams) and then heated slightly to initiate the reaction (130°F). At the fusion point of the mass, heating is terminated and an exothermic reaction continued. The temperature was recorded during polymerization. *Figure 1* indicates that larger batches would require cooling. This polymerization reaction was carried out in a dry box under dry nitrogen atmosphere and a viscous homogeneous reddish-brown resin was obtained. The resin was polymerized to a solid infusible plastic material in a compression press mold at 400°F for 15-30 minutes under a pressure of about 5000 psi. The formaldehyde to titanium (IV) phenoxide mole (gram molecular weight) ratio must be greater than 5 in order to obtain an infusible solid. An insufficient quantity of paraformaldehyde produces a fusible polymer, which softens at higher temperatures. *Figure 2* shows crystals of the titanium (IV) phenoxide prepared.

Hafnium (IV) Phenoxide Preparation by Double Decomposition

Hafnium (IV) phenoxide (*Figure 3*) was prepared by the same method as titanium (IV) phenoxide. 75 grams of dry 95-96% pure hafnium tetrachloride (Millmaster Chemical Co.) was treated with 150 grams of phenol (Barrett or Oronite) heated to boiling then refluxed until evolution of hydrogen chloride gas ceased.

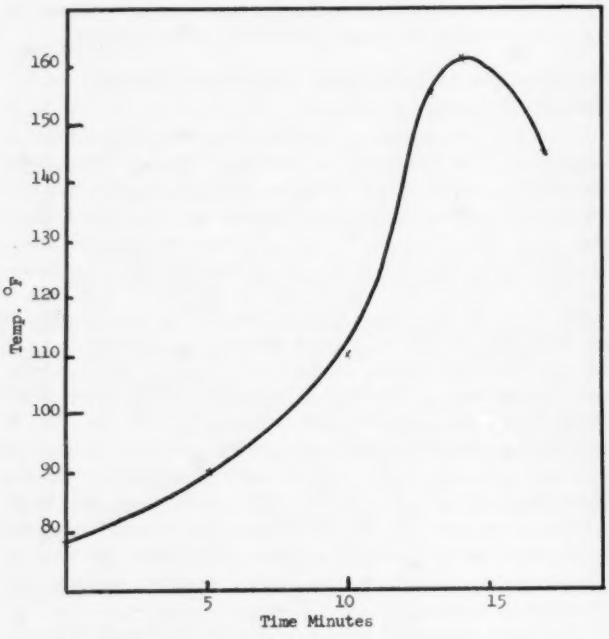

Figure 1. Exothermic reaction curve (hafnium phenoxyaldehyde)

Figure 2. Crystals of titanium phenoxide

The reddish-brown molten residue was separated from the mother liquor by decanting the liquid followed by washing with carbon tetrachloride and hexane and finally dried under a vacuum. Light yellow (almost white) hafnium (IV) phenoxide (melting point 327°F) resulted. The hafnium (as metal) obtained by analysis was 27.7% which is the theoretical calculated quantity.

Hafnium (IV) Phenoxyaldehyde Resin

Two different processes were employed in the preparation of the hafnium resin; namely the paraformaldehyde and acetal methods.

The Paraformaldehyde Method—32¼ grams of the purified hafnium phenoxide was mixed with 13½ grams of paraformaldehyde and heated slightly to initiate the reaction. An exotherm of 320°F was obtained with a 40 gram batch mixture. The product had an amber to light brown color. The decomposition temperature preceded the heat distortion point in a manner characteristic of phenolaldehyde resins.

Glacial acetic acid was evaluated as a catalyst (5) in one experiment, and no noticeable difference was detected. The hafnium (as metal) obtained was 22.5% by analysis.

The Acetal Resin—Acetal polymers such as Du Pont's Delrin resin are sources of aldehyde upon heating. Acetal resin was pulverized in a hammer type pulverizer mill to pass 100% through a 200 mesh sieve. 2.7 grams of the resin was mixed with 6.45 grams of the hafnium (IV) phenoxide, and the same procedure as the paraformaldehyde method was followed. The resulting resin was not as highly colored as the one obtained by the paraformaldehyde method. This resin was cured at 410°F to yield a brittle solid, therefore, was not evaluated further.

Compression Molded Nozzle Inserts and Cylindrical Shapes

Small cylindrical discs and nozzle inserts for a subcalibre experimental rocket were compression molded to shape from 50% by volume of hafnium or titanium resin and 50% titanium carbide powder as filler. The molding temperature was 400°F and pressure was 5000 psi.

Two mixing methods were employed (1) the two-roll mill method and (2) the hand mixing method. In the first method, the raw materials are shaped between two (2") rolls of a mill without circulating cold water until homogeneous and then introduced into the compression-mold cavity. In the second method, the raw materials are mixed by hand then transferred to the mold cavity. Hafnium resin nozzles made by the roll-mill method are shown in *Figures 4 and 5*. The results of the rocket firing is shown in *Figure 4*. Scrapings of the inner-peripheral surface of the nozzle will be analyzed for hafnium carbide at a future date.

The ratio of formaldehyde to hafnium (IV) phenoxide is as important as the reaction between phenol and formaldehyde in the preparation of conventional calorobic phenolformaldehyde resins. The resin was polymerized to an infusible solid by heating the phenoxyaldehyde mixture to 400°F and 760 mm pressure with a mole ratio of formaldehyde to phenoxide of 9/1. At a mole ratio of 5 to 1 an incompletely cured resin resulted

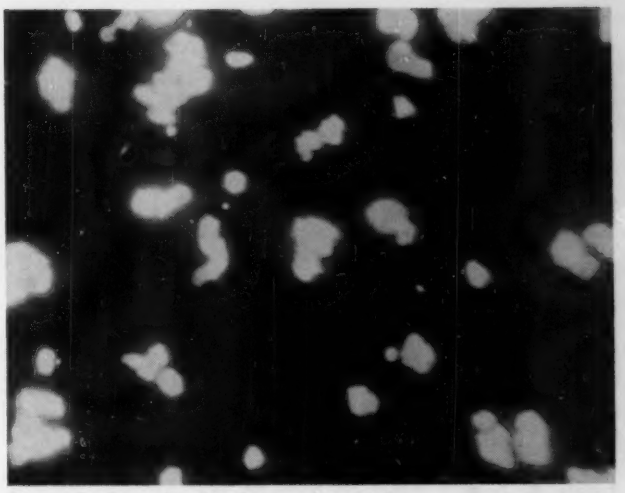

Figure 3. Crystals of hafnium phenoxide

which softened at high temperatures. At 300°F and ambient pressure, this resin was not satisfactorily cured. Further investigation is necessary to establish the optimum temperature, pressure and proper catalysts to produce optimum properties of the resin. Barcol hardness of nozzles shown in *Figures 4 and 5* are approximately 75, which compares favorably with similar calorobic-material nozzles made with phenolic resin and titanium carbide. Several nozzles were compression molded before a satisfactory uncracked nozzle was obtained.

Pyrolysis of Zirconium, Titanium, and Hafnium-Phenoxy-Formaldehyde

It is assumed, in the pyrolysis of the zirconium phenoxy-formaldehyde resin, that the residual zirconium oxide will be converted to the carbide (melting point 6386°F). It will not be converted to the zirconium cyanonitride, because of the excess carbon present (6). This reaction will occur at the nozzle surface exposed to the flowing exhaust gases during the combustion process. The gases and solid by-products from the nozzle material absorb energy, and the final solid products are assumed to be graphite and the carbides of zirconium, titanium, or hafnium.

The stability of one of these carbide nozzles would be determined by the environment. Zirconium carbide is unaffected by nitrogen or ammonia to 3270°F, and the nitride will form in the presence of hydrazine (at 1100-1300°F) which is explosive with potassium perchlorate at high temperatures (6). It is anticipated that the titanium and hafnium carbides will behave in a similar manner.

Conclusions and Recommendations

Glacial acetic acid as a catalyst in the paraformaldehyde reaction inhibits the formation of hydrous zirconia if the pH is less than 7.0 (7). Investigation of other catalysts is indicated.

Brittleness of the resins investigated can be minimized by (1) reducing the cross-linking of the phenoxide resin by blocking the para position of the phenol with preferably a methyl or other group; paramethyl phenol (Cresol) or other phenolics will therefore have to be substituted for phenol as a raw-material, (2) selecting dicyclopentadienyl-metal-dichloride of hafnium, titanium,

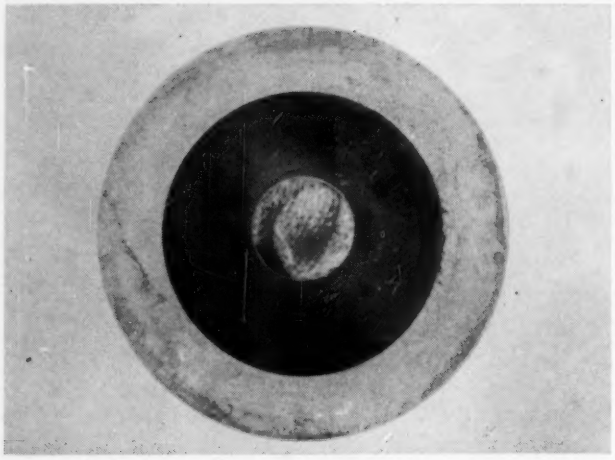

Figure 4. Nozzle insert of hafnium resin-titanium carbide (before firing)

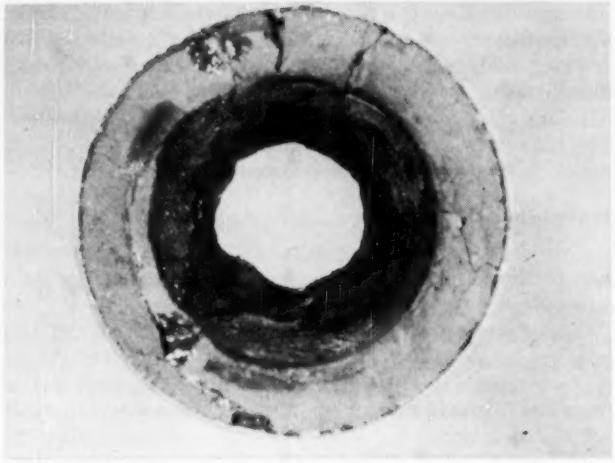

Figure 5. Nozzle insert of hafnium resin-titanium carbide mill mix (after firing)

or zirconium as raw materials instead of the metal tetrachloride and selecting a dicyclopentadienyl-metal-trichloride of columbium and tantalum instead of the metal pentachloride. Brittleness can also be prevented by using fibrous fillers.

Dicyclopentadienyl-tantalum (V)-triphenoxide could be prepared from the dicyclopentadienyl-tantalum (V)-trihalide then reacted with the aldehyde to form a resin. The same reaction is expected of columbium.

Dicyclopentadienyl-hafnium (IV)-diphenoxide may be derived from dicyclopentadienyl-hafnium (IV)-dichloride and reacted with an aldehyde to form the corresponding diphenoxy-aldehyde resin. Analogous resins of zirconium and titanium may be synthesized in this manner.

The molecular weight determinations of the intermediate titanium (IV)-phenoxide have shown it to be a monomer.

An infrared analysis of the resin would indicate the chemical structure and differential thermal analysis would shed information on the pyrolytic products.

The highest melting point (7619°F) of any known material is that of the system 4TaC + HfC (6). This system may be obtained as a pyrolytic by-product of a high polymer or of a hybrid mixture formed at the boundary of the nozzle surface during the rocket motor combustion period. The three approaches are to produce (a) a block polymer (b) a copolymer, and (c) a physical or hybrid mixture of tantalum and hafnium carbide. A block polymer may be formed by reacting the B-stage resin, or a lower degree of polymerization polymer of each of the hafnium (IV) phenoxyaldehyde with tantalum (V) phenoxyaldehyde. A copolymer of tantalum (V) phenoxyaldehyde and hafnium (IV) phenoxyaldehyde may be formed by mixing the proper molecular ratios of the hafnium and tantalum monomers with an aldehyde.

The physical mixture would consist of the TaC-HfC filler with hafnium (IV) phenoxy-formaldehyde resin as the binder. Hot pressed or sintered carbides of hafnium and tantalum have been prepared, but the difficulties and costs encountered in processing would restrict the use of the components so produced. The ease of forming the plastics components, and their consequent lower cost, would impose no such limitation on their application in the rocket propulsion field. The percentage of hafnium and tantalum present as a carbide will be lower than that obtained by the sintered process, but the high concentration of the graphite by-product may prove to be an advantage.

A solution of the hafnium and other resins mentioned above could be impregnated into porous graphite for evaluation as a calorobic material. Investigation of aldehydes other than those evaluated may be indicated.

Literature References

1. Porter, H. B. "What In Blazes Is High Temperature?" *Missiles and Rockets*, February 15, 1960 p. 24
2. Engineering Department, U. S. Naval Ordance Test Station, China Lake, Calif. "Some Results of Applied Research On Materials and Processes For Providing Heat-Resistant Rocket Components" *NAVORD Report 6390 and NAVWEPS Report 6390 Supplement 1*
3. Herzog, S. H. and Donaldson, W. E. "Ablation and Erosion In The Missile Environment" Parts I and II, U. S. Naval Ordnance Test Station China Lake, Calif. September 2, 1960. Paper delivered at the Third Pacific Area National Meeting of the American Society For Testing Materials. (1916 Race St. Philadelphia 3, Pa.) in San Francisco, Calif. October 11-16, 1959
4. Funk, H. and Roglet, E. "The Reaction of Some Metal Chlorides With Phenol and 2-Naphthol" Z. *Anorg. Chem.* 252, 323-328, 1944 of Chem. Abstract 40, 43117
5. Bradley, D. C. and Wardlow, W. "Zirconium Alkoxides" *Journal Chemical Society* (1951) p. 280
6. Blumenthal, W. B. "The Chemical Behavior of Zirconium" Van Nostrand, Princeton, N. J. c1958 pp 58-59
7. Bradley, D. C. and Wardlow, W. "Zirconium Alkoxides" *Journal Chemical Society* (1951) p. 351
8. Bailar, J. C. "Chemistry of the Coordination Compounds" Reinhold, N. Y. c1956 pp. 16, 393
9. Schlenker, F., "Epoxy Resin Compositions Containing Polyvalent Metal Phenolates or Phenol-Aldehyde Resins and The Process of Their Production" U.S. Patent 2,837,493, June 3, 1958

Resins from Cyclohexene Oxide Derivatives and Fatty Acids

C. W. McGary, Jr. and C. T. Patrick, Jr.

Union Carbide Chemicals Company
South Charleston, West Virginia

How concentrations of flexibilized curing agents and initiators affect flexibility and hardness of epoxy resins

Certain epoxy resins are useful in many applications that require mechanical and thermal shock resistance, such as potting and encapsulating electrical components. Resins have been prepared from glycidyl polyethers of bisphenol A and flexibilizing curing agents such as polyamides, polysulfides, reactive polyesters, polyisocyanates, and polymerized fatty acids (1). Flexible resins also have been obtained by using glycidyl polyethers of long-chain polyhydric alcohols. Many of these curable formulations, however, are expensive and have high viscosities and short pot lives; furthermore, the cured resins are often more rigid than desired and they tend to embrittle on aging. An investigation of resins derived from cyclohexene oxide derivatives and certain flexibilizing curing agents, accordingly, was undertaken.

It has been observed that certain cyclohexene oxide derivatives react faster than glycidyl ethers with carboxylic acids (3). For example, Unox epoxide 201*, 3,4-epoxy-6-methylcyclohexylmethyl, 3,4-epoxy-6-methylcyclohexanecarboxylate, and adipic acid react rapidly at 110-160°C,** and a crosslinked resin having a deflection temperature of 95° is formed at a carboxyl-epoxide ratio of 0.5. It was proposed that two reactions are responsible for the thermosetting polymerization.

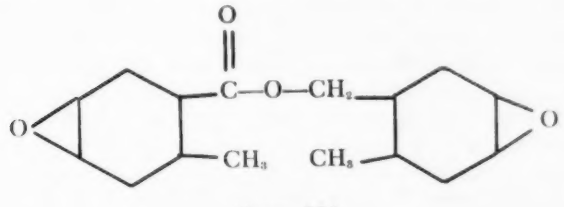

Unox 201

(1)

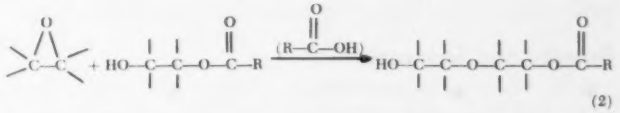

(2)

Diglycidyl ethers and dicarboxylic acids, in comparison, react stoichiometrically (reaction 1) in the presence of basic initiators and yield fusible, linear polymers. Reaction 2, however, can be accelerated by using either cyclohexene oxide derivatives or acidic catalysts, such as stannic chloride.

Epoxide 201 and dimerized unsaturated fatty acids react rapidly at 160-200° to form a gelled resin. The resins, however, cure very slowly after gelation, and tough, useful resins are not obtained without long, high temperature cures. In the presence of initiators such as stannous octoate, reaction occurs readily, and fully cured

* Trademark Union Carbide Corp.

** All temperatures in degrees centigrade

resins are obtained under mild curing conditions. This article is concerned with the resins derived from epoxide resin 201, polymerized fatty acids and stannous octoate.

Experimental

The materials were commercial products. The 201 resin, which is a diepoxide, had an epoxide equivalent weight of 156, a viscosity of 1450 cp. at 25°, and was substantially free of inorganic impurities. Commercial stannous octoate was used. Several fatty acid derivatives were used, as follows:

Material	Acid Composition, % Monomer	Dimer	Trimer
Tall oil acid (Unitol OT, Union Bag—Camp Paper Corp.)	100	0	0
Harcure dimer-870 (Harchem Div., Wallace and Tiernan, Inc.)	30-40	—60-70—	
Empol 1014 (Emery Industries, Inc.)	1	95	4
Empol 1022 (Emery Industries, Inc.)	3	75	22
3162-D (Emery Industries, Inc.)	0	21	79

The shelf life at 25° of a 60-g. sample of 201 resin fatty acid mixture was defined by viscosity measurements using a Brookfield viscometer, model LVF. Peak exotherm temperatures and gel times were obtained for 35-g. mixtures in stoppered, 4-oz. bottles in a circulating-air oven. The temperature in the center of the mixture was indicated by a thermocouple, and the gel time was arbitrarily recorded when a dropped lead shot did not penetrate the resin surface.

The ultimate tensile strength and percentage total elongation were determined at 23° in accord with ASTM method D638-58T at a speed of 0.2 in. per min. Several of the semi-rigid resins had yield points at about 10% elongation; it is believed that energy generated during the test raised the temperature above the deflection temperature in these cases. Deflection temperatures were obtained on 5 by ½ by ½ in. specimens by ASTM method D648-56 using a fiber stress of 264 psi. The Shore Durometer (type D) hardness was taken 10 seconds after penetration at 23° (ASTM method D1484-57T).

Results and Discussion

The effect of concentration of the 201 resin, dimer acid, and stannous octoate on the properties of cured resin was intensively investigated. Apparently, optimum physical properties, which do not change on aging, are obtained when the active groups react completely during the initial cure. *Table 1* shows the effect of stannous octoate concentration on properties for a resin derived from 0.5 carboxyl group for each epoxide group. At 0.5% concentration the highest deflection temperature, the lowest weight loss, and the smallest change in hardness upon aging at 120° were observed. Similar data were obtained for carboxyl-epoxide ratios of 0.3, 0.4, and 0.6 all indicating that 0.5% initiator is most effective in the 3 categories mentioned. At the lower carboxyl ratios the resins were more resistant to change on thermal aging; for example, at a 0.4 ratio with 0.5% initiator the hardness changed from 80 to 82 after aging and the weight loss was 0.2%. In all cases 0.5-2.0% of stannous octoate was very effective in producing stable resins. Concentrations outside this range gave resins that were more sensitive to thermal aging. It was observed that stannous octoate was somewhat deactivated by water and by basic materials, and therefore, 1-2% of initiator may be desirable if these contaminants are present.

The proportion of 201 resin and dimer acid had a marked influence on hardness and tensile properties of the resins as illustrated in *Table 2*. Change in the tensile properties upon aging correlates very well with change in hardness. The data indicate that 0.3-0.6 carboxyl group for each epoxide group produces satisfactory resins

Table 1. Effect of Stannous Octoate Concentration on Resin Properties[a]

Property	Stannous Octoate Conc., Wt. % 0.1	0.25	0.5	1.0	2.0	4.0	6.0
Deflection temp., °C.	11	17	43	41	31	13	6
Wt. loss, %[b]	2.3	1.8	1.2	1.7	2.3	4.7	6.0
Hardness, Durometer D							
Initial	47	65	78	78	76	58	43
24 hrs. at 120°	62	68	79	80	79	70	59
2100 hrs. at 120°	82	81	80	82	82	79	78

[a] Parts: Unox 201, 51; Empol 1022, 49 (0.5 carboxyl per epoxide). Cure: 2 hrs. at 120°, 4 hrs. at 160°.
[b] After aging 2100 hrs. at 120°.

Table 2. Physical Properties of 201 Resin—Acid Derivative (Emery-1022) Resins After Aging at 120°

Property	Aging Time, hrs.	Formulation, Carboxyl-Epoxide[a] 0.3	0.4	0.5	0.6	0.7	b
Tensile, psi	0	7000	4800	2400	1100	200	365
	48	6200	5100	2500	1300	300	438
	120	6900	5300	3000	1600	500	512
	240	7000	4700	3000	2000	1000	1285
Elongation, %	0	10	17	45	250	340	421
	48	15	14	50	170	180	189
	120	14	15	30	130	170	53
	240	16	18	35	100	100	6
Hardness, Durometer D	0	81	78	74	42	12	22
	48	81	79	76	50	22	28
	120	82	78	78	56	28	31
	240	82	79	78	61	42	37

[a] Initial cure cycle: 0.5 hr. at 80°, 1 hr. at 100°, 1 hr. at 120°, 4 hrs. at 160°; 2% stannous octoate.
[b] Diglycidyl ether of bisphenol A (38.5 g.), Emery trimer 3162-D (61.5 g.), and DMP-30 (1 g.). Cure: 3.5 hrs. at 120°.

Table 3. How Resin Properties Can Be Changed By Using Hardeners With Various Amounts of Trimer, Dimer and Monomer Acids

Formulation, parts	1	2	3	4	5
Unox 201	100	100	100	100	100
Trimer 3162-D	99				
Empol 1022		97		58	
Empol 1014			94		
Tall oil acid				34	
Harcure dimer 870					117
Stannous octoate	2	2	2	2	2
Properties of Mixture					
Viscosity (initial), cp. 25°	4100	1850	1860	520	1970
Pot life (time to 10,000 cp.), hrs. at 25°	8	16	20	50	28
Cure			**1 hr., 120°; 1 hr., 160°**		
Mechanical Properties					
Deflection temp., °C.	55	43	45	19	10
Hardness, Durometer D	79	78	77	40	60
Izod impact, ft.lb./in. notch	0.8	0.6	0.7	1.1	1.0
Tensile strength, psi	5500	3300	3400	700	2000
Elongation, %	9	40	40	240	140
Electrical Properties					
Dielectric strength, volts/mil stepwise	429	426	414	418	448
Surface resistivity, megohms	$>2 \times 10^7$	$>2 \times 10^7$	$>2 \times 10^7$	$>2 \times 10^7$	$>2 \times 10^7$
Volume resistivity, megohms-cm.	$>6.1 \times 10^7$	$>6.0 \times 10^7$	$>5.6 \times 10^7$	$>5.6 \times 10^7$	$>5.7 \times 10^7$
Dielectric constant, K (a) cycles/sec. at 23°					
60	2.85	2.71	2.75	3.18	3.14
10^3	2.82	2.64	2.83	2.99	2.97
10^6	2.42	2.26	2.30	2.44	2.44
(b) cycles at 80°					
60	3.37	3.71	3.78	4.49	4.69
10^3	3.01	3.25	3.25	4.18	4.25
10^6	2.49	2.39	2.47	2.89	2.98
(c) cycles at 135°					
60	3.82	3.78	3.82	4.16	4.31
10^3	3.80	3.78	3.79	4.12	4.29
10^6	2.96	3.04	3.02	3.52	3.61
(d) cycles at 175°					
60	3.69	3.65	3.59	4.06	4.54
10^3	3.66	3.61	3.56	3.73	4.09
10^6	3.30	3.30	3.26	3.50	3.77
Dissipation factor (a) cycles at 23°					
60	0.0063	0.0116	0.0119	0.0398	0.0335
10^3	0.0064	0.0095	0.0090	0.0284	0.0256
10^6	0.0080	0.0072	0.0075	0.0137	0.0123
(b) cycles at 80°					
60	0.0710	0.0659	0.0652	0.0320	0.0377
10^3	0.0555	0.0733	0.0709	0.0650	0.0714
10^6	0.0168	0.0191	0.0209	0.0555	0.0659
(c) cycles at 135°					
60	0.0086	0.0182	0.0147	0.174	0.0708
10^3	0.0149	0.0093	0.0114	0.015	0.0099
10^6	0.0645	0.0715	0.0702	0.0700	0.0759
(d) cycles at 155°					
60	0.047	0.115	0.0558	0.397	0.45
10^3	0.0078	0.0091	0.0061	0.027	0.032
10^6	0.0642	0.0598	0.0614	0.054	0.058
(e) cycles at 175°					
60	0.124	0.23	0.145	0.97	0.7
10^3	0.0097	0.015	0.010	0.067	0.054
10^6	0.0537	0.049	0.048	0.038	0.046

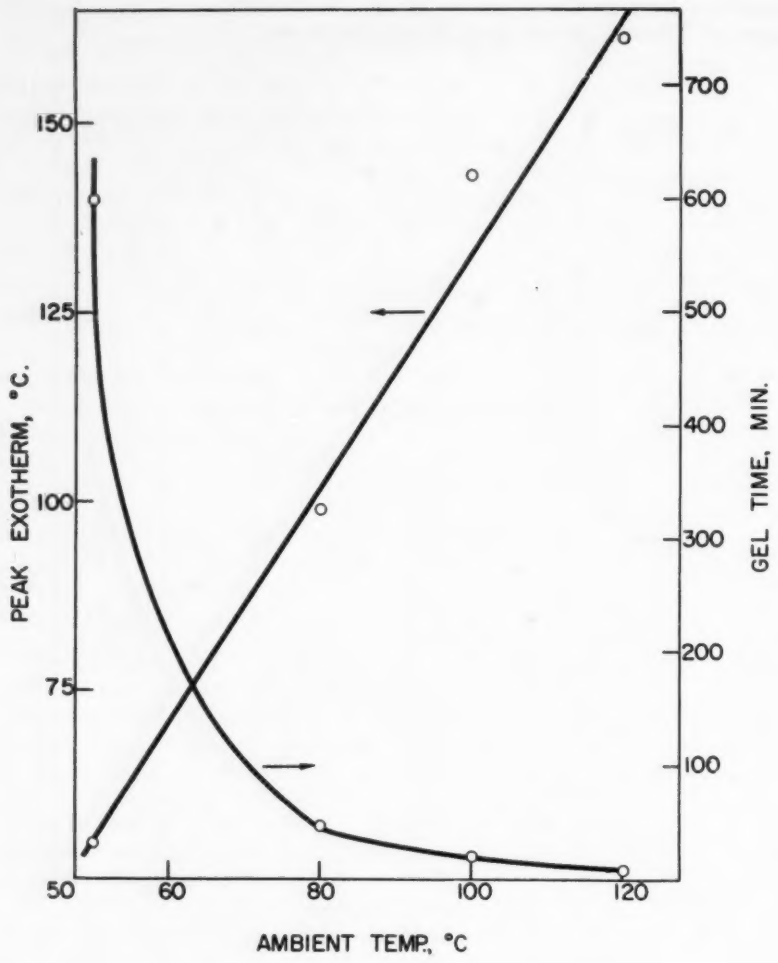

Figure 1. Peak exotherm temperature and gelation time as a function of ambient temperature

and that the higher proportions of dimer acid produce softer, more flexible resins. Formulations based on a 0.5 carboxyl ratio and 1% of stannous octoate were selected for further characterization since they had the best combination of toughness and resistance to thermal aging. The choice, however, would depend largely on the application, and other formulations may be more suitable depending on the flexibility required.

Mixtures of the 201 resin and dimer or trimer acid are completely miscible at 25° and have initial viscosities of 1800-4000 cpoise. The shelf life, or the time required to obtain a viscosity of 10,000 cpoise, is 8-20 hrs. when 1% of stannous octoate is employed. After 3-7 days a tough, cross-linked resin is obtained if reasonable care is taken to exclude moisture. The high reactivity at 80-120° is illustrated in *Figure 1* for a system containing 17.8, 17.2, and 0.35 g. of 201 resin, Empol 1022*, and stannous octoate, respectively. Apparently, the lower temperatures would be more suitable for larger batches since the reaction is exothermic. Curing for 0.5-1 hr. at 120° was adequate for near-ultimate properties and curing further produced only modest change. When a post-cure at higher temperatures was employed, little effect was observed, but when the total cure was effected at 160-200°, the resins were much more flexible. This phenomenon may be related to the relative amount of ester and ether formed during the reaction since the higher reaction temperatures favor esterification (2) and the structure of the polymer may be altered accordingly.

Resin properties can be changed by using hardeners with various amounts of trimer, dimer and monomer acids. *Table 3* summarizes the results obtained from 5 modifications and indicates that trimer acid leads to higher softening resins whereas addition of monomer acid, or tall oil acid, in limited quantities leads to lower softening resins. The data further illustrate the low viscosity and long shelf life of the curable mixtures and the excellent combination of toughness and electrical properties. Apparently, the unique electrical properties at temperatures up to 175° can be attributed to the high proportion of hydrocarbon in the resin.

Addendum

Other polyepoxides can be hardened with these fatty acids and catalysts, such as stannous octoate; for example, bis(3,4-epoxy-6-methyl cyclohexylmethyl) adipate, having an epoxide equivalent weight of 226 and Empol 1022 in the ratio of 0.5 carboxyl per epoxide group gave a resin with a tensile strength of 480 psi, an ultimate elongation of 360%, and a Durometer D hardness of 15. The resin was more flexible than that based on UNOX 201 and had excellent thermal shock resistance.

Literature References

1. Lee, H., and Neville, K., "Epoxy Resins", McGraw-Hill Book Co., Inc., New York, 1957.
2. McGary, C. W., Jr., Patrick, C. T., Jr., and Stickle, R., Jr., Paint Varnish Prod., Vol. 50, No. 3, 39 (1960).
3. Patrick, C. T., Jr., McGary, C. W., Jr., and Phillips, B., paper presented at the Miami ACS Meeting, April, 1957.

Acknowledgment

We are grateful to Dr. W. R. Proops for helpful suggestions and to Mr. W. R. Thomas for assistance in this project. Electrical properties were kindly supplied by Mr. F. L. Williamson of the Union Carbide Plastics Company.

* Trademark Emery Industries

Editorial

New Frontiers in the Field of Macromolecules

Prof. GIULIO NATTA

Director of the Institute of Industrial Chemistry, Polytechnic Institute of Milan

The discovery of stereospecific polymerizations has opened in the last seven years new horizons in the field of linear synthetic macromolecules and their applications as plastics, textile fibers, synthetic rubbers.

The first stereoregular high polymers obtained by stereospecific catalysis are already being produced on a wide commercial scale, such as isotactic polypropylene, isotactic polybutene, several stereoregular polydiolefins (polybutadienes, polyisoprenes etc.).

Among the latter, cis-1,4 polybutadiene is now produced with a steric purity even higher than the one of natural or synthetic polyisoprene.

The obtainment of polymers having a high steric purity and the regulation at will of their crystallinity (which can be achieved either by regulating the steric purity of the single macromolecules or by introducing some irregularities of chemical nature by means of copolymerization) permits us to remarkably modify the properties of the macromolecules.

Thus, they can vary in a continuous way from highly crystalline products having high melting temperatures, to products having a lower degree of crystallinity and lower melting temperatures, lower hardness and higher elasticity, and finally to completely amorphous products having the properties of elastomers.

An example of the latter are the ethylene-propylene or ethylene-butene copolymers which give very low cost synthetic rubbers having good elastic and dynamic properties and, at the same time, a chemical resistance higher than that of polydiolefins.

Ethylene-propylene copolymers which contain unsaturations randomly distributed in the chain can now be vulcanized by the conventional methods used with unsaturated rubbers; however they substantially maintain the mechanical and dynamic properties and the chemical resistance characteric of saturated copolymers which would normally require special vulcanization processes.

New polymers in which the melting temperature can be regulated without altering their crystallinity are obtained by copolymerization of monomers. The monomeric units of these monomers behave as isomorphous, in the sense of yielding crystalline copolymers having reticular constants and melting temperatures which are intermediate between those of the corresponding homopolymers. Thus, diolefin polymers of different types can be obtained which have high melting points, elastic moduli and tensile strengths in the desired ranges of temperatures.

Stereospecific polymerizations have enabled the use as raw materials for the production of crystalline macromolecules, new monomers of very low cost which in the past could not be used to produce valuable products.

These new monomers allow us to produce, besides plastics materials having interesting properties, also textile fibers which are extremely light and possess high mechanical characteristics as well as sufficient thermal resistance.

The properties of these fibers and their dyeability, now already achieved by several different methods permit us to forecast very wide developments for highly crystalline polypropylene fibers (produced in Italy under the trade-name "MERAKON"*).

The synthesis of polytactic polymers, containing several sites of optical or geometrical asymmetry, has resulted in new classes of stereoregular polymers, including some which are optically active. It should be noted that the synthesis is started from monomers *not* containing sites of optical asymmetry.

This fact differentiates the new synthetic polymers from the natural ones derived from the condensation of already optically active monomers (for instance cellulose from glucose, natural silk from L-aminoacids).

Asymmetric synthesis of polytactic optically active polymers represents a more advanced stage of stereospecific polymerization, which mostly yields highly crystalline polymers.

In these last years, stereospecific catalysis has been extended to new classes of monomers containing oxygen, nitrogen, chlorine etc. Ordinarily these monomers are not polymerizable with the metal-organic catalysts employed in alpha-olefin polymerization.

Crystalline polymers were also obtained by stereospecific polymerization or copolymerization of monomers containing inner double bonds.

Of particular interest is the synthesis of crystalline polyesters through polymerization or copolymerization of oxygen-containing unsaturated monomers such as, the polymerization of ketenes and their copolymerization with ketones, aldehydes, etc.

These monomers permit the synthesis of crystalline polymers reaching a melting temperature between 200 and 300°C. Such a range is not reached by linear alphaolefin polymers.

An already reached frontier is the one of high chemical and thermal stability, an example of which is some saturated polymers not containing secondary or tertiary carbon atoms. These polymers are obtained by polyaddition of unsaturated, oxygen-containing monomers.

The new, almost unlimited possibilities recently opened by the production of new classes of macromolecules having different properties and characteristics (from old as well as from new monomers) will allow us to select special products suitable for special uses at very low costs.

We can therefore foresee that in the near future the variety and quantity of applications and hence the consumption of plastics, fibers, and synthetic rubbers will be expanded throughout the world at a rate still higher than in the past, reaching and even exceeding the most optimistic forecasts.

---

* Registered trade-mark.

A *preview* of several articles accepted for publication in the next issue of SPE TRANSACTIONS

The Thermodynamics Biaxial Elongation

by Richard S. Stein

An important article which extends thermodynamic analysis to the case of two dimensional deformation, of interest in elucidating the molecular mechanisms of such processes. Must reading for workers in biaxial orientation.

Dynamic Measurement of Mechanical Moduli I: Equipment for Automatic Recording of Shear and Flexural Amplitude-Time Curves in Free Vibration

by Armand F. Lewis and Marvin C. Tobin

An article on a subject on which there is little data but for which there is a high demand—Poisson's ratio. Equipment is described for measurement of Young's and shear modulus on the same identical polymer sample, by a free vibration method. Young's modulus and damping, shear modulus and damping, and Poisson's ratio are reported over a range of temperature for polypropylene, Nylon 66, and poly(methylmethacrylate).

Relationships Between the Structures of Organic Phosphites and Their Effectiveness in Poly(Vinyl Chloride) Stabilization

by James P. Scullin, Marvin Rosen, and Theodore A. Girard

Following structural variations were evaluated: Aryl; alkyl; alkenyl; aralkyl; alkaryl; cycloaliphatic; mixed alkyl aryl tertiary phosphites; cyclic tertiary phosphites; bis-tertiary phosphites; and phosphites containing carbon-sulfur-phosphorus linkages.

Bibliography on Ultraviolet Degradation and Stabilization of Plastics

by N. Z. Searle and R. C. Hirt

Literature references on the stabilization of plastics, arranged in chronological order except for the categories of photochemistry, phosphorescence, and fluorescence, which are arranged in alphabetical order by subject. Of special interest: The compact four-letter CODEN designation has been used in place of the chemical abstracts system, to save space and allow the references to be presented on a single line and to be printed directly from IBM punched cards.

SPE TRANSACTIONS